Institute of Bioorganic Chemistry, Polish Academy of Sciences
Department of Plant Functional Metabolomics

DOCTORAL THESIS

SERHII KOZIN

ENGINEERING OF TRYPTOPHAN SPECIALIZED METABOLISM IN *ARABIDOPSIS THALIANA* FOR PLANT IMMUNITY

Supervisor:
prof. dr. habil. Paweł Bednarek

Poznań 2026

To my wife, Anastasiia, my closest collaborator in life.

I would like to express my deepest gratitude to my supervisor, prof. dr. habil. Paweł Bednarek, for his scientific support, valuable guidance, and patience, without which this thesis would never have been written, and would almost certainly have been much worse.

I am also deeply grateful to dr. habil. Anna Piasecka for the knowledge she shared, the time she devoted, and her invaluable help with metabolomics analyses, which at several points seemed to understand my project better than I did.

I would also like to thank Mariola Bednarek for her help with plant handling and for her practical advice, which made everyday work with plants much easier.

Moreover, I would like to thank Lokesh Veeresh for his help with the more routine side of laboratory work, which was made much more bearable and enjoyable thanks to him.

I thank all former and current members of the Department of Plant Functional Metabolomics, thanks to whom daily work in the laboratory was not only a valuable scientific experience, but also a genuine pleasure.

I would also like to thank my colleagues from the Department of Molecular Plant Physiology, whose advice, suggestions, and timely interventions rescued more than one experiment from a tragic end.

Finally, I thank my friends for their constant support, motivation, and for tolerating my repeated claims that the thesis was "almost finished."

The work described in this thesis has been carried out at the Institute of Bioorganic Chemistry, Polish Academy of Sciences in Poznań in the Department of Plant Functional Metabolomics under the supervision of prof. dr. habil. Paweł Bednarek. This work was supported by the OPUS grant 2019/35/B/NZ1/03731 (National Science Centre, Poland), "Interspecies metabolic engineering as a tool to investigate immune functions of plant specialized metabolites."

TABLE OF CONTENTS

Page

ABBREVIATIONS

4OGlcI3F	4-O-β-Glucosyl-Indol-3-yl Formamide
4OHI3G	4-Hydroxyindol-3-ylmethyl Glucosinolate
4MI3G	4-Methoxyindol-3-ylmethyl Glucosinolate
1MI3G	1-Methoxyindol-3-ylmethyl Glucosinolate
AAP1	Amino Acid Permease 1
ABCG	ATP-binding cassette transporter, subfamily G
AGL	Aliphatic Glucosinolate
BABG	Brassinin-Associated β-Glucosidase
CERK1	Chitin Elicitor Receptor Kinase 1
CGP1	Cysteinylglycine Peptidase 1
cDNA	Complementary DNA
DAMP	Damage-Associated Molecular Pattern
DHCA	Dihydrocamalexic Acid
DNA	Deoxyribonucleic Acid
DTC	Dithiocarbamate
DTC-MT	Dithiocarbamate *S*-Methyltransferase
EFR	Elongation Factor Tu Receptor
ER	Endoplasmic Reticulum
ETI	Effector-Triggered Immunity
ESP	Epithiospecifier Protein
FLS2	Flagellin-Sensing 2
flg22	22-Amino Acid Flagellin Epitope
GGP	Gamma-Glutamyl Peptidase
GSH	Glutathione
GL	Glucosinolate
GST	Glutathione *S*-Transferase
HCX	Hydroxycamalexin
HCX-Hex	Hydroxycamalexin Hexoside
HCX-Hex-Mal	*O*-Malonyl-Hydroxycamalexin Hexoside
HR	Hypersensitive Response
I3A	Indol-3-ylmethylamine

I3CA	Indole-3-Carboxylic Acid
I3G	Indol-3-ylmethyl Glucosinolate
IAN	Indole-3-Acetonitrile
IAOx	Indole-3-Acetaldoxime
IGL	Indole Glucosinolate
ITC	Isothiocyanate
JA	Jasmonic Acid
LC-MS/MS	Liquid Chromatography-Tandem Mass Spectrometry
LC-UV/FLD	Liquid Chromatography with UV and Fluorescence Detection
MAMP	Microbe-Associated Molecular Pattern
MAPK	Mitogen-Activated Protein Kinase
MCX	Methoxycamalexin
NLR	Nucleotide-Binding Leucine-Rich Repeat Receptor
PAD3	Phytoalexin Deficient 3
PAMP	Pathogen-Associated Molecular Pattern
PCS1	Phytochelatin Synthase 1
*Pc*BMM	*Plectosphaerella cucumerina* Strain BMM
PEN2	Penetration 2
PR proteins	Pathogenesis-Related Proteins
PRR	Pattern-Recognition Receptor
PTI	Pattern-Triggered Immunity
RA	Raphanusamic Acid
RLK	Receptor-Like Kinase
RLP	Receptor-Like Protein
RNA	Ribonucleic Acid
ROS	Reactive Oxygen Species
RT	Retention Time
RT-qPCR	Reverse Transcription Quantitative PCR
SA	Salicylic Acid
SAR	Systemic Acquired Resistance
SD	Standard Deviation
SM	Specialized Metabolite

SOT16	Sulfotransferase 16
SUR1	Superroot 1
UV	Ultraviolet
WT	Wild Type

INTRODUCTION

1.1. Plant specialized metabolism

Specialized metabolites (SMs), classically known as secondary metabolites, are organic compounds that, unlike primary metabolites, are not directly involved in the normal growth, development, or reproduction of the organism. The historical aspect of this metabolism classification is the concept of "dispensability" versus "indispensability." Specialized metabolites were often regarded as nonessential by-products - akin to "the ebbs and flows on the metabolism beach" - or even as waste or detoxification products (Aharoni and Galili, 2011). Today, it is well established that many SMs function as crucial chemical signals and defensive agents in the ecosystem. Thus, although they may be considered dispensable for the processes of growth and development (except for pathways responsible for hormone synthesis), they are indeed indispensable for the survival and adaptive success of a species. Furthermore, the distinction between primary and specialized metabolism is frequently based on function rather than structure, as individual compounds can serve dual roles depending on context (Harborne, 1977). Notably, the features of SMs include their extensive structural diversity, their often taxonomically restricted distribution to particular families or genera, and their high degree of variability both between and within species.

1.1.1. History of SM study

Over the past centuries, the study of SMs has evolved from merely identifying these compounds to understanding their biosynthesis, localization, and ecological functions. The earliest work was devoted to the isolation of such alkaloids as morphine and quinine, which were known to exhibit medicinal properties (Garba Mikail et al., 2022). The early 20th century was marked by a period during which scientists tried to distinguish between SMs and the metabolites considered primary (Fraenkel, 1959). By the middle of the 20th century, the discovery of terpenoids, phenolics, and glucosinolates (GLs) expanded the scope even more. These compounds had to await the development of chromatographic and spectroscopic techniques to isolate and characterize them properly and then identify their correct structure, along with their physiological and ecological

functions. In the genomics era, emerging advanced technologies have fundamentally transformed the understanding of plant SM functions. These include metabolomics, which continually enriches our knowledge of the chemical diversity and biosynthetic complexity of these compounds. The availability of whole-genome sequences for a growing number of plant species enables detailed investigation of the genomic basis of SM production (Zhao et al., 2013). As we move further in time, vast numbers of genes and gene products involved in SM metabolism have been identified and characterized. It has been proven that terpenoids, phenols, alkaloids, and oxidized fatty acids play critical roles in plant growth, environmental adaptation, and interactions with other organisms. Recent combined biological, biochemical, and metabolomic studies have underscored that SMs serve as essential chemical signals in ecosystems, mediating complex communication networks and thereby contributing to ecosystem configuration, biodiversity, and coevolution (Bohlmann and Keeling, 2008; Thompson, 1982). As a result of this scientific progress, nowadays, the older view of these compounds as merely secondary or nonessential is no longer tenable.

Currently, one can state that one of the most pronounced roles of SMs is acting in plant defense mechanisms. For instance, particular polyphenols are synthesized constitutively and serve as a deterrent against insect herbivores by inhibiting feeding and exhibiting toxicity (Moctezuma et al., 2014). This defensive strategy is not only crucial for the survival of the plant but also plays a significant role in shaping its ecological interactions. Besides defense, SMs mediate a spectrum of non-defensive ecological interactions - pollinator and seed-disperser attraction, symbiosis signaling, plant-plant communication, and abiotic stress mitigation are among them (Lv et al., 2022). Volatile organic compounds emitted by plants can attract pollinators or repel herbivores, demonstrating the relationship between plants and their environment (Haruta et al., 2001).

The study of SMs also links with the field of pharmacology, as many of these compounds exhibit bioactive properties that can be beneficial for human health (Duan et al., 2025; Peng et al., 2025). For example, terpenoids and alkaloids have been extensively studied for their therapeutic effects, including anti-inflammatory, anti-cancer, and antimicrobial activities (Jiang et al., 2016; Masyita et al., 2022). Understanding the biosynthetic pathways of these metabolites can lead to the development of novel drugs and therapeutic agents derived from plant sources.

Moreover, SMs are increasingly recognized for their potential applications in agriculture and the food industry (Tiedge et al., 2025). The manipulation of biosynthetic

pathways through genetic engineering and synthetic biology has opened new avenues for enhancing the production of valuable metabolites (Roell and Zurbriggen, 2020; Tariq et al., 2023). For instance, researchers have successfully engineered plants to produce higher yields of flavonoids and other beneficial compounds, which can be harnessed for food and nutraceuticals (Butelli et al., 2008; Tariq et al., 2023). This biotechnological approach not only improves the economic value of crops but also contributes to sustainable agricultural practices by reducing the need for synthetic pesticides and fertilizers (Butelli et al., 2008; Jiang et al., 2016; Tiedge et al., 2025).

1.1.2. Classification of SMs

The classification of plant SMs supports understanding their diverse roles in plant biology, ecology, and their applications in medicine and agriculture. These compounds can be broadly categorized into several classes based on their chemical structure and biosynthetic pathways, which include phenylpropanoids, terpenoids, alkaloids, and others (Kabera et al., 2014). In addition, SMs can be classified based on their physiological functions, with phytoalexins being a notable example.

1.1.2.1. Main structural classes of SMs. Phenylpropanoids (Fig. 1.1), represent one of the largest groups of SMs in plant kingdom, characterized by the presence of one or more hydroxyl groups attached to aromatic rings. These compounds, derived from phenylalanine via a C_6–C_3 scaffold, can combine antioxidant capacity with direct antimicrobial or anti-herbivore toxicity (Korkina, 2007; Yadav et al., 2020). Flavonoids, a subclass of phenylpropanoids, are particularly abundant and involved in various physiological processes, including UV protection, pollinator attraction, and defense against microbial infections. (Treutter, 2006; Winkel-Shirley, 2002).

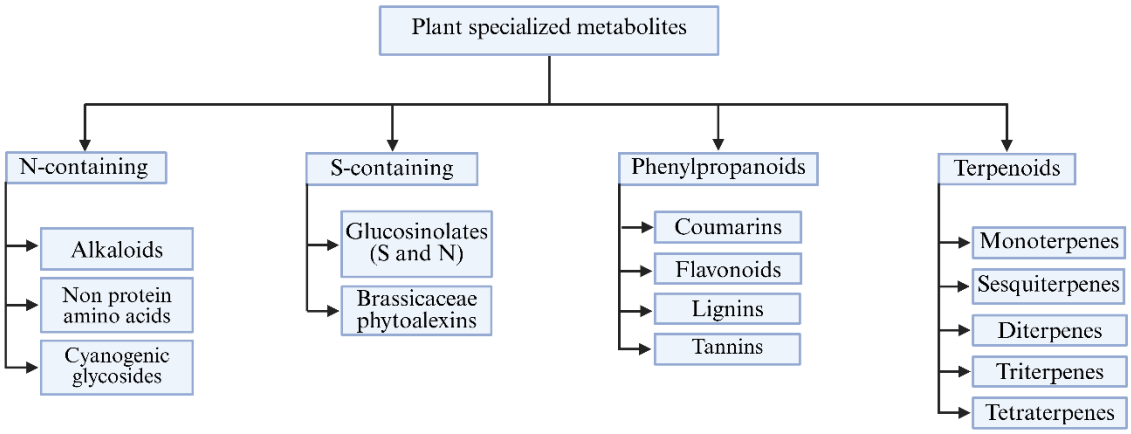

Fig. 1.1. Simplified classification of plant specialized metabolites

Terpenoids represent the largest and most structurally diverse class of SMs in plants. They are synthesized through the polymerization of five-carbon isoprene units and are known for their diverse structures and functions. For example, they act as defensive compounds by repelling herbivores and attracting their natural enemies (Bohlmann and Keeling, 2008); they contribute to the aromatic properties that facilitate pollinator attraction (Carrillo-Gavilán et al., 2015). Their complex biosynthetic pathways enable the production of compounds such as essential oils, which have significant applications in perfumery and aromatherapy (Kabera et al., 2014)

Alkaloids, the most diverse group representing N-containing metabolites characterized by their nitrogenous heterocyclic structures, constitute a crucial SM class with diverse ecological and pharmacological roles. Intrinsic toxicity of many alkaloids contributes to plant defense by deterring pests. For example, the bitter taste and toxicity of nicotine effectively discourage herbivory, a phenomenon not commonly observed with other classes such as terpenoids, which often serve more as attractants or volatile signals (Harborne, 2001). Moreover, these metabolites have been harnessed in human medicine for their analgesic and anti-inflammatory properties (Xiang et al., 2022).

Unlike N-containing, S-containing SMs are not ubiquitous in the plant kingdom. Such metabolites are mainly produced by plant species belonging to the Brassicales order, including the Brassicaceae family. This family includes important crop and vegetable plants like oilseed rape (*Brassica napus*), cabbage (*Brassica oleracea* var. *capitata*), broccoli (*Brassica oleracea* var. *italica*), and mustard (*Sinapis alba*), as well as the model plant *Arabidopsis thaliana*. Plants representing Brassicales order evolved pathways for biosynthesis of GLs and S-containing phytoalexins (Halkier and Gershenzon, 2006; Sønderby et al., 2010; Pedras et al., 2011). These compounds are synthesized from amino

acids and play crucial roles in plant defense mechanisms against herbivores and pathogens. Research using *A. thaliana* has significantly advanced our understanding of GL biosynthesis. The availability of its complete genome has enabled functional genomics approaches that have identified numerous genes encoding proteins involved in this pathway.

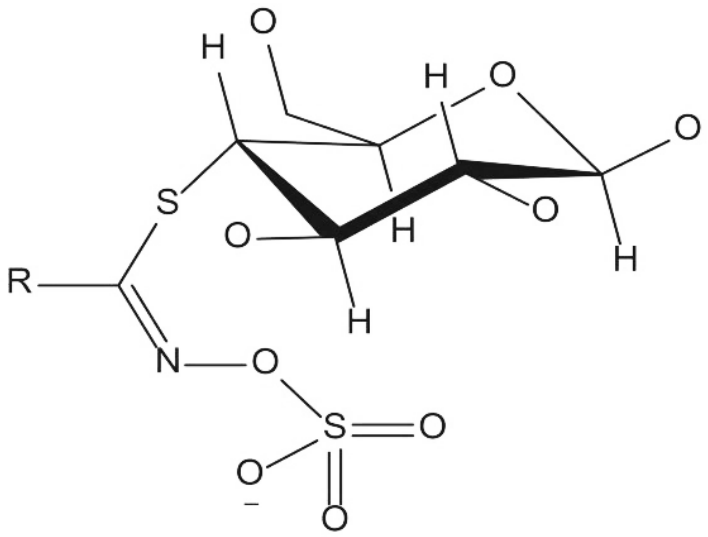

Fig. 1.2. General structural formula of a glucosinolate molecule. R – side chain.

Collectively, Brassicaceae plants have been reported to synthesize at least 120 distinct GLs, which are structurally grouped into three main classes - aliphatic, indolic, and benzyl - based on their precursor amino acids (Fig. 1.2) (Fahey et al., 2001). Aliphatic GLs (AGLs) are derived from Met and other aliphatic amino acids such as Ala, Ile, Leu, and Val. Indolic glucosinolates (IGLs) originate from Trp, while benzyl GLs from Phe or Tyr (Sønderby et al., 2010). All GLs share a core structure consisting of a β-D-glucopyranose moiety linked via sulfur to a (*Z*)-*N*-hydroximinosulfate ester, with a variable side chain determined by the amino acid precursor (Fahey et al., 2001).

1.1.2.2. Phytoalexins – an example of a functional SM class. Phytoalexins (Fig. 1.3) are defined as low-molecular-weight antimicrobial compounds synthesized *de novo* in response to pathogen invasion, and are therefore considered components of an inducible defense mechanism (Paxton, 1981; VanEtten et al., 1994). Notably, despite the function of these compounds in plant-microbe interactions, their biosynthesis can be frequently triggered by abiotic stresses, including UV-radiation and metal ions (Pedras et al., 2011).

In grapevine (*Vitis vinifera)*, representing phenylpropanoids resveratrol accumulates specifically at sites of fungal invasion and directly inhibits growth of *Botrytis*

cinerea (Adrian et al., 1997; Schouten et al., 2002). This compound directly inhibits conidial germination and mycelial growth *in vitro*, with studies reporting ~70 % inhibition of conidial germination at 100 µg mL^{-1} (Caruso et al., 2011). Scopoletin, a coumarin-type phytoalexin, accumulates rapidly upon pathogen detection in several dicots. This has been observed in tobacco (*Nicotiana tabacum*) leaves after tobacco mosaic virus or *Alternaria alternata* infection, and also in cassava (*Manihot esculenta*), sunflower and *A. thaliana* (Chong et al., 2002; Costet et al., 2002; Stringlis et al., 2019; Tal and Robeson, 1986). Another well-characterized example of a phenylpropanoid phytoalexin is glyceollin, prenylated pterocarpan derived from the isoflavonoid branch of the flavonoid pathway existing in the form of three isomers (I, II and III). It is found in soybean (*Glycine max*), and exhibits antifungal activity against *Phytophthora sojae*, *Sclerotinia sclerotiorum*, and other pathogens (Jahan et al., 2020; Lygin et al., 2013; Ng et al., 2011).

Brassicaceae plants produce a diverse array of S-containing phytoalexins, with individual compounds often confined to narrow phylogenetic sub-clades of this family (Pedras et al., 2007). A well-characterized example of Brassicaceae phytoalexins is camalexin, first discovered in *Camelina sativa* (Browne et al., 1991). This compound is the major phytoalexin of *A. thaliana*, which is induced by a wide range of pathogens (Glawischnig, 2007). Camalexin is lipophilic and disrupts fungal membranes and interferes with signal transduction in *B. cinerea*, *Alternaria brassicicola* and *Pseudomonas syringae* (Rogers, 1996; Sellam et al., 2007). Consequently, *A. thaliana* mutants deficient in camalexin are hypersusceptible to selected pathogens, including the necrotrophic fungus *A. brassicicola* (Thomma et al., 1999). Beyond combating pathogens, camalexin shapes the root microbiome and primes systemic defenses, linking direct chemical action to broader immune signaling in the plant (Koprivova et al., 2023).

In cultivated *Brassica* species, phytoalexin blends commonly include brassinin and its derivatives, including cyclobrassinin and spirobrassinin (Pedras et al., 2014). In roots of rutabaga (*B. napus* ssp. *napobrassica*) and turnip (*B. rapa* ssp. *rapa*), UV radiation induced higher production of brassinin and cyclobrassinin than inoculation with the biotrophic fungus *Albugo candida* (Pedras and Adio, 2008). In UV-radiated turnip tissue, brassinin accumulation was reported to become evident within 8 h and to reach a maximal level reported as ~17 µg/g (freeze-dried tissue) (Monde et al., 1991). Brassinin downstream metabolite, brassilexin, has been isolated from *B. juncea* and is characterized by a thiazole ring fused to the indole core (Devys et al., 1988). Brassilexin inhibits the

growth of the black-leg pathogen *Leptosphaeria maculans* at 2–6 µM, and inhibits several *Alternaria* isolates at ≤10 µM (Pedras et al., 2004).

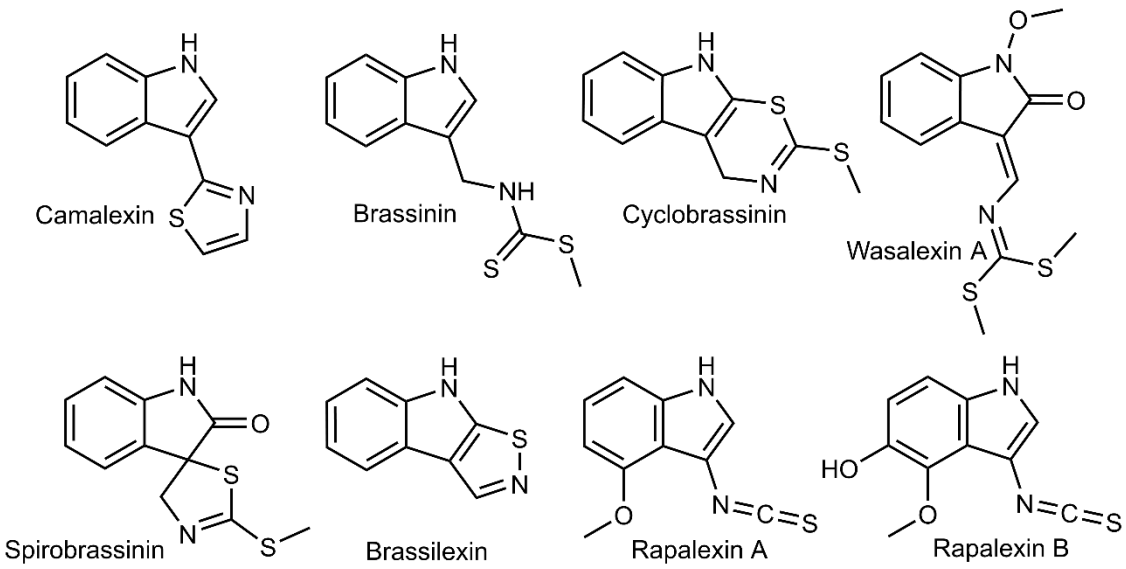

Fig. 1.3. Chemical structures of selected indole-type S-containing phytoalexins of Brassicaceae.

Other lineage-restricted phytoalexins are nasturlexins C and D from *Barbarea vulgaris* and *Barbarea verna*, which display antifungal activity against *A. brassicicola*, *L. maculans* and *S. sclerotiorum* (Pedras et al., 2015). Rapalexins A and B are indole isothiocyanate (indole-ITC) phytoalexins first isolated from *B. rapa* (Pedras and Adio, 2008). They were later detected in *Eutrema salsugineum* (syn. *Thellungiella halophila*) and in *A. thaliana* following abiotic or biotic elicitation (Pedras and Adio, 2008). Rapalexins have been shown to display antifungal activity against *L. maculans* and *Colletotrichum* spp. (Pedras and Adio, 2008; Pedras and Thapa, 2020; Plaszkó et al., 2021). Rutexin-series phytoalexins (rutexin, isalexin and brassicanate A) form another branch of Brassicaceae indole-sulfur phytoalexins (Pedras et al., 2004; Pedras and Yaya, 2010). To date, they have been detected in rutabaga (*B. napus* ssp. *napobrassica*) and *B. rapa* (Pedras et al., 2004). All three are synthesized de novo in wounded or pathogen-challenged roots, reaching low-to-mid µg/g levels within 24 h (Pedras et al., 2004). *In vitro* assays indicate inhibition of *L. maculans* at low µM concentrations (Pedras et al., 2004). Wasalexins A/B found in salt cress (*E. salsugineum*) are believed to originate from the IGL pool. In accordance with this assumption, UV, $AgNO_3$ and heavy-metal ions strongly induce not only biosynthesis of these compounds, but also IGL biosynthetic genes in *Thellungiella salsuginea* (Mucha et al., 2015). Pathogens like *L. maculans*,

Albugo candida, and *B. cinerea* elicit rapid wasalexin formation without visible disease in *T. salsuginea* foliage (Pedras et al., 2010).

1.2. *A. thaliana* as a model organism

Plant research relies heavily on model species that offer both genetic accessibility and experimental versatility. Among these, *A. thaliana*, a small flowering plant from the Brassicaceae family, has become the leading model system for studying plant defense mechanisms (Meinke et al., 1998). Scientific interest in this species dates back to the 1940s, when Friedrich Laibach first proposed its use due to its small genome and ease of cultivation (Koornneef and Meinke, 2010). However, it wasn't until the 1980s and 1990s that its model status was solidified, driven by the work of scientists such as George Rédei and Maarten Koornneef, who developed extensive genetic tools, including mutant libraries and mapping populations (Redei, 1975; Koornneef et al., 1983). This foundation culminated in the launch of the Arabidopsis Genome Initiative in 1996 and the completion of its full genome sequence in 2000 - the first for any plant species (The Arabidopsis Genome Initiative, 2000). This achievement enabled high-throughput gene discovery, transcriptomics, and large-scale functional studies.

A. thaliana offers many practical advantages: a short life cycle of ~six weeks, small size, prolific seed production, and the ability to grow in simple lab conditions under low light (Clough and Bent, 1998; Koornneef and Meinke, 2010). Its seeds are so small and uniform that thousands can be germinated on a single petri dish, facilitating high-throughput experiments. Furthermore, its self-pollinating nature and high tolerance to homozygosity are ideal for genetic studies, while its compatibility with tools like floral dip transformation and modern genome-engineering tools such as CRISPR/Cas9 (Feng et al., 2013), make gene editing routine.

In addition, a vast seed-stock infrastructure multiplies these genetic tools. Public repositories such as the Arabidopsis Biological Resource Center (ABRC) and the Nottingham Arabidopsis Stock Centre (NASC) now distribute more than 800 000 distinct seed stocks. Of these, more than 700 000 sequence-indexed T-DNA insertion lines, ~360 000 have mapped flanking-sequence tags covering ≈ 90 % of annotated genes (Alonso and Ecker, 2006; NASC Bioinformatics; Pucker et al., 2021). Beyond T-DNA collections, both repositories also maintain chemically induced, CRISPR and natural-accession panels

(NASC Bioinformatics; The European Arabidopsis Stock Centre - The University of Nottingham). Ready access to these mutants lets researchers knock out, stack or complement virtually any gene to test its role in SM biosynthesis, transport or regulation within days rather than seasons (Koornneef and Meinke, 2010).

These attributes, alongside a fully sequenced and annotated genome (~135 Mbp), have made Arabidopsis a cornerstone of plant research in developmental biology, hormone signaling, and environmental adaptation. Discoveries made using Arabidopsis have extended well beyond plant biology, offering insights into molecular and cellular processes relevant to other organisms, including humans (Koornneef and Meinke, 2010). However, as with any model system, Arabidopsis has some limitations. It is a eudicot angiosperm adapted to specific temperate environments and does not fully represent the vast diversity of over 400,000 known plant species, which span gymnosperms, monocots, ferns, mosses, algae, and more. Many important biological traits - such as symbiotic interactions with arbuscular mycorrhizal fungi, C4 or crassulacean acid metabolism photosynthesis, and cereal crop-specific morphologies - are absent in *A. thaliana* (Cosme et al., 2018; Sharma et al., 2023). Despite these limitations, Arabidopsis remains the foundational reference species for comparative genomics and molecular studies, which enables us to identify conserved and divergent mechanisms across the plant kingdom.

1.2.1. *A. thaliana* and specialized metabolism research

Because its genome is compact, *A. thaliana* has become the reference plant for dissection of key specialized-metabolism pathways. Forward- and reverse-genetic analyses, together with biochemical studies, enabled detailed elucidation of GL and camalexin biosynthesis in this species (The Arabidopsis Genome Initiative, 2000; Halkier and Gershenzon, 2006; Glawischnig, 2007). Similar type of studies mapped the entire coumarin branch that frees iron under alkaline conditions (F6′H1 → S8H → fraxetin/sideretin) and demonstrated its physiological importance for Fe ions uptake (Rajniak et al., 2018; Tsai et al., 2018). Functional studies have also revealed root-exuded triterpenes that remodel the rhizosphere microbiome and modulate root architecture, pointing to ecological roles beyond defense (Bai et al., 2021; Huang et al., 2019). Finally, the thalianol, marneral, and arabidiol/baruol triterpene clusters - compact, co-expressed gene islands that were first dissected genetically in Arabidopsis and later shown to be organized by distinct chromatin interaction domains (Nützmann et al., 2020)

At the same time, Arabidopsis chemistry is phylogenetically narrow. It lacks the benzoxazinoids that dominate cereal defense metabolism, the diterpenoid phytoalexins such as momilactone and oryzalexin, characteristic of rice (Frey et al., 2009), and the triterpenoid avenacin saponins that protect oat roots against soil fungi (Mylona et al., 2008). These lineage gaps explain why discoveries in Arabidopsis increasingly serve as blueprints for pathway mining and engineering in chemically divergent crop models, rather than as a complete catalogue of plant specialized metabolism.

1.2.2. *A. thaliana* in the context of plant immunity

Despite its widespread use as a model organism in various fields of plant biology, *A. thaliana* was initially not considered a suitable model for studying plant-pathogen interactions. Early perceptions regarded this common weed as lacking specific pathogenic microorganisms. However, by the 1990s, it was demonstrated that the cauliflower mosaic virus and the bacterium *Xanthomonas campestris* pv. *campestris* could infect Arabidopsis (Love et al., 2005; Van Hulten et al., 2019). Shortly thereafter, additional pathogens capable of infecting *A. thaliana* in natural environments were identified (Mauch-Mani and Slusarenko, 1993). These findings positioned this species as a valuable model for testing hypotheses related to immune responses in other plant species, exemplified by its application in functional genomics studies of tomato.

In the 1990s, the first protocols for studying plant-pathogen interactions using *A. thaliana* were developed (Mauch-Mani and Slusarenko, 1993). Since then, experiments involving this species have led to the identification of numerous key components of the plant immune system (Jones and Dangl, 2006; Nishimura and Dangl, 2010), including the recognition of microbe-associated molecular patterns (MAMPs) and the mechanisms of pattern-triggered immunity (PTI) (Yuan et al., 2021). Furthermore, studies utilizing Arabidopsis have provided insights into how virulence effectors enter plant cells, how they are recognized, and how this recognition activates effector-triggered immunity (ETI) (Jones and Dangl, 2006). The use of *A. thaliana* as a model has significantly enhanced our understanding of the roles of SMs in immune responses, including functions of GLs derivatives and phytoalexins like camalexin (Glawischnig et al., 2004; Bednarek et al., 2009). These studies demonstrated mechanistic connections between specialized metabolism and phytohormone-dependent immunity, including pattern-triggered responses coordinated by jasmonic acid (JA) and salicylic acid (SA) signaling.

Gene expression studies have yielded significant insights into transcriptomic changes triggered by pathogen detection (Corwin et al., 2016). In addition to standard gene expression analyses, co-expression studies using *A. thaliana* have identified genes associated with plant immune responses (Tully et al., 2014). These analyses enabled construction of complex networks of gene interactions, facilitating the identification of previously unknown genes that may play critical roles in immune responses (Nishimura and Dangl, 2010). This broad applicability, together with its genetic simplicity and extensive molecular toolkit, ensures that Arabidopsis will continue to be an indispensable system in understanding the complexities of plant-pathogen interactions and, by extension, driving strategies forward for crop improvement (Jones and Dangl, 2006; Nemri et al., 2010; Klepikova et al., 2016).

1.3. Molecular mechanisms of plant immunity

Plants have evolved a decentralized, multilayered innate immune system in which every cell functions as both sentinel and defender (Dangl and Jones, 2001; Jones and Dangl, 2006). This system (Fig. 1.4) can be activated in response to general elicitors, which include exogenous chemicals, molecules derived from microorganisms (MAMPs) and damage signals (Damage-associated molecular patterns; DAMPs), and to specific elicitors, namely pathogen-secreted effectors, historically termed avirulence (Avr) proteins (Block et al., 2008; Boller and Felix, 2009; Zipfel, 2014).

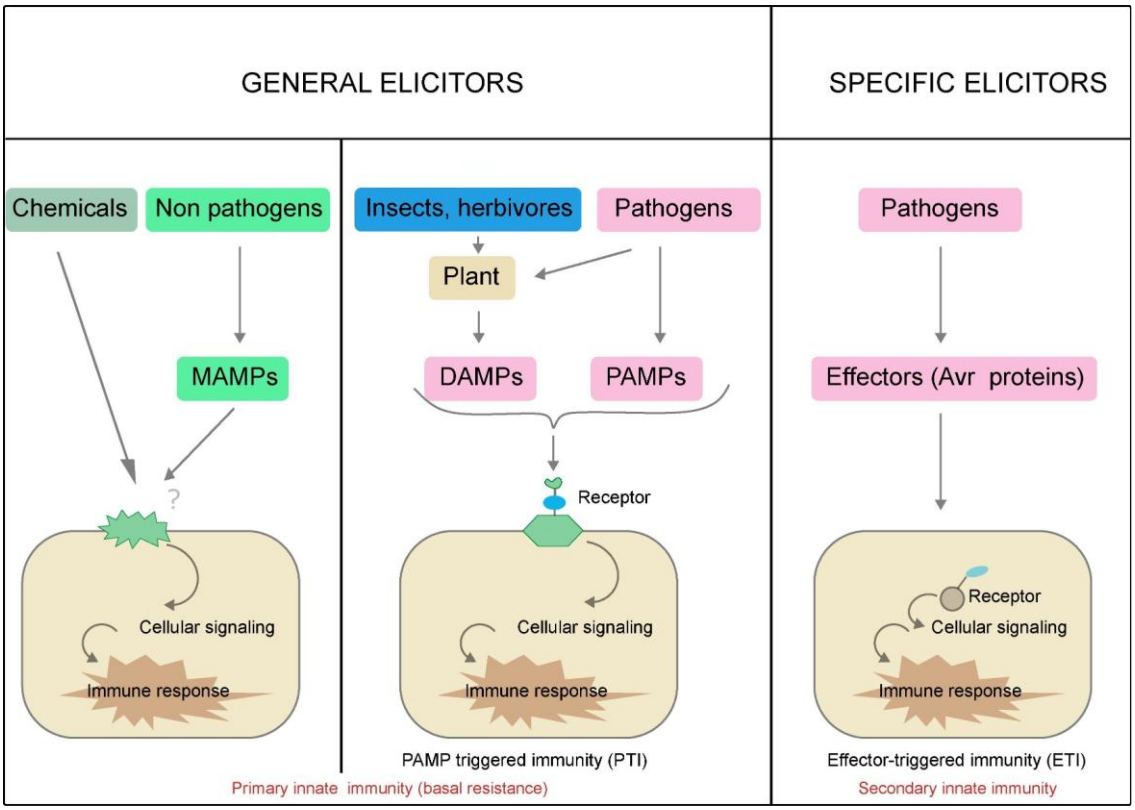

Fig. 1.4. Layers of inducible plant immunity. General elicitors like MAMPs and DAMPs trigger PTI via surface receptors, while pathogen effectors activate ETI through intracellular recognition.

1.3.1. Pattern-triggered immunity

PTI is a rapid, broad-spectrum response that constitutes the first layer of inducible plant immunity and is activated upon recognition of chemical elicitors (e.g. β-aminobutyric acid), MAMPs or DAMPs. MAMPs are molecular features conserved among microbial subclasses, such as bacterial lipopolysaccharide, flagellin-derived peptides (e.g. flg22) or fungal chitin fragments, which may be released by pathogens, non-pathogens or weakly interacting microbes (Gómez-Gómez and Boller, 2000; Miya et al., 2007). DAMPs are generated when insects, herbivores or pathogens injure plant tissues and liberate host-derived molecule fragments (e.g. oligogalacturonides) that feed back to amplify defense (Denoux et al., 2008; Boller and Felix, 2009). All these general elicitors are perceived by plasma membrane localized pattern-recognition receptors (PRRs) such as flagellin sensing 2 (FLS2), elongation factor thermo unstable receptor (EFR), and chitin elicitor receptor kinase 1 (CERK1). This recognition occurs at the host-environment interface, in which PRRs function as molecular triggers that guide immune responses upon the detection of a threat (Jones and Dangl, 2006).

PRRs are typically classified into two main types. Receptor-like kinases (RLKs) contain extracellular domains, usually leucine-rich repeats that bind MAMP or DAMP, and an intracellular kinase domain that functions in transmitting signals inside the cell. Receptor-like proteins (RLPs) lack a kinase domain, and they mostly need to interact with RLKs for signal propagation (Liebrand et al., 2013). Upon activation, PRRs form complexes with co-receptors such as BAK1 (brassinosteroid insensitive 1-associated kinase 1) to enhance signal transduction (Chinchilla et al., 2007). Signaling pathways activated by PRRs are highly multilayered and include Ca^{2+} influx, reactive oxygen species (ROS) production and mitogen-activated protein kinase (MAPK) signaling cascades that lead to transcriptional reprogramming (Jones and Dangl, 2006; Ramírez-Zavaleta et al., 2022). This in turn leads to production of PR proteins, antimicrobial peptides, antimicrobial SMs and signaling molecules. Other responses include the reinforcement of physical barriers to infection, such as deposition of callose at cell walls, which constitutes a structural defense (Jacobs et al., 2003). Overall, PTI includes a broad array of defense responses that strongly enhance the robustness against infections (Felix et al., 1999).

1.3.2. Effector-triggered immunity

Despite the broad-spectrum nature of PTI, many adapted pathogens deploy effector proteins to suppress or circumvent these early immune responses. In turn, plants have evolved a more specialized defense layer known as ETI initiated by intracellular nucleotide-binding leucine-rich repeat receptors (NLRs), encoded by resistance (R) genes, which monitor some effector proteins (Dodds and Rathjen, 2010; Yuan et al., 2021). NLRs either recognize effectors directly or detect perturbations in host proteins manipulated by effectors, a concept referred to as the "guard" or "decoy" model (Chen et al., 2022). Upon direct binding of an effector or indirect detection of its host-target perturbation, NLRs switch from an autoinhibited monomer to an oligomeric active “resistosome” form. Depending on the NLR class these resistosomes can function either as a Ca^{2+}-permeable channel or as an NADase enzyme, thereby initiating defense signaling (Martin et al., 2020; Contreras et al., 2023). Within minutes after binding an effector, the NADPH oxidase RBOHD-primed by PRRs at the plasma membrane - produces a signal in form of ROS (Ngou et al., 2021); this is followed by SA accumulation, extensive transcriptional reprogramming and, frequently, a localized

hypersensitive (HR) cell death that walls off the pathogen (Yuan M., Jiang Z., 2021). Because effector variants and matching NLR genes diversify across populations, the ETI types and variations are highly dynamic and an important target for crop improvement (Van de Weyer et al., 2019).

Recent work shows that ETI does not act in isolation. Key PRR components of PTI are indispensable for full ETI output, and ETI subsequently amplifies multiple PTI defense responses evolution (Ngou et al., 2021; Yuan et al., 2021). Conceptually, this integration is outlined in the mentioned “zig-zag” model of host-pathogen co-evolution, where successive cycles of effector innovation and NLR diversification drive escalating immune strength until pathogens devise new countermeasures (Jones and Dangl, 2006).

1.3.3. PTI-ETI synergy: Go in for the kill

Upon PAMP (pathogen-associated molecular pattern) or MAMP perception, PRR-co-receptor complexes phosphorylate the NADPH-oxidase RBOHD, releasing a rapid ROS burst, moderate SA production and the first wave of SAR (systemic acquired resistance) signals (Yuan et al., 2021). When NLRs subsequently sense effectors, ETI transcriptionally and post-translationally amplifies those same PTI components, generating a second, high-amplitude ROS/SA pulse that delimits the HR-response zone (Ngou et al., 2021).

Importantly, the PTI-ETI circuit is involved in triggering the biosynthesis of phytoalexin classes. In rice (*Oryza sativa*), diterpenoid phytoalexins - including momilactones, phytocassanes and oryzalexins - are produced from tightly linked gene clusters that are first induced during PAMP-triggered MAPK activity and then induced during effector-triggered responses to *Magnaporthe oryzae* (Shimura et al., 2007; Hasegawa et al., 2010; Kishi-Kaboshi et al., 2010; Wu et al., 2011). In soybean and other legumes, isoflavonoid-derived glyceollins are synthesized de-novo; PTI secures precursor availability, while ETI-induced MYB and bHLH transcription factors elevate pathway flux, resulting in glyceollin levels that inhibit *Phytophthora sojae* and correlate with field resistance (Cheng et al., 2018; Jahan et al., 2020; Lin et al., 2023). Collectively, these data indicate that while the chemical structures differ, the regulatory logic is conserved, PTI establishes baseline transcription of phytoalexin pathways, ETI intensifies production, and the resulting metabolites contribute to local containment of pathogens and, in some cases, to systemic signaling.

1.4. Glucosinolates

1.4.1. Biosynthetic insights

GL biosynthetic pathway has been almost completely characterized in the model plant *A. thaliana* (Jensen et al., 2014; Somssich et al., 2025). Studies in other species confirmed strong conservation of this pathway in the Brassicaceae family. GLs biosynthetic pathway is composed of three separate phases: phase 1 - precursor modification, phase 2 – core biosynthesis, and phase 3 core structure tailoring.

The 1st phase usually involves addition of a methylene group to the side chain of Met and Phe/Tyr (Fig. 1.5). Phe and Tyr undergo only one methylene addition, yielding 2-phenylethyl-GL and 2-hydroxy-2-phenylethyl-GL, respectively (Liu et al., 2016). Met-derived GLs, in contrast, vary in side-chain length. Their elongation starts in the cytosol, where branched-chain aminotransferase 4 (BCAT4) converts Met to 4-methylthio-2-oxobutanoate. This 2-oxo acid is then transported into chloroplasts by bile acid transporter 5 (BAT5) and enters the iterative methylthioalkylmalate synthase-isopropylmalate isomerase-isopropylmalate dehydrogenase cycle in the plastid (Sønderby et al., 2010). Each cycle adds one methylene unit. BCAT3 likely completes the elongation, especially in the formation of short-chain aliphatic GLs (Knill et al., 2008). The resulting chain-elongated 2-oxo acids are then returned to the cytosol and serve as precursors of aliphatic GLs (Sønderby et al., 2010).

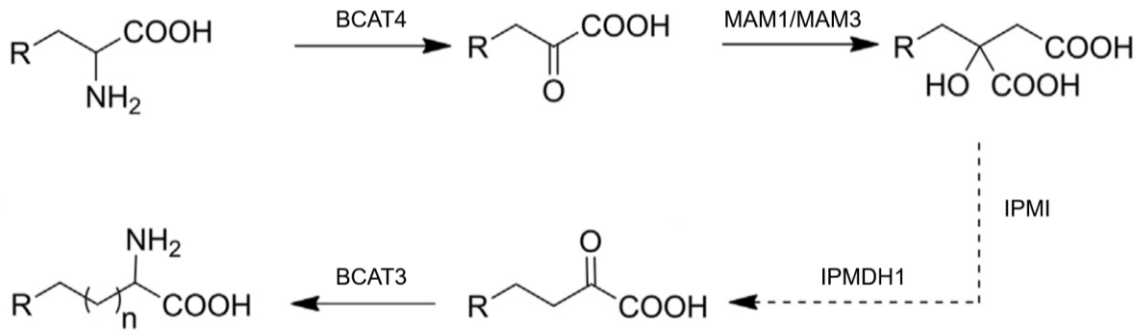

Fig. 1.5. Simplified scheme of Met chain elongation during GL biosynthesis.

In the core GL structure biosynthesis, which occurs during 2nd phase, elongated Met and modified Phe or Tyr are converted into corresponding aldoximes by CYP79F and CYP79A isoforms, respectively. Trp is converted by redundant CYP79B2 and

CYP79B3. The resulting aldoximes are then oxidized to reactive intermediates - *aci*-nitro compounds by CYP83 enzymes, CYP83B1 acts on indolic and benzyl aldoximes, while CYP83A1 metabolizes aliphatic ones (Fig. 1.6) (Bak and Feyereisen, 2001; Denekamp and Smeekens, 2003).

Following oxidation of the aldoximes, the resulting *aci*-nitro intermediates are poised for conjugation with glutathione (GSH) as the sulfur donor (Jensen et al., 2014). The reaction results in the formation of *S*-alkylthiohydroximates, intermediates whose production is crucial for subsequent GL core assembly. The next step involves the cleavage of the γ-glutamyl residue from the GSH conjugated by redundant γ-glutamyl peptidases (GGP1 and GGP3), thereby converting the GSH conjugate into a thiohydroximate (Geu-Flores et al., 2011). This processing is essential because the free amino group present in the thiohydroximate is required for the activity of the subsequent enzyme in the pathway, the C–*S* lyase SUR1 (Superroot1), which catalyzes the removal of the remaining peptide portion. The liberated thiohydroximate is then glycosylated by a UDP-glucose-dependent glycosyltransferases (UGT74B1 and UGT74C1) to yield a desulfoglucosinolate. In the final step, specific sulfotransferases (SOT16, SOT17, and SOT18) utilize 3′-phosphoadenosine-5′-phosphosulfate to sulfate the desulfoglucosinolate, resulting in the mature GL structure (Grubb et al., 2014).

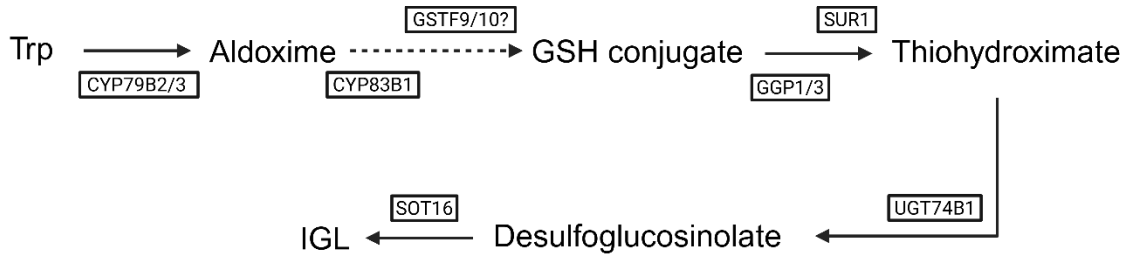

Fig. 1.6. Simplified scheme of core IGL structure biosynthesis.

In IGL biosynthesis, the 3rd phase (GL core-structure tailoring) involves the CYP81F sub-family enzymes that introduce hydroxyl groups at the N-1 and C-4 positions of the indole core. There are four CYP81F enzymes in *A. thaliana*. CYP81F4 provides the root-centric *N*-hydroxy gateway and mediates introduction of OH group at N-1. CYP81F2 is the primary 4-hydroxylase (Bednarek et al., 2009; Pfalz et al., 2009). CYP81F3 is another 4-hydroxylase while CYP81F1 retains the catalytic capacity for both reactions, but under normal growth contributes marginally to IGL modification (Pfalz et al., 2011). 4-hydroxy-I3G (4OHI3G) can be further *O*-methylated by IGL *O*-

methyltransferases 1-4 (IGMT1-4) to yield 4-methoxy-I3G (4MI3G). In parallel, the 1-hydroxy intermediate is methylated by IGMT5 (Pfalz et al., 2016) to form 1-methoxy-I3G (1MI3G), which accumulates mainly in roots (Pfalz et al., 2011).

Late-tailoring reactions also diversify the AGLs, a flavin-dependent glucosinolate *S*-oxygenase (FMO; GSOX1), converts methyl-thioalkyl side-chains into their methyl-sulfinyl counterparts, while the 2-oxoglutarate-dependent dioxygenases AOP2 and AOP3 (2-oxoglutarate-dependent oxygenase) desaturate or hydroxylate those chains to yield alkenyl- and hydroxyalkyl-GSLs, respectively (Lambrix et al., 2001; Hansen et al., 2007). For the benzoyloxy branch of AGLs, the peroxisomal benzoyl-CoA ligase supplies the benzoyl-CoA starter, but the acyl-transferase that actually transfers the benzoyl group to the glucosinolate scaffold has not yet been identified (Kliebenstein et al., 2007).

1.4.2. Glucosinolate hydrolysis

GLs molecules are chemically stable and intrinsically inert, to fulfill their physiological roles, they must first be activated by hydrolysis mediated by myrosinases (β-thioglucoside glucohydrolases; TGGs) (Fig. 1.7) (Halkier and Gershenzon, 2006; Somssich et al., 2025). GLs are cleaved to unstable aglycones that are subsequently converted into a range of bio-active end-products, including nitriles, epithionitriles, oxazolidine-2-thione, thiocyanates and ITCs (Fahey et al., 2001; Wittstock et al., 2016). The exact breakdown product formed depends on the GL side-chain, the reaction conditions and the presence of so-called epithiospecifier proteins (ESP) (Lambrix et al., 2001; Wittstock and Burow, 2010). For instance, low pH, iron ions and ESP favor nitrile formation, whereas in the absence of ESP the reaction typically yields ITCs (Lambrix et al., 2001).

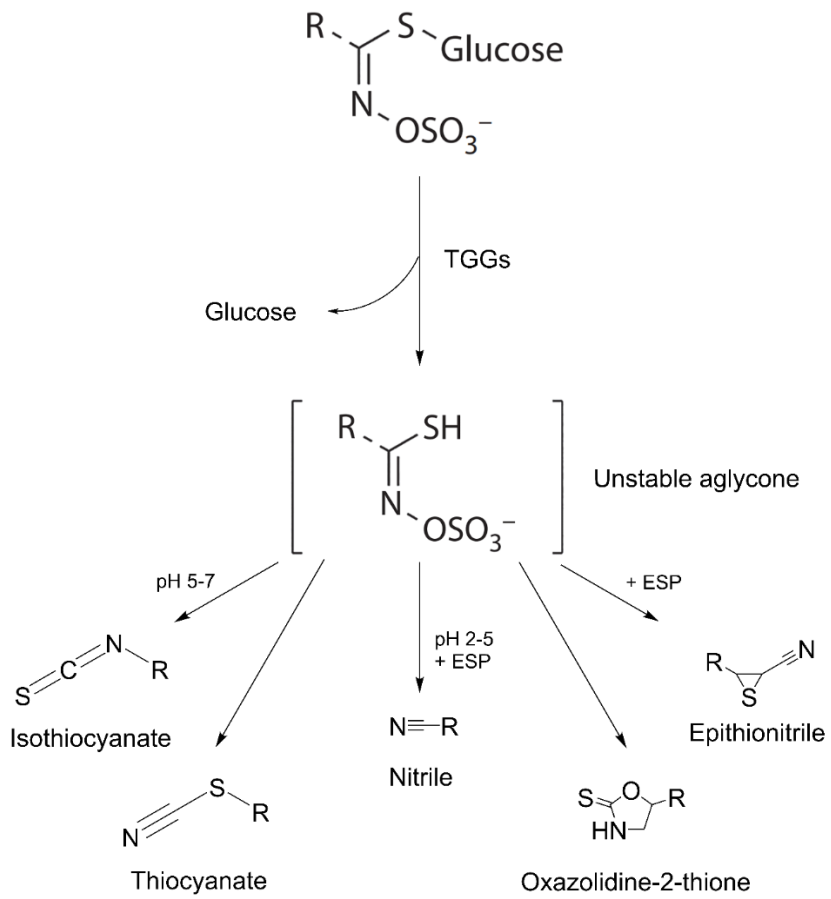

Fig. 1.7. Simplified scheme of glucosinolate hydrolysis. Only the most commonly formed products are shown. ESP – epithiospecifier proteins.

Under normal physiological conditions, GLs are spatially separated from myrosinases at the cellular or sub-cellular level, so degradation is not constitutive. Enzyme-substrate contact occurs only when tissue integrity is compromised (e.g. by wounding) or under stress conditions, triggering hydrolysis as a defense response (Wittstock and Burow, 2010).

Myrosinases of Brassicaceae plants belong to two phylogenetic clades. The QE-type clade (TGG1-TGG6) carries a glutamine in one of the two catalytic sites (Andersson et al., 2009), whereas the EE-type clade - including PEN2 (Penetration2), PYK10, BGLU21 and BGLU18 - have the glutamine residue replaced by glutamic acid (Bednarek et al., 2009; Nakano et al., 2017). Many myrosinases show clear organ and sub-cellular specificity. For example, in *A. thaliana*, TGG1 and TGG2 are leaf enzymes, whereas TGG4 and TGG5 are characteristic of roots (Andersson et al., 2009). PYK10 and BGLU21 are localized to endoplasmic-reticulum (ER) bodies in cotyledons and roots; BGLU18 occurs in ER bodies of leaves and PEN2 is found mainly anchored in the

membranes of peroxisomes and mitochondria of leaf and root cells (Yamada et al., 2011; Fuchs et al., 2016; Nakano et al., 2017).

1.4.3. Biological activity of GL-derived products.

Among the GLs hydrolysis products, simple nitriles are generally the least reactive, whereas ITCs exhibit the highest toxicity toward most organisms (Hanschen et al., 2014). However, biological effects are dose-dependent, so even nitriles or epithionitriles can be highly toxic to livestock (Tripathi and Mishra, 2007). It has also been shown that GLs-derived nitriles can enhance the accumulation of defense-related phytohormones SA, JA and abscisic acid in *A. thaliana* (Ting et al., 2020). Because of both their toxic and signaling activities, which are activated upon tissue damage or pathogen recognition, GLs have long been considered a key element of Brassicaceae defense against herbivorous insects and pathogenic microbes (Hopkins et al., 2009; Wittstock and Burow, 2010). Respective studies indicated that AGLs and corresponding ITCs confer protection primarily against leaf-chewing herbivores (Hopkins et al., 2009). IGLs and their breakdown products deter piercing–sucking insects that feed from the phloem (Kim and Jander, 2007); whereas benzyl GLs and their isothiocyanates contribute to resistance against plant-parasitic nematodes (Zasada and Ferris, 2003; Schroeder and Macguidwin, 2010).

Research has also demonstrated that, beyond defense functions, GLs are active in responses to abiotic stress and influence other physiological processes. For example, they mediate stomatal opening in leaves (Ahuja et al., 2016), regulate root hydraulic conductivity under salt stress (Martínez-Ballesta et al., 2014), and IGLs turnover intermediates contribute to auxin biosynthesis (Sugawara et al., 2009). Taken together, the constitutive presence and structural diversity of GLs in plant tissues appear essential for providing Brassicaceae species with effective resistance towards diverse pests and tolerance of various abiotic stresses.

1.4.4. Role of IGLs and PEN2 pathway in pre-invasive immunity

Brassicaceae species deploy a pre-invasive chemical barrier, which controls entry of filamentous pathogens into plant tissue and is largely mediated by IGLs and the PEN2 myrosinase. Unlike the classical “mustard oil bomb” (where GLs are stored in specialized

cells and activated upon tissue damage), this pathway is rapidly triggered, likely by PTI, in intact living cells (Bednarek et al., 2009; Clay et al., 2009). Upon pathogen recognition, mitochondria-associated fraction of PEN2 re-localizes in attacked epidermal cells to the pathogen contact sites where it catalyzes IGL hydrolysis to chemically unstable indol-3-ylmethyl-ITCs (I3M-ITCs) (Fig. 1.8) (Bednarek et al., 2009; Fuchs et al., 2016). These compounds are promptly conjugated with GSH by glutathione *S*-transferase U13 (GSTU13) to form corresponding GS-ITCs adducts known as GS-I3M-dithiocarbamates (GS-I3M-DTCs) (Piślewska-Bednarek et al., 2018). In the next step, an unknown γ-glutamyl peptidase is needed to remove the γ-Glu moiety to produce Cys-Gly-I3M-DTCs, in theory it could be GGP1/3, but the involvement of these enzymes remains unproven. Another peptidase likely excises Gly to produce Cys-I3M-DTCs, but the identity of this enzyme remains vague. Candidates include cysteinylglycine peptidase 1 and phytochelatin synthase 1 (PCS1), as both possess the required enzymatic activity (Hématy et al., 2020; Miyaji et al., 2024). Indol-3-ylmethyl GL (I3G)-derived Cys-I3M-DTC is further processed to indole-3-ylmethylamine (I3A) and raphanusamic acid (RA) that accumulate upon pathogen infection in PEN2-competent plants. (Bednarek et al., 2009). In addition to activation of PEN2, pathogen recognition activates CYP81F2, specifically in the attacked epidermal cells to hydroxylate I3G at the position C-4, which then serves as the substrate for PEN2 (Bednarek et al., 2009; Fuchs et al., 2016). Strikingly, Cys-I3M-DTC conjugate derived from the IG substituted at the position 4 (4MI3G or 4OHI3G) undergo a different conversion yielding 4-*O*-β-glucosyl-indol-3-yl formamide (4OGlcI3F) as detectable end product (Fig. 1.8) (Lu et al., 2015).

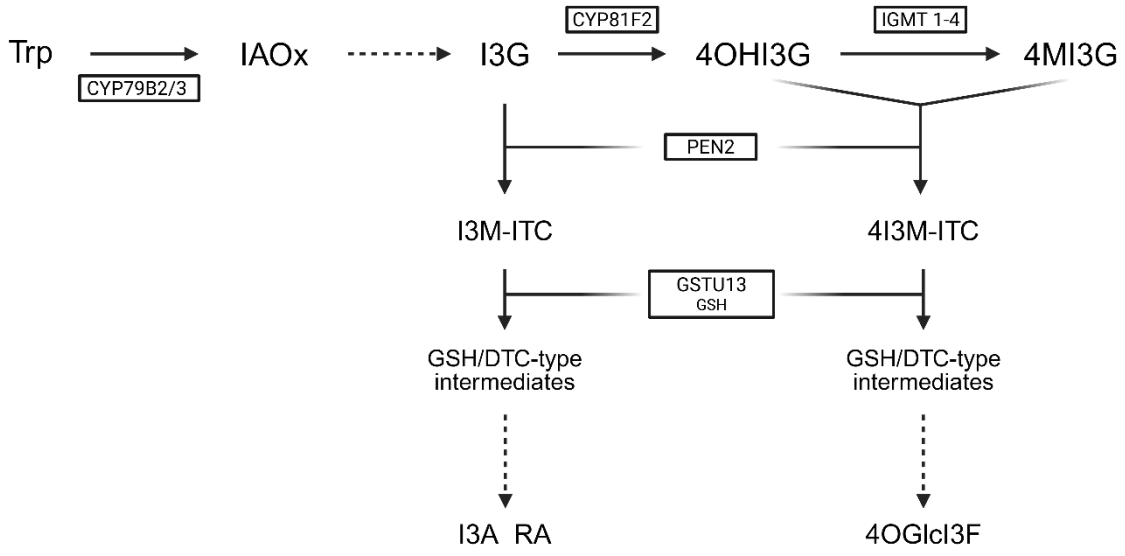

Fig. 1.8. Simplified scheme of PEN2-mediated IGL hydrolysis.

In accordance with the proposed metabolic pathway, null alleles of *PEN2*, *CYP81F2*, *GSTU13* and *PCS1* reveal greatly reduced accumulation of respective IGL derived metabolites (Fig. 1.8). Moreover, it has been shown that mutations in these genes lead to enhanced penetration into epidermal cells of a broad range of filamentous pathogens including necrotrophic, biotrophic and hemibiotrophic fungi (Hiruma et al., 2010; Schlaeppi et al., 2010; Pastorczyk and Bednarek, 2016; Piślewska-Bednarek et al., 2018; Hématy et al., 2020). This defect is particularly striking for non-adapted pathogens that are inefficient or even completely disabled in penetrating into epidermal cells of wild-type (WT) Arabidopsis plants. Moreover, infection phenotypes of *pen2* and *cyp81f2* single and double mutants indicated that only PEN2-mediated hydrolysis of 4OH- and/or 4MI3G is critical for immunity while hydrolysis of I3G is dispensable to control fungal penetration (Bednarek 2009). Importantly, despite enhancing pathogen entry rates, defects in the PEN2 pathway components do not support further colonization of plant tissue (Bednarek et al., 2009; Pastorczyk et al., 2020). For these reasons, CYP81F2/PEN2-mediated IGL metabolism is considered a component of the pre-invasive resistance, which specifically prevents penetration of non-adapted filamentous pathogens into epidermal cells.

1.5. Camalexin and brassinin as representatives of Brassicaceae phytoalexins

1.5.1. Camalexin and its derivatives

Camalexin is the key phytoalexin in *A. thaliana*. This compound is 3-thiazol-2-yl-indole, a bicyclic aromatic system consisting of an indole ring covalently linked to a thiazole ring, a five-atom heterocycle containing both sulfur and nitrogen (Pedras et al., 2011). Importantly, camalexin production is not unique to *A. thaliana*, other members of the Camelinae tribe (*Arabidopsis lyrata, Arabidopsis helleri, C. sativa*, *Capsella bursa-pastoris, Capsella rubella, Olimarabidopsis pumila, Olimarabidopsis cabulica* and *Neslia paniculata*) also synthesize this compound (Bednarek et al., 2011; Pedras et al., 2011; Pedras and Alavi, 2020).

Collectively, Camelinae plants produce several camalexin derivatives that expand the chemical space of this defensive metabolic branch. These modifications encompass

hydroxylation and subsequent *O*-methylation (6-methoxy-; 7-methoxy, dimethoxy-camalexin) or *O*-glycosylation (hydroxy-camalexin hexosides) (Böttcher et al., 2009; Pedras and Alavi, 2020). Methoxy-camalexin (MCX) was first detected in *C. sativa* leaves following infection by the fungus *A. brassicae* (Browne et al., 1991). Later on, it was detected in *C. bursa-pastoris* challenged by the same pathogen, moreover, the exact position of substitution at C-6 was identified (Jimenez et al., 2005). A comparative survey of Camelineae species revealed the presence of the same camalexin derivative in *N. paniculata, C. rubella* and *Olimarabidopsis* spp. while tested *Arabidopsis* spp. have not been shown to accumulate this metabolite (Bednarek et al., 2011). However, two hexose conjugates of hydroxy-camalexin (HCX-Hex) together with an acylated derivative of one of those (HCX-Hex-Mal) have been detected at low levels in *A. thaliana* leaves infected with *Phytophthora infestans* or treated with silver nitrate or silver nanoparticles (Böttcher et al., 2009; Kruszka et al., 2020). It has been noted that for these hexosides the position of the substituent on the indole ring could not be determined by mass spectrometry, so the assumed 6-*O* linkage remains unproven (Böttcher et al., 2009). HCX-Hex and HCX-Hex-Mal appear together, transiently, when the parent camalexin pathway is strongly induced, and every report of them to date comes from *A. thaliana* - no other camalexin producing plant species has yet been analyzed for the accumulation of these conjugates (Böttcher et al., 2009; Kruszka et al., 2020).

1.5.1.1. Camalexin biosynthetic pathway. Camalexin biosynthesis (Fig. 1.9) starts with the enzymatic oxidation of tryptophan to indole-3-acetaldoxime (IAOx) by CYP79B2 and CYP79B3 enzymes, which is shared with IGLs biosynthesis.

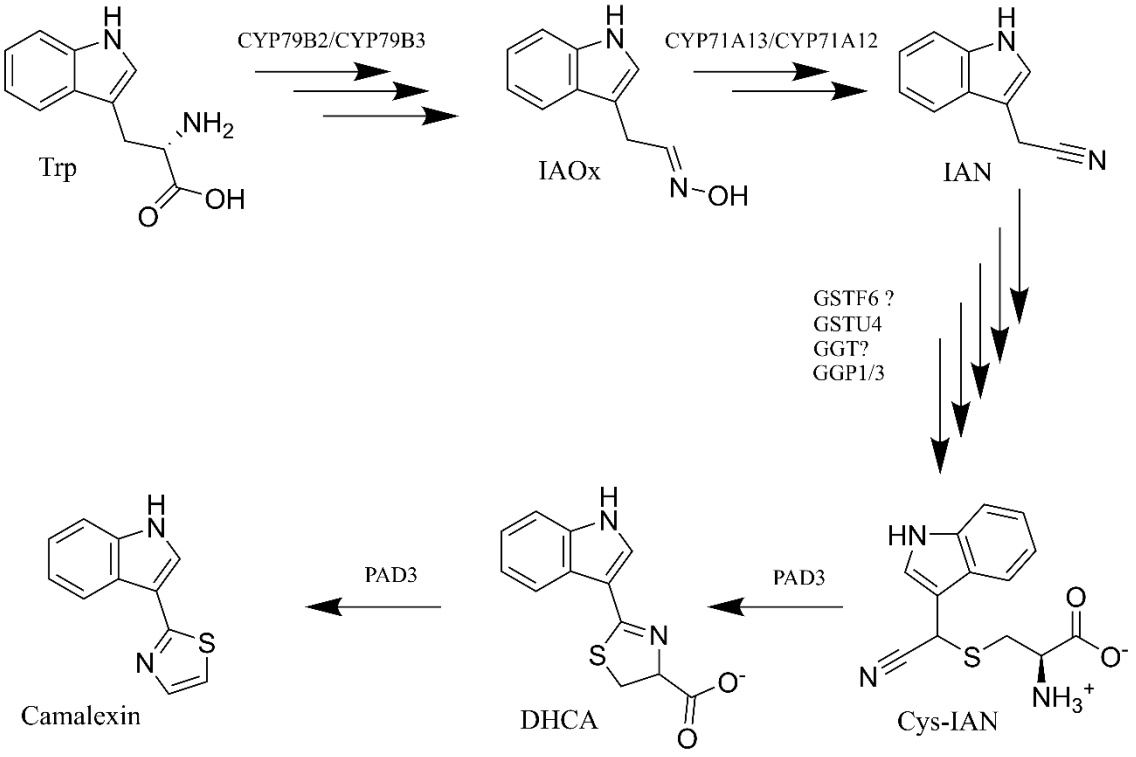

Fig. 1.9. Camalexin biosynthesis from tryptophan in *A. thaliana*.

In the camalexin-specific pathway, IAOx is further processed by two redundant cytochrome P450 enzymes CYP71A13 and CYP71A12, which catalyze the oxidative decarboxylation of IAOx to yield indole-3-acetonitrile (IAN) (Nafisi et al., 2007; Møldrup et al., 2013; Müller et al., 2015). This step is essential for diverting the metabolite from IGL biosynthesis into the production of camalexin (Glawischnig, 2006). IAN is conjugated with GSH to form GSH-IAN conjugate (GS-IAN). This reaction is partially catalyzed by GSTF6 (glutathione *S*-transferase F6) (Su et al., 2011). GS-IAN is further processed by GGP1 and GGP3, which remove the γ-glutamyl residue to produce Cys-Gly-IAN (Geu-Flores et al., 2011). The subsequent conversion of Cys-Gly-IAN to Cys-IAN likely requires removal of Gly by a Cys-Gly dipeptidase; CGP1 is a plausible candidate for this step, although its role in camalexin biosynthesis has not yet been demonstrated directly (Su et al., 2011; Miyaji et al., 2024). This compound is then metabolized by CYP71B15 (PAD3; Phytoalexin deficient 3) to obtain dihydrocamalexic acid (DHCA). The role of PAD3 is to catalyze the oxidative cyclization of the dipeptide intermediate to form the thiazole ring, however, this reaction can proceed also in a non-enzymatic way (Glawischnig, 2007). The final step in the pathway is oxidation of DHCA to camalexin, also catalyzed by PAD3. This reaction completes the thiazole ring structure and confers bioactive properties (Schuhegger et al., 2006). It has been hypothesized that

on the pathway leading to its derivatives, camalexin is first converted to HCX by an unknown oxidase and this intermediate is immediately methylated or hexose-conjugated (Böttcher et al., 2009).

Recent investigations have markedly refined our mechanistic understanding of the camalexin biosynthetic cascade. Notably, convergent evidence supports the existence of a dedicated biosynthetic metabolon - a spatially controlled supramolecular assembly comprising cytochrome P450 isoforms CYP79B2/B3, CYP71A13, and PAD3 - that facilitates highly efficient substrate channeling while concurrently attenuating the diffusion and deleterious loss of reactive intermediates under stress-induced conditions. This enzyme complex is hypothesized to be strategically assembled in the immediate microenvironment of pathogen ingress, thereby ensuring a rapid, localized accrual of camalexin that reinforces the plants defensive capacity (Mucha et al., 2019).

1.5.1.2. Metabolic engineering of camalexin pathway. Building directly on the biosynthetic genetic insights, Møldrup et al. re-assembled the entire camalexin pathway in *Nicotiana benthamiana*. To this end, they applied transient co-expression of *CYP79B2/3, CYP71A13, GGP1,* and *CYP71B15* yielding 10–35 µg camalexin per g of fresh weight, a concentration comparable to strongly elicited Arabidopsis leaves. With these experiments, it has been confirmed that co-expression of CYP79B2/3, *CYP71A13*, *GGP1* and *CYP71B15* is sufficient to produce camalexin in a non-Brassicaceae host, provided that endogenous host activities support the GSH-conjugation step and the remaining intermediate processing reactions (Møldrup et al., 2013).

1.5.1.3. Camalexin in post-invasive resistance. Investigation of camalexin function has been strongly supported with availability of *pad3* single and *cyp71a12 cyp71a13* double mutants deficient in biosynthesis of this phytoalexin (Fig. 1.10). Pathogen assays with these mutant lines indicated that, unlike IGLs, CYP81F2 and PEN2, camalexin does not contribute to the control of pathogen entry rates. Interestingly, multiple mutants combining defects in PEN2 pathway and in camalexin biosynthesis (e.g. *pen2 pad3* and *pen2 cyp71a12 cyp71a13*) revealed enhanced susceptibility as compared with respective single mutant plants. Detailed investigation of infection phenotypes observed in these mutants possess defects not only in pre-invasive defense, but also in controlling further pathogen spread from initially penetrated epidermal cells into the mesophyll layer (Bednarek et al., 2009; Pastorczyk et al., 2020). Similar enhanced susceptibility was observed in *cyp79b2 cyp79b3* double mutant that is defective in production of all Trp-derived SMs (Bednarek et al., 2009; Schlaeppi et al., 2010; Hiruma

et al., 2013; Frerigmann et al., 2016; Pastorczyk et al., 2020). Overall, these studies indicated that camalexin is involved in post-invasive resistance towards controlling the spread of filamentous pathogens from initially penetrated epidermal into further plant tissue. According to this proposed function, live-cell imaging of Arabidopsis lines expressing fluorophore-tagged PAD3 protein showed that this enzyme is anchored to cortical ER strands that traverse mesophyll cells and accumulate directly beneath fungal contact sites. Co-immunoprecipitation combined with proteomics as well as FRET-FLIM assays revealed that PAD3 with CYP71A13 and its partially redundant paralogue CYP71A12 form a metabolon on these mesophyll-localized ER domains (Mucha et al., 2019). The mesoscale localization of PAD3/CYP71A13 contrasts with peroxisome-anchored PEN2 in the epidermis, but both systems converge at the cell periphery, jointly forming a multilayer defensive chemical barrier (Fig. 1.10). Despite this clear evidence for specific contributions of IGLs and camalexin, it remains still not known if their functions in pre- and post-invasive resistance are dependent on the timing and localization of their biosynthesis or/and on their unique chemical and biological activities.

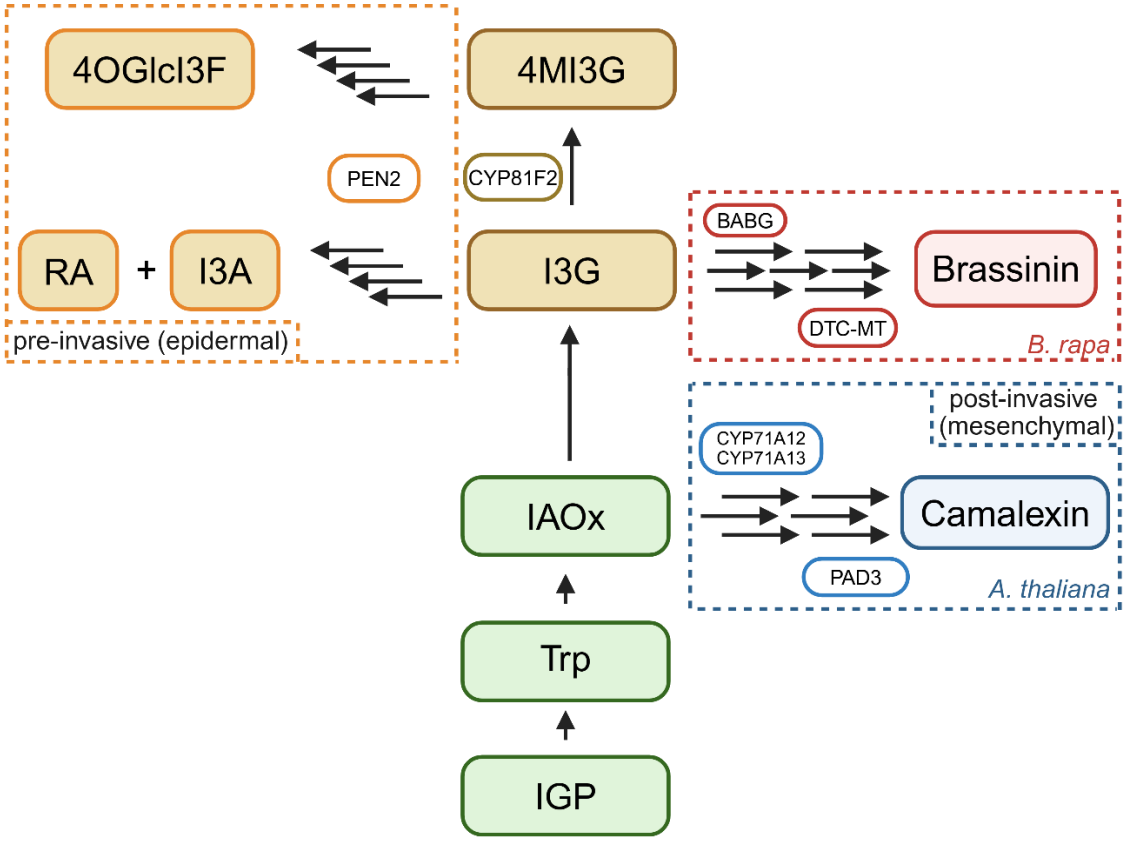

Fig. 1.10. Biosynthetic divergence of Trp-derived metabolites and their specific roles in pre- and post-invasive resistance.

1.5.2. Brassinin

Brassinin is methyl *N*-(1H-indol-3-ylmethyl)-DTC, an achiral indole-derivative whose DTC tail provides the high-sulfur reactivity and soft-ligand character that confer both its antimicrobial/IDO-inhibitory activity and its role as the direct biosynthetic progenitor of cyclobrassinin, spirobrassinin and brassilexin (Pedras et al., 2006; Klein and Sattely, 2017).

1.5.2.1. Brassinin biosynthetic pathway. Brassinin originates from Trp and its biosynthesis diverges from the IGL pathway (Fig. 1.11). The direct precursor of this phytoalexin is I3G, at this branch point, the redundant β-thioglucosidases BABG.a (brassinin-associated β-glucosidase a) and BABG.b hydrolyze I3G, releasing the short-lived I3M-ITC (Klein and Sattely, 2017). This intermediate is bonded with reduced GSH to give the GS-I3M-DTC adduct. Currently, it is not clear if this reaction is spontaneous or supported by enzymatic GST activity. The GSH adduct is then channeled through unknown peptidases, supposedly GGP1/3, to remove the γ-Glu residue. The resulting Cys-I3M-DTC becomes the substrate for SUR1, the same enzyme that acts in IGL biosynthesis, which excises the entire cysteine scaffold to yield free I3M-DTC (Klein and Sattely, 2017).

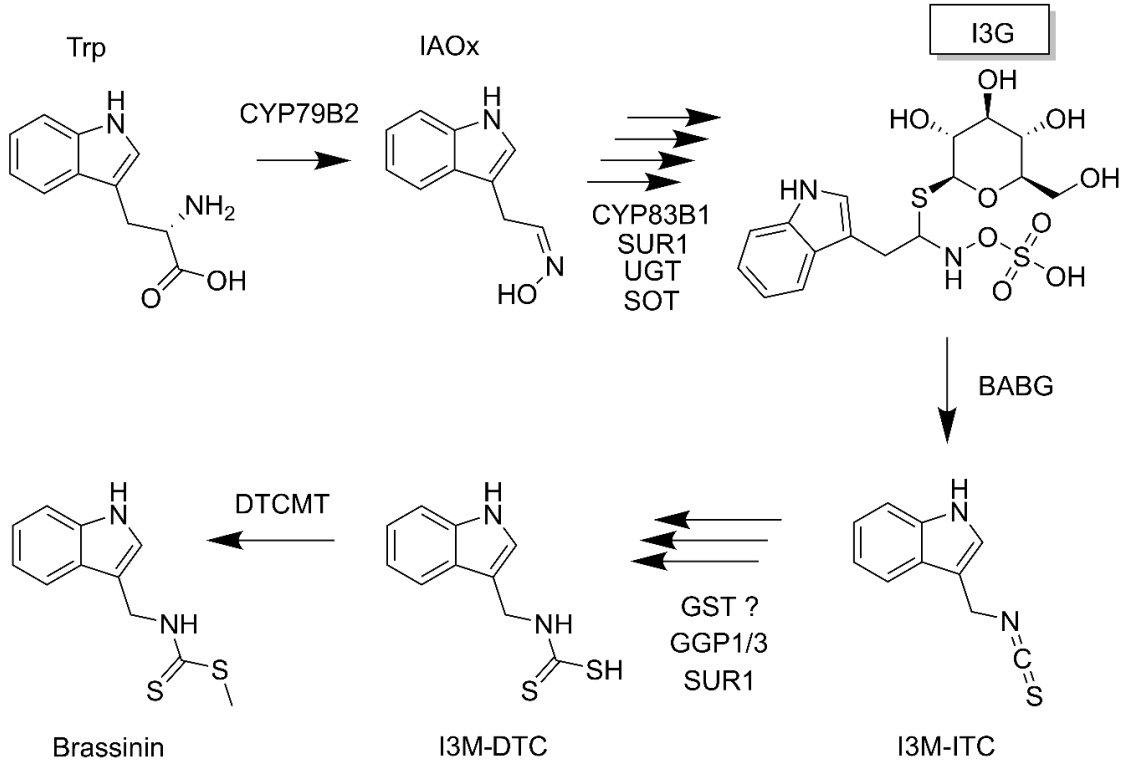

Fig. 1.11. Brassinin biosynthesis from Trp in *B. rapa*.

Finally, dithiocarbamate *S*-methyltransferase (DTC-MT) uses *S*-adenosyl-L-methionine to methylate the sulfhydryl of I3M-DTC, converting this intermediate into its *S*-methyl ester. This single-step can both stabilizes the molecule and completes the pharmacophore that supports brassinin antifungal activity (Pedras et al., 2004; Klein and Sattely, 2017). The route from I3G to I3M-DTC parallels partially the PEN2 metabolic branch starting with a myrosinase (BABG) that hydrolyses I3G, followed by GSH capture. The later steps parallel a portion of the core GL biosynthetic pathway, involving GGP1/3-mediated peptide trimming and the involvement of SUR1(Bednarek et al., 2009; Klein and Sattely, 2017).

After the synthesis of brassinin, downstream modifications can result in the formation of spirobrassinin and cyclobrassinin. These transformations are catalyzed by two cytochrome P450 enzymes, CYP71CR1 and CYP71CR2, which have been identified and studied in *Brassica rapa* (Klein and Sattely, 2015). The conversion of brassinin to spirobrassinin includes the reaction of oxidative cyclization guided by CYP71CR1. The enzyme introduces a spirocyclic structure by forming a five-membered lactam ring. The cyclization to spirobrassinin is suggested to provide additional stability and resistance towards enzymatic degradation by pathogens (Klein and Sattely, 2015). CYP71CR2 catalyzes the production of cyclobrassinin, another brassinin derivative. Cyclobrassinin is formed by a fused, rigid bicyclic structure formed via oxidative closure of the indole and DTC moieties. Its structural rigidity may influence its interaction with microbial enzymes and its antifungal properties, though further research is needed to confirm its exact mechanism of action. Studies on structurally similar antifungal compounds suggest that molecular rigidity and sulfur reactivity can play key roles in enzyme interactions and bioactivity (Pedras et al., 2014).

The accumulation of downstream indole phytoalexins highlights the plasticity of chemical defenses in *Brassica* spp., cyclobrassinin outperforms its precursor *in vitro* assays with *B. cinerea* and still inhibits pathogens such as *S. sclerotiorum* (Pedras et al., 2004; Pedras and Yaya, 2010). Spirobrassinin, by contrast, shows lower antifungal activity and no study has demonstrated superior potency (Pedras et al., 2006).

1.5.2.2. Engineering the brassinin pathway. A study on brassinin engineering in a non-GL plant species, *N. benthamiana*, revealed the minimal set of enzymes required for biosynthesis of this phytoalexin. First of all, eight *B. rapa* genes (*CYP79B2, CYP83B1, GSTF9, GGP1, SUR1, UGT74B1, SOT16* and adenosine-5′-phosphosulfate

(APS) kinase 1 (*APK1*)) were transiently expressed in *N. benthamiana*, driving *de novo* accumulation of I3G. Co-expression of genes encoding selected myrosinases, either TGG4 or one of the *Brassica*-specific BABG.a/b, led to hydrolysis of this IGL in intact cells initiating I3M-DTC formation. Addition of DTC-MT.a converted this intermediate into brassinin. When DTC-MT was omitted, the DTC was efficiently glycosylated by endogenous *N. benthamiana* UGTs. With BABG and DTC-MT on top of the IGL module, tobacco leaves accumulated ~400 pmol/mg DW brassinin - levels comparable to elicited *Brassica* tissue. Further channeling to spirobrassinin or cyclobrassinin was achieved by appending *CYP71CR1* or *CYP71CR2*, respectively (Klein et al., 2013; Klein and Sattely, 2015, 2017). Overall, the reconstitution in tobacco confirmed that processing of the GS-I3M-DTC intermediate involves the same GSH-processing machinery as IGL biosynthesis. This in turn indicates that in I3G-producing species minimal pair of BABG and DTC-MT should be sufficient to create brassinin biosynthesis.

1.5.2.3. Immune functions of brassinin. Existing evidence supports brassinin primarily as a locally induced defense metabolite produced in response to infection with numerous pathogens (Pedras et al., 2011; Pedras and Abdoli, 2017). For instance, challenge with *L. maculans* elicits brassinin accumulation in resistant *B. juncea* and *B. napus* cultivars within 24 h, coincident with HR-like lesions (Rouxel et al., 1991). Moreover, flg22 and chitin treatments of *B. rapa* leaves rapidly induce *BABG* and *DTC-MT* transcripts within 30–180 min, indicating that pattern-triggered immunity controls brassinin biosynthesis (Kim et al., 2020).

Based on its antibiotic properties, it has been proposed that brassinin is toxic to many microbial pests. For instance, this phytoalexin displays an $EC_{50} \approx 81$ μM against germ-tube elongation of *A. brassicicola* (Sellam et al., 2007) and impairs mitochondrial respiration, provoking oxidative and lipid-membrane stress in the fungus (N'Guyen et al., 2021). Although its dedicated exporter has not been identified, brassinin and downstream indole-sulfur phytoalexins are recoverable from intercellular (extracellular) fluids of infected cotyledons, showing that the compound accumulates outside living cells rather than being conclusively secreted into the apoplast (Dahiya and Rimmer, 1988).

Brassinin-derived phytoalexins such as brassilexin and cyclobrassinin surge within 12-48 h after infection by avirulent *L. maculans* isolates in *B. juncea* and *B. napus*, temporally coinciding with HR lesions (Rouxel et al., 1991). The ability to accumulate high levels of these phytoalexins correlates genetically with HR resistance across *Brassica* accessions (Rouxel et al., 1991). However, despite these findings on its

antimicrobial properties and correlations between brassinin accumulation and resistance the function of brassinin has been not specifically assigned to pre- or post-invasive resistance. The main reason for this is lack of *Brassica* mutants (e.g. *babg*) specifically deficient in biosynthesis of this phytoalexin.

OBJECTIVES

The primary objective of this doctoral thesis is to elucidate the roles of tryptophan-derived specialized metabolites, specifically the indole phytoalexins, camalexin and brassinin, in the immune responses of Brassicaceae plants. While camalexin is established in restricting post-invasive pathogen growth, the precise function and spatiotemporal action of brassinin remain unclear. We hypothesize that the immune functions of these metabolites are determined by their unique spatial and temporal production patterns rather than solely by their inherent chemical properties.

To test this hypothesis, we will re-engineer camalexin and brassinin biosynthesis in *pen2 cyp71a12 cyp71a13* Arabidopsis background. We will place respective genes under the control of epidermis-active promoters (*PEN2, CYP81F2*) so that metabolite production is confined to cells at the pathogen entry site. Generated transgenic lines will be assayed for transgene expression and metabolite production, including all pathway intermediates and possible side products**.** Finally, selected transgenic lines will be challenged with a fungal pathogen to determine whether re-localized phytoalexin synthesis enhances immunity.

Expected outcome: This research will provide valuable insights into the mechanisms by which indole phytoalexins contribute to plant immunity. Understanding these mechanisms could inform future crop protection strategies, including the genetic engineering of plants with optimized secondary metabolite profiles for improved disease resistance.

MATERIAL AND METHODS

3.1. List of reagents used

Enzymes:

- DNase I free of RNases (Qiagen, Germany)
- Restriction enzymes AscI, SbfI, EcoRI, AsiSI, KasI, NotI (New England Biolabs, USA)
- RNase inhibitor RNasin Plus RNase Inhibitor (Promega, USA)
- T4 DNA Ligase (Promega, USA)
- GoTaq DNA Polymerase (Promega, USA)
- PfuTurbo Hotstart DNA Polymerase (Agilent, USA)
- Phusion High-Fidelity DNA Polymerase (Thermo Scientific, USA)

Nucleic Acid Working Kits:

- DNA Clean & Concentrator Kit (Zymo Research, USA); kit for purifying PCR reaction products from the reaction mixture
- iTaq Universal SYBR Green Supermix (Bio-Rad, USA); kit for performing quantitative PCR with reverse transcription
- Omniscript RT Kit (Qiagen, Germany); kit for reverse transcription
- RNeasy Plant Mini Kit (Qiagen, Germany); kit for isolating total RNA from plant tissues
- Zymoclean Gel DNA Recovery Kit (Zymo Research, USA); kit for purifying DNA fragments from agarose gel after electrophoresis
- Zyppy Plasmid Miniprep Kit (Zymo Research, USA); kit for isolating plasmids from bacterial suspensions
- GeneArt™ Seamless Cloning and Assembly Kit (New England Biolabs, USA)
- EurX Plant and Fungi DNA Extraction Kit (EURx, Poland); kit for isolating genomic DNA from plants and fungal pathogen

Antibiotics:

- Ampicillin (BioShop, Canada)
- Kanamycin (BioShop, Canada)

- Carbenicillin (BioShop, Canada)
- Rifampicin (BioShop, Canada)

Solvents and reagents:

- Acetonitrile, LC-MS grade (VWR, USA)
- Agar (BioShop, Canada)
- Agarose (BioShop, Canada)
- Glufosinate-ammonium (phosphinothricin ammonium) (Cayman Chemical Co)
- β-Mercaptoethanol (Sigma-Aldrich, Germany)
- Purple Gel Loading Dye Buffer (New England Biolabs, USA)
- Lysogeny Broth (LB) Miller (BioShop, Canada)
- Magnesium Chloride (Sigma-Aldrich, Germany)
- Deoxyribonucleotides dATP, dCTP, dGTP, dTTP (Promega, USA)
- Dimethyl Sulfoxide (DMSO) (BioShop, Canada)
- Sodium Dodecyl Sulfate (SDS) (VWR, USA)
- Yeast Extract (BioShop, Canada)
- Beef Extract (BioShop, Canada)
- Ethanol (Merck, Germany)
- Glycerol (Chempur, Poland)
- Isopropanol (VWR, USA)
- Formic Acid (Merck, Germany)
- Acetic Acid (POCH, Poland)
- Hydrochloric Acid (POCH, Poland)
- Wersen Acid, EDTA (BioShop, Canada)
- Peptone (BioShop, Canada)
- Murashige & Skoog Medium (Duchefa, Netherlands)
- Sucrose (Chempur, Poland)
- Silwet L-77 (PhytoTechnology Laboratories, USA)
- Oligo(dT) Primer (Genomed, Poland)
- SYBR Green Safe DNA Gel Stain (Invitrogen, USA)
- Tris(hydroxymethyl)aminomethane, Tris (BioShop, Canada)
- Sodium Hydroxide (POCH, Poland)

Analytical standards:

- Brassinin (Sigma-Aldrich, Germany)
- Camalexin (Synthetic standard)
- I3A (Synthetic standard (Bednarek et al., 2009))
- 4OGlcI3F (Synthetic standard (Lu et al., 2015))

Buffer and media recipes:

- Edwards Buffer (200 mM Tris/HCl pH 7.5; 250 mM NaCl; 25 mM EDTA; 0.5% SDS)
- Yeast Extract Beef Medium (YEB; 5 mg/ml beef extract, 1 mg/ml yeast extract, 5 mg/ml peptone, 5 mg/ml sucrose, and 0.5 mg/ml $MgCl_2$)

3.2. Plant material

Plant lines used in this study:

- *A. thaliana*, Columbia-0 ecotype (Col-0) (Nottingham Arabidopsis Stock Centre)
- *A. thaliana*, mutant line *pen2 cyp71a12 cyp71a13*, triple mutant (Pastorczyk et al., 2020)
- *A. thaliana,* double mutant *pen2-1 pad3* (Bednarek et al., 2009)
- *B. rapa*, rapid-cycling, flowering, ecotype FPsc (Nottingham Arabidopsis Stock Centre)

3.3. Experimental workflow

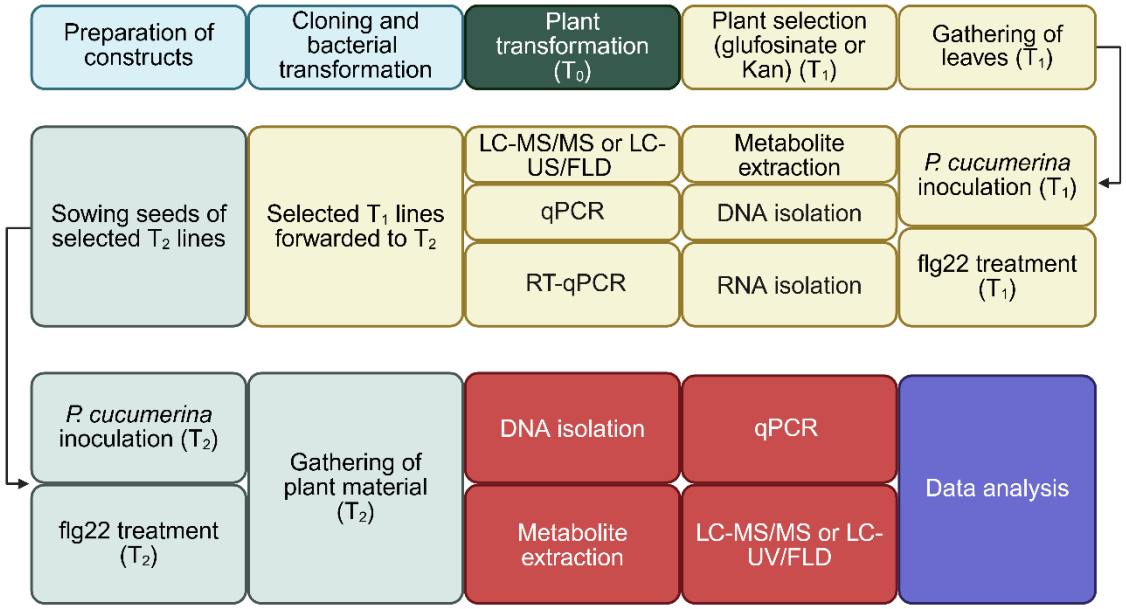

3.4. General methods for plant cultivation

A. thaliana seeds were cold-stratified (4°C, darkness) prior to sowing on soil (9 × 9 cm pots). Plants were cultivated in a growth chamber at 22°C and 60% relative humidity under short-day conditions (8 h light/16 h dark) with regular watering, consistent with standard short-day cultivation used for *A. thaliana* rosette growth in controlled conditions (Lu et al., 2015). Two-week-old seedlings were transplanted to 44 mm Jiffy-7 peat pellets (Jiffy Group, Norway) pre-moistened with 0.1% (v/v) Wuxal Universal fertilizer solution and grown for an additional 2–3 weeks. Plants intended for seed production or for transformation were transferred at the age of about 8 weeks to pots with soil and moved to long-day conditions (16 h light/8 h dark) and cultivated until maturity and flowering.

B. rapa plants were cultivated in the same phytotron program as *A. thaliana* (short day for vegetative growth; long day for flowering and seed set), long-day growth at approximately 22°C is consistent with standard controlled-environment cultivation of *B. rapa*.

3.5. Preparation of plasmids and bacterial strains for plant transformation

To generate transgenic lines of *A. thaliana*, we prepared genetic constructs containing the genes of interest with appropriate promoters in the binary vector pAMPAT (https://novoprolabs.com/vector/Vgmydooa) obtained from the Max Planck Institute for Plant Breeding Research (Cologne, Germany). We obtained the plasmid that already possessed *PEN2* promoter instead of the original 35S promoter. pAMPAT can be used for plant transformation using *Agrobacterium tumefaciens* bacteria and additionally contains sequences that allow its replication in *Escherichia coli*. Its sequence includes a gene encoding an enzyme conferring resistance towards two antibiotics: ampicillin (in *E. coli*) and carbenicillin (in *A. tumefaciens*), enabling the selection of bacteria after transformation with this vector. Additionally, it also contains a gene encoding a protein conferring resistance towards glufosinate ammonium herbicide, allowing for subsequent selection of transgenic plants after transformation.

pAMPAT plasmid was amplified in appropriate *E. coli* strains (*E. coli* NEB® 10-beta electrocompetent cells) and purified using the Zyppy Plasmid Miniprep Kit (Zymo Research, USA). The correctness of enzymatic digestion reactions and PCR reactions was verified by electrophoretic separation in a 1% agarose gel. PCR products were purified using the DNA Clean & Concentrator Kit (Zymo Research, USA). Products of enzymatic digestions were separated electrophoretically in a 1% agarose gel and then purified using the Zymoclean Gel DNA Recovery Kit (Zymo Research, USA).

3.5.1. Template genomic DNA isolation

Genomic DNA from *A. thaliana* and *B. rapa* was isolated from the leaves of approximately 4-week-old plants using a modified Edwards method. Approximately 50 mg of collected plant tissue was homogenized using mini pestles (Eppendorf, Germany) in 300 µl of Edwards buffer. The homogenized tissue was incubated for 10 minutes at 65°C while shaking at 500 rpm, followed by an additional 10-minute incubation on ice. In the next step, 200 µl of chloroform was added, the mixture was shaken to allow phase separation and centrifuged for 5 minutes at 4°C at 15,000 rpm. Subsequently, 200 µl of the supernatant was transferred to a clean tube, 200 µl of cold isopropanol was added,

mixed, and centrifuged as before. After centrifugation, the supernatant was poured off, leaving only the pellet, to which 500 µl of 70% ethanol was added, shaken, and centrifuged for 3 minutes at 4°C at 15,000 rpm. The ethanol wash and centrifugation were repeated, after which the supernatant was poured off, and the pellet was dried at room temperature until complete ethanol evaporation. The dried pellet was resuspended in 100 µl of sterile water. The purity and concentration of the isolated genomic DNA were verified using a NanoDrop spectrophotometer (Thermo Scientific, USA). Isolated DNA was used to amplify genes encoding enzymes selected for the reconstruction of camalexin and brassinin pathways (Tab. 3.1).

Tab. 3.1. List of genes selected for engineering camalexin and brassinin biosynthesis in *A. thaliana* and *B. rapa*.

	***A. thaliana* gene ID**	***B. rapa* gene ID**
CYP71A13	AT2G30770.1	
CYP71B15	AT3G26830.1	
BABG.a		Brara.D02695
DTC-MT.a		Brara.B01660
CYP71CR1		Bra005870
CYP71CR2		Bra009149

3.5.2. Constructs containing camalexin biosynthetic genes

A plasmid containing *PAD3* and *CYP71A13* genes under *PEN2* and *CYP81F2* promoters, respectively, was prepared. A separate plasmid variant containing only *CYP71A13* gene under *CYP81F2* promoter was also engineered for better understanding and evaluating the roles of introduced genes as parts of the complex camalexin biosynthesis pathway. To amplify the selected regions, respective primers have been used (Tab. 3.2) with Phusion polymerase (Thermo Fisher, USA). Amplification protocol is presented in Tab. 3.3.

Tab. 3.2. Primer sequences used for the amplification of selected fragments of *A. thaliana* genomic DNA.

Starter name	**Sequence (5'-3')**
Asis1PAD3EcoR1_For	ATGCGATCGCATGTCGGTTTTCCTCTGTTTCCTC
Asis1PAD3EcoR1_Rev	CGGAATTCTCACTTGTCGTCATCGTCTTTGTAGTCCA
PromCYP81F2AsisI_For	CTAGAGCGTGGTGAAGAACTTGAAAGAA
PromCYP81F2AsisI_Rev	TTGGCGCGCCACAATCTAGTCACACTAACTCACG
AsisICYP71a13KAS1_For	ATGCGATCGCCAAAACGTAATCCATTTTTTTTTC
AsisICYP71a13KAS1_Rev	ATGCGATCGCATGAGCAATATTCAAGAAATG
Kas1CYP83b1Asc1_For	TTGGCGCGCCACTAGTGCCGGCCTGCAGTCTAGAG
Kas1CYP83b1Asc1_Rev	GAGCGGCCGCCCGGTCACTGGATTTTGGTTTT

Classical restriction assembly was used for preparation of the constructs (Fig. 3.1), utilizing the restriction sites available in the backbone vector. Overall, to achieve the goal restriction enzymes AscI, AsiSI, KasI, EcoRI, and NotI (New England Biolabs, USA) were utilized. Ligation was performed using the enzyme T4 DNA Ligase (Promega, USA). The resulting reaction mixture, after incubation and enzyme deactivation, was used to transform *E. coli*.

Tab. 3.3. PCR program for the amplification of genomic DNA fragments.

Initial Denaturation	**98°C, 30 seconds**
Denaturation	98°C, 10 seconds per cycle
Annealing	65°C, 30 seconds per cycle
Extension	72°C, 30 seconds per kb of target
Final Extension	72°C, 5 minutes
Hold	4°C, ∞

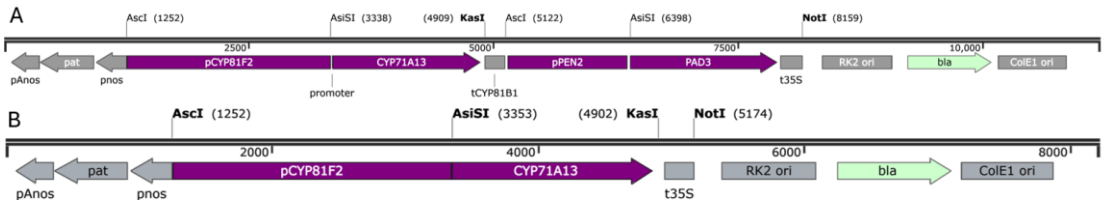

Fig. 3.1. Maps of the pAMPAT plasmid-based constructs; A, *CYP71A13* and *PAD3* gene under the *CYP81F2* and *PEN2* promoters respectively; B, *CYP71A13* gene under the *CYP81F2* gene promoter.

3.5.3. Constructs containing brassinin biosynthetic genes

A construct containing two genes involved in the brassinin biosynthetic pathway, *BABG* and *DTC-MT*, was engineered. To control the expression of the *BABG* gene, the *PEN2* promoter was used, while the native *CYP81F2* promoter was introduced for *DTC-MT* (Fig. 3.2).

Gibson assembly was used for preparation of this construct, utilizing GeneArt™ Seamless Cloning and Assembly Kit (New England Biolabs, USA). This method is a cloning technique that facilitates the joining of multiple DNA fragments without the need for restriction enzymes or traditional ligation methods. This method employs overlapping homologous sequences at the ends of each DNA fragment, which are seamlessly fused together through a proprietary enzyme-mediated, single-tube reaction process.

DTC-MT.a was amplified from *B. rapa* genomic DNA using phusion polymerase (Thermo Fisher, USA) using the respective primers (Tab. 3.4). Additionally, a construct containing only *BABG.a* gene was synthesized *de novo (*SynBio Technologies USA).

Tab. 3.4. Primer sequences used for the amplification of selected fragments of genomic DNA used for preparation of brassinin-related constructs.

Starter name	Sequence (5'-3')
Frag1-For-CYP81F2	CGTTTCCCGCCTTCGGTTTGGGCGCGCCACAATCTAGTCACACTA
Frag1-Rev-CYP81F2	ATGCGATCGCTTTTTTTTCCTTTGTGTTGATTTTT
Frag2-For-DTC-MT	GGAAAAAAAAGCGATCGCATGGCTCCGACGTACAC
Frag2-Rev-DTC-MT	ATATATAGCAGGCGCCTTACTTTTCGAACTGCGGG
Frag3-For-PEN2	GTAAGGCGCCTGCTATATATATCATTAGGACGTTT
Frag3-Rev-PEN2	ATCTTTGGTTGGCCGGCCAAGCTTATCGATACCGTCGACCTCG
Frag4-For-BABG	TTGGCCGGCCAACCAAAGATGACACAAGGAAAGAG
Frag4-Rev-BABG	GATCCCCCTCCACCGCGGTGGCGGCCGCCCGGTCACTGGATTTTG

For-CR1	ATATGCGATCGCGGAAAAAAAAATGGATCAAATCATCCTCAACT
Rev-CR1	ATATCCTGCAGGTTAGGCATTGCTCTTAAACCTT
For-CR2	ATATGCGATCGCGGAAAAAAAAATGGAGCAGATCCTCTCTAACT
Rev-CR2	ATATCCTGCAGGCTACACCCTGCGAACTGGTATA

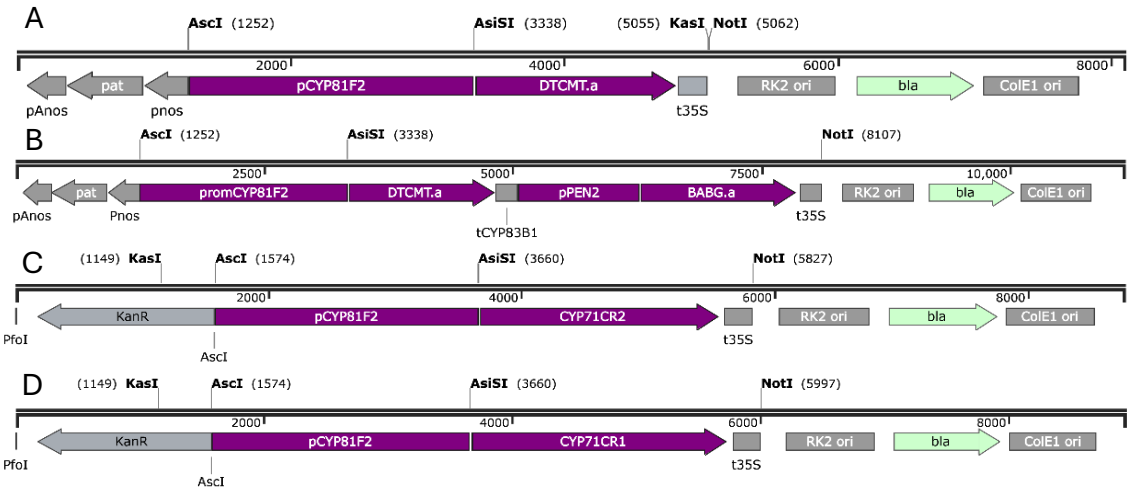

Fig. 3.2. Maps of the pAMPAT plasmid-based constructs; A, *DTC-MT* gene under the *CYP81F2* promoter; B, *DTC-MT* and *BABG.a* gene under the *CYP81F2* and *PEN2* promoters respectively; C, *CYP71CR1* gene under the *CYP81F2* promoter; D, *CYP71CR2* gene under the *CYP81F2* promoter.

CYP71CR1/2 were amplified from *B. rapa* genomic DNA using the primers listed (Tab. 3.4). Finally, utilizing restriction cloning technique, constructs containing genes encoding enzymes required for the biosynthesis of cyclobrassinin and spirobrassinin were engineered. As these plasmids were supposed to be transformed in plants that are already glufosinate-resistant the backbone in these plasmids was pAMPAT with glufosinate resistance gene replaced by kanamycin resistance gene. This plasmid variant was generated previously at our laboratory.

3.5.4. Transformation of *E. coli*

25 µl of a glycerol stock suspension of electrocompetent *E. coli* strain DH10β bacteria (New England Biolabs, USA), stored at -80°C, were thawed and incubated on ice for 30 minutes. Subsequently, 10 µl of the ligation mixture was added to the bacteria. Electroporation was performed in a cuvette with a gap width of 0.1 cm (Bio-Rad, USA)

using a MicroPulser (Bio-Rad, USA), applying a single electrical pulse at 1.8 kV. For recovery, the bacteria were immediately resuspended in 965 µl of liquid LB medium and incubated at 37°C with shaking at 220 rpm for 1 hour. Then, 200 µl of the bacterial suspension was plated onto selective LB agar plates containing ampicillin at a concentration of 100 µg/ml for selection. The sealed bacterial plates were incubated at 37°C for 16 hours. Individual colonies that grew were resuspended in 3 ml of liquid LB medium containing ampicillin at the same concentration as before and incubated again for 16 hours at 37°C with shaking at 200 rpm. Plasmids were isolated from the bacteria, and the successful acquisition of the intended genetic construct was preliminarily confirmed by PCR using primers employed for cloning, as well as by restriction digestion verifying the unique digestion pattern of the obtained plasmid. In cases of positive results from these reactions, sequencing of the obtained plasmid was commissioned to confirm the sequence and exclude the presence of point mutations.

3.5.5. Transformation of *A. tumefaciens*

50 µl of prepared electrocompetent *A. tumefaciens* strain GV3101:pMPRK bacteria (obtained from the Max Planck Institute for Plant Breeding Research in Cologne; a strain resistant to rifampicin and kanamycin), stored at -80°C, thawed and incubated on ice for 30 minutes. One microliter of the purified plasmid solution was added to the bacteria, and electroporation was performed similarly to the *E. coli* transformation, with the only change being the voltage set to 2.2 kV. Subsequently, the bacteria were resuspended in 950 µl of YEB medium and incubated at 28°C with shaking at 220 rpm for 1 hour. Next, 100 µl of the bacterial suspension was plated onto selective YEB agar plates containing antibiotics: carbenicillin (100 µg/ml), rifampicin (100 µg/ml), and kanamycin (50 µg/ml). The bacterial plates were incubated at 28°C for approximately 2.5 days. Individual bacterial colonies were resuspended in 2 ml of liquid YEB medium with antibiotics at the same concentrations as before and incubated again at 28°C with shaking at 200 rpm for 2.5 days. Subsequently, to verify the presence of the plasmid in the transformed *A. tumefaciens* bacteria, a PCR reaction was conducted using the obtained bacterial suspensions.

3.6. Plant transformation

A. tumefaciens containing the appropriate plasmids were cultured in 2 ml of liquid YEB medium with antibiotics (as described above). The incubation was carried out at 28°C with shaking at 200 rpm for 2.5 days. Subsequently, 100 µl of the bacterial suspension was transferred to a conical flask containing 20 ml of YEB medium with antibiotics and incubated again under the same conditions for 1.5 days. In the next step, 500 µl of the bacterial suspension was transferred to 10 ml of YEB medium with antibiotics, continuing incubation under the same conditions. During incubation, the optical density at 600 nm (OD600) of the bacterial suspensions was measured approximately every hour, and when the value reached ~0.6, the suspension was centrifuged at room temperature at 4000 rpm for 15 minutes. The supernatant was poured off, leaving only the pellet, which was resuspended in 50 ml of 5% sucrose solution and 30 µl of the surfactant Silwet L-77 was added. Stems of flowering (approximately 8-10-week-old) plants of *A. thaliana pen2 cyp71a12 cyp71a13* or *cyp81f2 cyp71a12 cyp71a13* lines were dipped for 30 seconds in the prepared *A. tumefaciens* suspensions and then placed in darkness for 24 hours. After this period, the plants were returned to the growth chamber and cultivated until maturity and seed production. The dried seeds were collected, cleaned of any remaining seed silique debris, and subjected to stratification at 4°C for at least 2 weeks.

3.6.1. Selection of transgenic plants with glufosinate

Seeds collected from T_0 plants were sown into trays filled with soil. Approximately one week after seed germination, T_1 generation seedlings were sprayed with glufosinate ammonium solution at a concentration of 75 mg/l. The spray was repeated three times at 3-day intervals. Subsequently, seedlings showing resistance towards this herbicide were transferred to Jiffy-7® peat pellets and grown in a growth chamber for an additional 4-5 weeks.

3.6.2. Selection of transgenic plants with kanamycin

For plants transformed with constructs carrying the kanamycin-resistance marker we performed *in vitro* on-plate selection. Seeds from T_0 plants were surface-sterilized (20% bleach, 10 min), rinsed 3-5 times in sterile water, suspended in 0.3 % agarose + ½-strength Murashige and Skoog salts and spread onto ½-strength Murashige and Skoog plates (1% plant agar, 4.3 g/l ½-MS salts, 0.5 g/l MES, 0.1 g/l myo-inositol, pH 5.7) supplemented with 50 µg/ml kanamycin. Plates were sealed and cold-stratified for 3 d at 4°C, then transferred to 22°C short-day conditions; seedlings showing fully green cotyledons and visible primary roots after 7–10 d were scored as kanamycin-resistant and transplanted to Jiffy-7® peat pellets for further cultivation.

3.7. Investigation of transgenic plants

3.7.1. Inoculation with *Plectosphaerella cucumerina* spores

For pathogen inoculation, we utilized the necrotrophic fungus *Plectosphaerella cucumerina* strain BMM (*Pc*BMM), which is adapted to *A. thaliana*. This strain was obtained from prof. Antonio Molina (Centro de Biotecnología y Genómica de Plantas, Universidad Politécnica de Madrid, Spain). Spore suspensions were prepared by rinsing spores from mycelium grown on potato dextrose agar medium using plastic laboratory spreaders. The concentration of spores was determined using a Bürker counting chamber and adjusted to 0.8×10^8 spores/ml. These suspensions were then stored in a 20% glycerol solution at -80°C.

In case of experiments with T_2 plants, 5-week-old plants were inoculated by spraying them with a spore suspension prepared by diluting the initial spore solution in deionized water to achieve a final concentration of 10^7 spores/ml (for metabolic analysis) or 4×10^6 spores/ml (fungal biomass assays). Concurrently, control plants were treated with deionized water. After spraying, the plants were placed in sealed containers with transparent lids to maintain humidity. Depending on the analysis, samples were collected at various time points post-inoculation: for metabolite extraction, 48 hours in case of camalexin producing transgenics and 72 hours in case brassinin, five days for genomic DNA extraction (fungal biomass assays). Each sample comprised leaves from different

plants to minimize biological variability, with fresh weights ranging from 50–70 mg for DNA and RNA extractions and 100–200 mg for metabolite extractions. Immediately after collection, the samples were flash-frozen in liquid nitrogen and stored at -80°C.

For screening of the first generation of plants (T_1), individual leaves of single-5-week-old plants were collected, placed on square Petri plates and inoculated with suspension of 10^7 *Pc*BMM spores/ml, the plates were covered to keep humidity. Leaves were collected after 24 hours for RNA extraction or after 48 hours for metabolite extraction. Immediately after collection, the samples were flash-frozen in liquid nitrogen and stored at -80°C. Preserved and validated T_1 plants were replanted into soil from the Jiffy pots to pots to grow them for seeds. When the rosettes started to form (2-3 weeks), plants were moved to long day conditions.

3.7.2. Treatment of plants with bacterial flagellin epitope

The MAMP used in our experiments was flagellin epitope (flg22), a 22-amino acid peptide derived from bacterial flagellin, synthetized by ProteoGenix (Schiltigheim, France). To achieve a final concentration of 5 µM flg22, we first diluted 10 µl of a 10 mM stock solution in 990 µl of deionized water. Subsequently, 500 µl of this intermediate solution was further diluted in 9.5 ml of deionized water, and 12.5 µl of the adhesion agent Tween 20 was added. Plants were sprayed with this final solution, while control samples were sprayed with 10 ml of deionized water containing 12.5 µl of Tween 20. Samples for metabolite analysis (100 to 200 mg) were collected 24 hours after flg22 treatment. The samples were immediately flash-frozen in liquid nitrogen and stored at –80°C.

3.7.3. RNA isolation and gene expression analysis

For the isolation of total RNA, approximately 50 mg of frozen plant tissue was utilized. The extraction was performed using the RNeasy Plant Mini Kit (Qiagen, Germany) following the manufacturer's protocol. Additionally, DNase I (Qiagen, Germany) was employed to eliminate any genomic DNA contamination from the RNA samples. The concentration and quality of the isolated RNA were assessed using a NanoDrop spectrophotometer (Thermo Scientific, USA). Subsequently, 2 µg of RNA underwent reverse transcription using the Omniscript RT Kit (Qiagen, Germany)

according to the provided instructions. To prevent RNA degradation during this process, the RNase inhibitor RNasin Plus (Promega, USA) was added.

The resulting complementary DNA (cDNA) from the reverse transcription was diluted to a concentration of 25 ng/µl. This cDNA served as the template for quantitative reverse transcription PCR (RT-qPCR). The RT-qPCR reactions were conducted using the iTaq Universal SYBR Green Supermix (Bio-Rad, USA) and a CFX Real-Time PCR Detection System (Bio-Rad, USA), with *actin* gene employed as the reference. Primer sequences for the specific genes were designed using GenScript web software. All primer sequences used in the RT-qPCR analyses are listed in Tab. 3.5, and all reactions were performed according to the protocol outlined in Tab. 3.6.

Tab. 3.5. Primer sequences used for performing RT-qPCR of selected genes.

Starter name	**Sequence (5'-3')**
F-CYP71A13-RT	ATGCCCCGGGATAAATCTT
R-CYP71A13-RT	GAGAAAACATGTTACACAACCG
F-PAD3-RT	TGCTCCCAAGACAGACAATG
R-PAD3-RT	GTTTTGGATCACGACCCATC
F-DTC.MT-RT	AGAAGCAATGGAGAGGACAAATGAG
R-DTC.MT-RT	TTACTTTTCGAACTGCGGGTGGCT

Tab. 3.6. Thermal cycling program for RT-qPCR analysis.

Step	**Temperature**	**Time**	**Cycles**	**Read**
DNA denaturation	95 °C	20–30 s (for cDNA)	1	no
Denaturation	95 °C	2–5 s	35	no
Annealing/extension	60 °C	15–30 s	35	plate read
Melt curve	65–95 °C	0.5 °C increments, 2–5 s/step	1	plate read

The relative transcript level of each target gene was determined by the $2^{-\Delta Cq}$ method using *actin* as the reference gene. For each sample, ΔCq was calculated as Cq(target) − Cq(reference), and relative expression was calculated as $2^{-\Delta Cq}$. This corresponds to normalization of the target transcript to the internal reference gene within the same sample.

3.7.4. Metabolite extraction and LC analysis

Samples containing approximately 200 mg of collected plant tissues, frozen in liquid nitrogen, were subjected to extraction in DMSO (2.5 µl per 1 mg of fresh tissue) using 1 mm diameter zirconia beads (Carl Roth, Germany). For MS analysis camphorsulfonic acid (0.5 mM) and lidocaine (0.5 mM) (both Sigma-Aldrich, Germany) were added as internal standards to the extraction buffer. Utilizing a consistent solvent volume relative to the fresh tissue mass across all samples allowed for the comparison of individual metabolite concentrations among the analyzed samples. The extraction process was performed using a Precellys Evolution homogenizer (Bertin Instruments, France) with a shaking speed of 8,000 rpm for 2 × 30 seconds for leaves. Following homogenization, the samples were centrifuged for 20 minutes at 15,000 rpm and 4°C. The resulting supernatant was then transferred to chromatographic vials and prepared for LC- UV/FLD (liquid chromatography with ultraviolet and fluorescence detection) or LC-MS/MS (liquid chromatography coupled to tandem mass spectrometry) analyses.

3.7.4.1. Analysis of leaf extracts with LC-UV/FLD. Chromatographic separations were performed on a Thermo Scientific Dionex Ultimate 3000 LC-UV/FLD system (Thermo Fisher Scientific, Waltham, MA, USA), equipped with a quaternary pump, an autosampler, a column oven, and both UV and FLD detectors. Chromatograms were recorded and integrated using Chromeleon software. Analyses were performed under conditions outlined in Tab. 3.7. Waters Atlantis T3 column (2.1 × 150 mm, 3 µm particle size) extended with Waters Atlantis T3 extension column (2.1 × 5 mm, 3 µm particle size) was used for all analyses. Columns were maintained at 20°C inside. All LC-UV/FLD targeted metabolomics was done using corresponding standards. Peak area was used to estimate metabolite abundance.

Peak identities were assigned by comparing retention times and spectral characteristics (UV-absorption or fluorescence) to those of authentic standards or reference data. Quantitation was performed based on peak areas. Camalexin was quantified using external calibration curves prepared from serial dilutions of respective standards analyzed under the same LC conditions as the samples. Peak areas were converted to compound in tissue concentrations (nanomoles of compounds per gram of the leaf tissue fresh weight; nmol/gFW), accounting for the extraction and injection volumes (Danzer and Currie, 1998).

Tab. 3.7. Conditions of chromatographic separation used during LC-UV/FLD analysis

		UV-detection		**Fluorescence**			
		Brassinin		Camalexin HCX-Hex		I3A	
Detector wavelength		273 nm		Ex 318 nm Em 386 nm		Ex 275 nm Em 350 nm	
Gradient		Time	%B	Time	%B	Time	%B
		2 9 23 26 27 34 35	0 10 22 50 100 100 0	2 20 27 28 38	0 100 100 0 0	2 9 20 21 26 27 37	0 10 19 100 100 0 0
Temperature		20 °C					
Injection volume		7 µl					
Flow rate		0.250 ml/min					
Phase composition	A	0.1% trifluoroacetic acid in H_2O (v/v)		H_2O			
	B	98% acetonitrile 1.9% H_2O 0.1% trifluoroacetic (v/v)		98% acetonitrile in H_2O (v/v)			

3.7.4.2. Analysis of leaf extracts by LC-MS/MS. Samples were subjected to LC-MS/MS analysis using an UltiMate 3000 RS system (ThermoFisher Scientific) coupled to a TIMS-TOF mass spectrometer (Bruker Daltonics, Germany). Chromatographic separation was carried out on a BEH RP C18 column (2.1 × 150 mm, 1.8 µm particle size) at 30°C with a mobile phase flow rate of 0.25 mL/min.

The elution (Tab. 3.8) was performed using:

- Solvent A: water containing 0.1% formic acid (Sigma–Aldrich),
- Solvent B: acetonitrile (VWR Chemicals, France) containing 0.1% formic acid,

Tab. 3.8. Gradient program used for LC separation

Time (min)	**% B (acetonitrile)**
0 – 5	10 → 30

5 – 12	30 → 100
12 – 15	100 (isocratic)
15 – 15.5	100 → 10
15.5 – 20.5	10 (re-equilibration)

The mass spectrometer was calibrated with sodium formate salt clusters as an internal calibrant prior to each analysis. MS detection was performed under the conditions listed in Tab. 3.9. Instrument was operated in positive and negative ionization modes with data-dependent fragmentation (ddMS/MS). Data acquisition was supervised by Compass HyStar version 6.0 (Bruker Daltonic).

Tab. 3.9. Key MS operating parameters

Parameter	**Value**
Ion source voltage	–4.5 kV / +4.5 kV
Nebulizer pressure	2.2 bar
Gas flow rate	10 L/min
Source temperature	220 °C
m/z range	95–1000
Resolution	>30,000 FWHM

Raw LC-MS/MS data were processed using MS-Dial ver. 4.74 followed by MSCleanR. Processing steps included peak detection, annotation using spectral MS/MS public metabolomic libraries (http://prime.psc.riken.jp/compms/msdial/main.html), elimination of adducts, alignment, and gap filling by compulsion.

3.7.5. Quantification of fungal biomass using qPCR

To estimate fungal biomass in plant tissues, a qPCR-based method was employed. This technique allows for the precise detection and quantification of fungal DNA relative to plant DNA in infected plant tissue, using species-specific marker genes for both the fungus and the host plant.

Plant tissues were inoculated with 4×10^6 spores/ml. Concurrently, control plants were sprayed with 25 ml of deionized water. Six independent samples were collected at 5 days post inoculation (dpi). Each sample consisted of leaves with a total mass of 100 mg of fresh weight. Samples were immediately frozen in liquid nitrogen upon collection and later stored at -80°C. Approximately 100 mg of frozen plant leaves were ground into a fine powder using a mortar and pestle in liquid nitrogen. DNA was then extracted using the EurX Plant and Fungi DNA Extraction Kit, following the manufacturer protocol. The extracted DNA was eluted in the provided buffer and quantified using a nanodrop to determine concentration and purity. DNA integrity was confirmed by agarose gel electrophoresis. All samples were normalized to contain 15 ng of DNA before proceeding to amplification.

Primers specific to the fungal *Tubulin* gene were used to quantify fungal DNA, while primers targeting the *AAP1* (Amino Acid Permease 1) gene were employed to normalize the data against plant DNA (Tab. 3.10).

Tab. 3.10. Primer sequences used in fungal DNA quantification.

Starter name	Sequence (5'-3')
For-AAP1	GAATCGGTCTAGCCATCGCA
Rev-AAP1	ATGAGCCAAAAGGGCTCGAA
For-tub	CAAGTATGTTCCCCGAGCCGT
Rev-tub	GGTCCCTTCGGTCAGCTCTTC

Both primer sets were validated for amplification efficiency and specificity. Reactions were conducted in technical triplicates for each biological replicate. The thermal cycling protocol included as presented in Tab. 3.11.

Tab. 3.11. qPCR protocol for *Pc*BMM biomass estimation.

	Temperature and time	Number of cycles
Initial Denaturation	98°C, 3 minutes	
Denaturation	98°C, 10 seconds	35
Annealing	62°C, 30 seconds	
Extension	72°C, 1 minute	
Final Extension	72°C, 5 minutes	

The ΔCq method was used to calculate relative fungal biomass, normalized to the plant *AAP1* gene. This allowed for consistent comparisons of fungal colonization across experimental conditions. Statistical analyses were performed to identify significant differences in fungal biomass.

RESULTS

4.1. Spatiotemporal reengineering of camalexin metabolic pathway

We selected the camalexin-deficient *pen2 cyp71a12 cyp71a13* (*pen2 cyp71a12/13*) triple mutant as the background to spatially re-engineer the biosynthesis of this phytoalexin. In addition to camalexin deficiency, this line lacks the pre-invasive IGL-metabolism pathway, making it susceptible at both the pre- and post-invasive stages of infection. To restore camalexin production, we reintroduced the gene encoding the entry enzyme CYP71A13 (Fig. 3.1) under *CYP81F2* promoter, which provides pathogen-inducible expression in epidermal cells contacting the pathogen (Fuchs et al., 2016). In addition, our construct included gene encoding the terminal P450 monooxygenase PAD3 (CYP71B15) (Fig. 3.1) driven by the *PEN2* promoter that also provides epidermal expression (Lipka et al., 2005; Fuchs et al., 2016). Apart from these two enzymes, camalexin biosynthesis requires the obligatory peptidase step provided by the redundant GGP1/GGP3, which are the enzymes acting also in the IGL pathway and have been shown to be induced in pathogen-inoculated epidermal cells (Hunziker et al., 2020). For this reason, we did not include any of them in our pathway reconstruction. In addition, a dedicated GST has been postulated to contribute, but camalexin biosynthesis has been implemented in tobacco without adding a specific GST (Su et al., 2011; Møldrup et al., 2013), and hence we also omitted it in our constructs. Overall, we assumed that combining prom*CYP81F2*::*CYP71A13* with prom*PEN2*::*PAD3* constitutes the smallest sufficient module to provide camalexin production at infection sites. Promoter control was taken from the enzymatic components of the pre-invasive epidermal metabolic pathway. By placing *CYP71A13* and *PAD3* under *CYP81F2* and *PEN2* promoters, respectively, we aimed to redirect camalexin biosynthesis to the initial pathogen entry sites. Apart from the construct containing two genes (prom*CYP81F2*::*CYP71A13* / prom*PEN2*::*PAD3*; hereafter p*81F2*::*71A13*/p*PEN2*::*PAD3*) we also generated and transformed individually into the *pen2 cyp71a12/13* plants single-gene control construct prom*CYP81F2*::*CYP71A13* (p*81F2*::*71A13*).

4.1.1. Transgene induction in T_1 p*81F2*::*71A13* plants

To trigger transgene expression, we spray-inoculated Col-0 (WT reference), the *pen2 cyp71a12/13* line, and both single-gene transgenics with the Arabidopsis-adapted strain of necrotrophic fungal pathogen *Pc*BMM. This fungus strongly engages Trp-derived defenses and progressively breaches the leaf surface, making entry-site chemicals decisive and well suited to test altered epidermal processes. We first quantified transgene expression using RT-qPCR across independent T_1 p*81F2*::*71A13* transformants. As expected, *CYP71A13* transcript levels varied among individual plants. Three lines (#13, 14, 18) showing Col-0-like expression have been chosen for subsequent assays (Fig. 4.1.1).

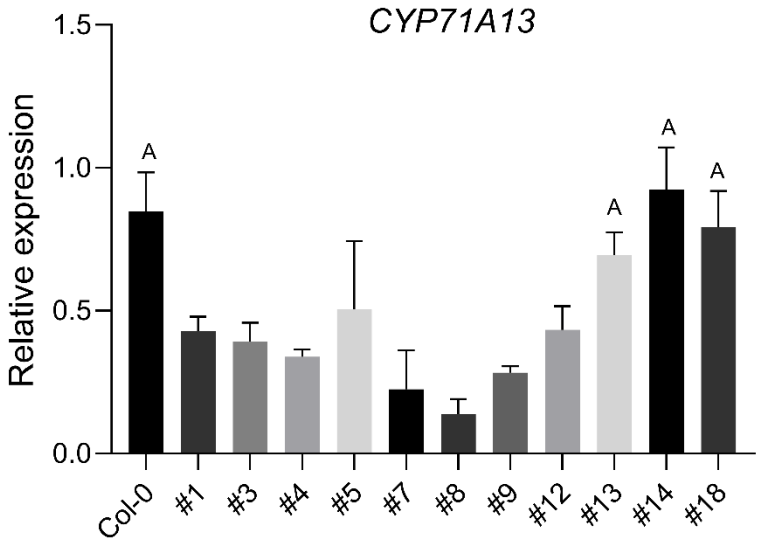

Fig. 4.1.1. RT-qPCR of *CYP71A13* in *Pc*BMM-inoculated leaves (48 hpi) of T_1 plants carrying construct p*81F2*::*71A13*. Expression was normalized to the reference gene *actin*. Bars show mean ± SD of biological replicates (n = 3). Letters above bars denote homogeneous groups from one-way ANOVA with Tukey's post hoc test ($\alpha = 0.05$). Col-0 (WT) included as a reference.

We next asked if PAD3 provided by the native *PAD3* gene, still present in the *pen2 cyp71a12/13* background, can be affected with p*81F2*::*71A13* expression. In the panel of our T_1 plants, expression of endogenous *PAD3* was pathogen-inducible but varied among p*81F2*::*71A13* individuals. Notably, lines #13 and #14 with highest *CYP71A13* expression (Fig. 4.1.1) showed slightly lower levels of *PAD3* transcript compared to the Col-0 and other *CYP71A13* lines (Fig. 4.1.2).

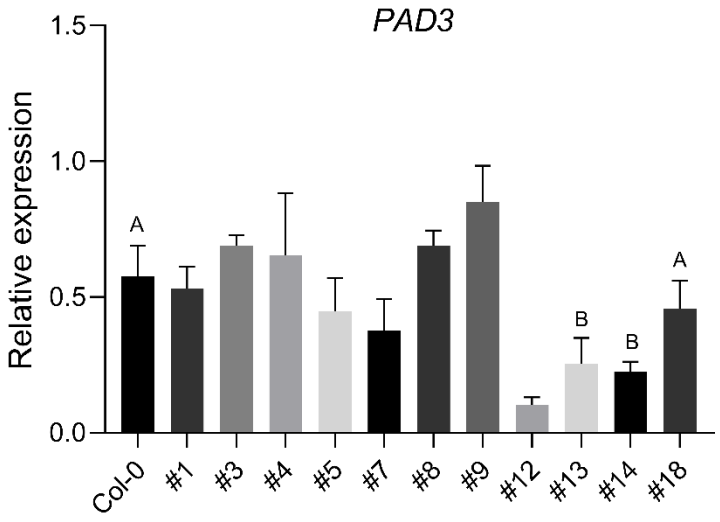

Fig. 4.1.2. RT-qPCR of *PAD3* in *Pc*BMM-inoculated leaves (48 hpi) of T_1 plants carrying the p*81F2*::*71A13* construct. Expression was normalized to *actin*; bars show mean ± SD of biological replicates (n = 3).

4.1.2. Verifying camalexin biosynthesis in *CYP71A13* lines

We next examined pathway outputs at the camalexin level upon *Pc*BMM infection and upon treatment with the bacterial flagellin epitope flg22 in the T_2 progeny of the selected T_1 *CYP71A13* plants (#13, #14, #18) using the same LC-FLD method. As expected, Col-0 leaves accumulated camalexin after *Pc*BMM infection, but not upon flg22 treatment, whereas in *pen2 cyp71a12/a13* this compound remained not detected across all treatments (Fig. 4.1.3). In the *CYP71A13* transgenic plants, *Pc*BMM likewise triggered camalexin biosynthesis, but clearly below levels observed in Col-0. flg22-treatment resulted in no detectable camalexin accumulation in transgenic lines and in Col-0. Camalexin detection in tested p*81F2*::*71A13* lines upon *Pc*BMM inoculation was somewhat expected because the endogenous *PAD3* locus is intact in the *pen2 cyp71a12/13* background, providing the terminal monooxygenase required to convert Cys-IAN to DHCA and further to camalexin (Fig. 1.9). Moreover, this also confirmed that the GGP1/3 peptidases are natively available in the epidermal cells, where the *CYP81F2* promoter is active upon pathogen inoculation (Fuchs et al., 2016; Hunziker et al., 2020). However, the observed modest camalexin levels, relative to Col-0, suggest that, as assumed, the reengineered CYP71A13 does not fully co-localize with PAD3. This raised a direct question whether re-targeting the terminal step to epidermal cells by

driving *PAD3* with the *PEN2* promoter can elevate local camalexin output compared with reliance on endogenous *PAD3* expression profiles.

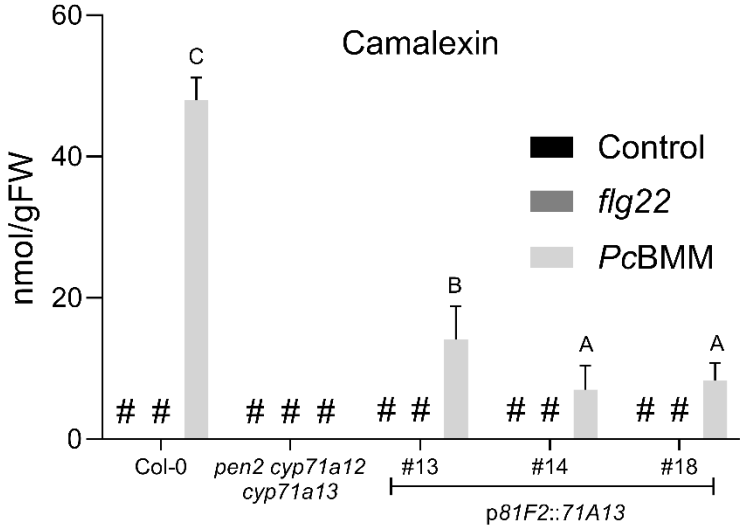

Fig. 4.1.3. LC-FLD quantification of camalexin accumulation in leaves of selected p*81F2*::*71A13* T_2 lines in response to flg22 treatment (24 hpi), and *Pc*BMM inoculation (48 hpi). Col-0 and *pen2 cyp71a12/13* lines included as positive and negative controls, respectively. Bars show mean ± SD of biological replicates (n = 6); "#", below the detection limit; statistical groupings above bars indicate differences from one-way ANOVA with Tukey's post hoc test (α = 0.05).

4.1.3. Epidermal-targeted PAD3 completes the CYP71A13-initiated camalexin route

Confirming camalexin biosynthesis in p*81F2*::*71A13* lines, we further proceeded with the generation and selection of p*81F2*::*71A13*/p*PEN2*::*PAD3* transgenics. As our analysis of p*81F2*::*71A13* confirmed that the re-engineering of *CYP71A13* under the *CYP81F2* promoter supports camalexin biosynthesis, we based our initial screens of p*81F2*::*71A13*/p*PEN2*::*PAD3* T_1 plants on metabolite output. Based on respective LC-FLD analysis, we selected three plants (#15, #21, #23) that showed the strongest camalexin accumulation in response to *Pc*BMM infection in T_1 to collect the T_2 seeds (Fig. 4.1.4).

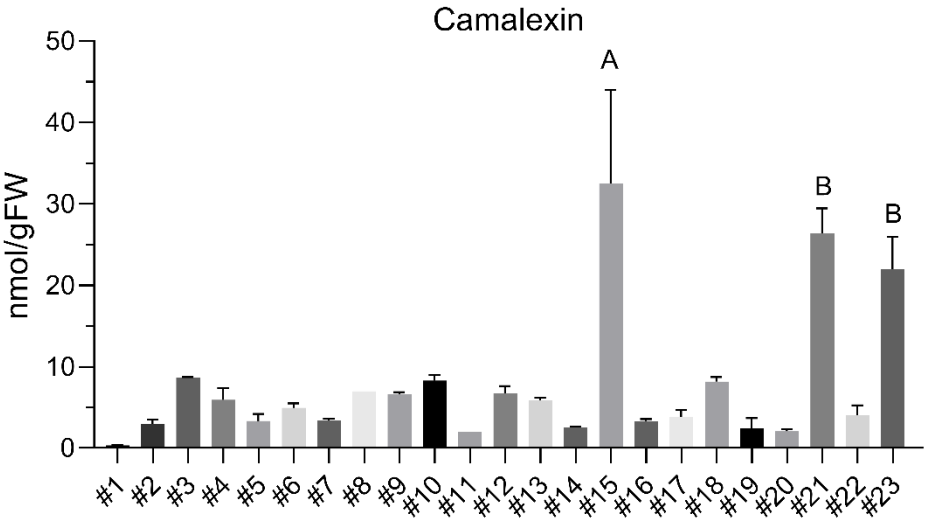

Fig. 4.1.4. LC-FLD screening of camalexin accumulation in *Pc*BMM-inoculated leaves of T_1 p*81F2*::*71A13*/p*PEN2*::*PAD3* plants (48 hpi). Bars show mean ± SD of biological replicates (n = 3); statistical groupings above bars indicate differences from one-way ANOVA with Tukey's post hoc test (α = 0.05).

We re-tested camalexin accumulation in p*81F2*::*71A13*/p*PEN2*::*PAD3* T_2 plants in response to *Pc*BMM inoculation (48 hpi) and flg22 treatment (24 hpi). Camalexin was clearly induced in response to fungal infection in our transgenic plants, particularly in line #15, while remaining below the detection limit after flg22 treatment (Fig. 4.1.5).

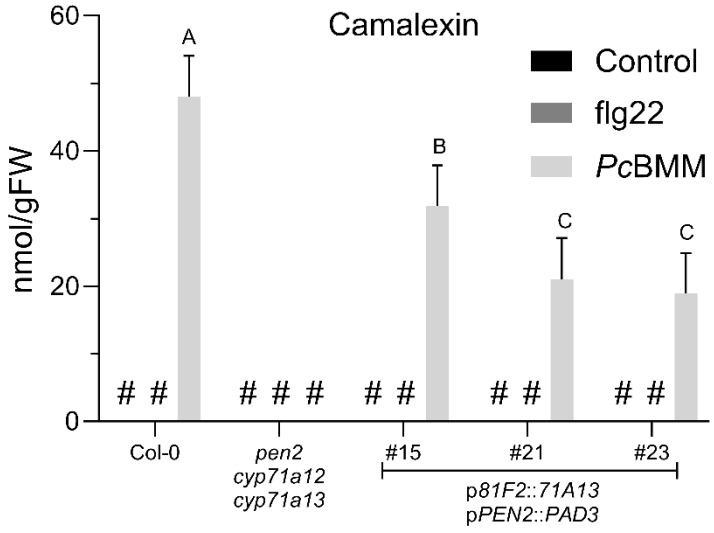

Fig. 4.1.5. LC-FLD quantification of camalexin accumulation in leaves of selected T_2 p*81F2*::*71A13*/p*PEN2*::*PAD3* lines in response to flg22 treatment (24 hpi) and *Pc*BMM inoculation (48 hpi). Col-0 and *pen2 cyp71a12/13* lines were included as positive and

⟶ negative controls, respectively. Bars show means ± SD of biological replicates (n = 6). "#", below the detection limit. Statistical groupings above bars indicate differences based on one-way ANOVA with Tukey's post hoc test (α = 0.05).

Under our chromatographic method, camalexin eluted at RT ≈ 18 min on the FLD chromatograms (Ex/Em 318/386 nm). We also inspected these chromatograms for additional treatment-responsive peaks specific for p*81F2*::*71A13*/p*PEN2*::*PAD3* lines. These revealed two smaller, earlier-eluting peaks present at RT ≈ 11.8 min (Peak_1) and RT ≈ 13 min (Peak_2; Fig. 4.1.6). These minor peaks were more abundant in samples obtained from *Pc*BMM infected and flg22-treated p*81F2::71A13*/p*PEN2::PAD3* plants, and from infected Col-0 plants, as compared with respective control samples. Both were absent in extracts obtained from *pen2 cyp71a12/13* plants (Fig. 4.1.10). This accumulation pattern suggested that both peaks represent camalexin derivatives. To identify these metabolites, we coupled LC-FLD system with MS/MS detector and monitored ions eluting at the same retention times. This revealed two signals at *m/z* 379.09, which corresponds to the molecular weight of camalexin hexosides reported to accumulate upon infection with *P. infestans* (Böttcher et al., 2009). For this reason, we designated these peaks as HCX-Hex #1 and HCX-Hex #2 isomers (Fig. 4.1.8).

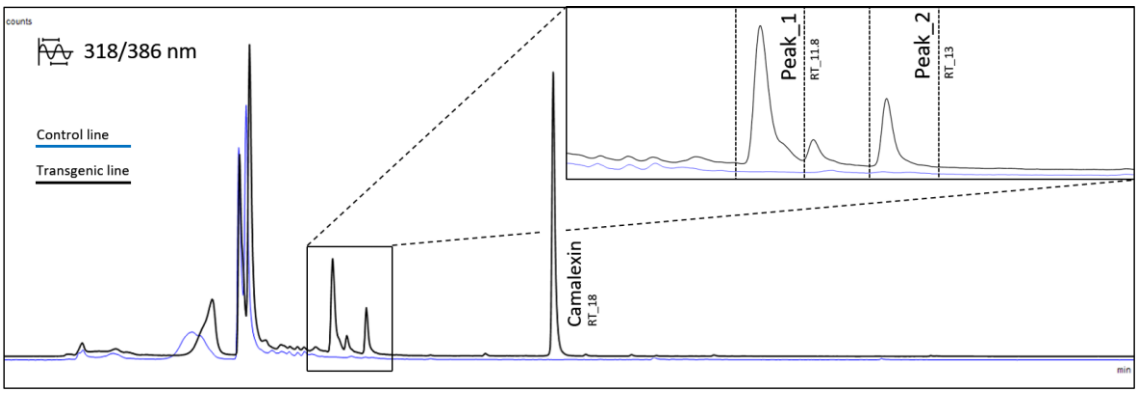

Fig. 4.1.6. LC-FLD chromatograms (Ex/Em = 318/386 nm) of extracts from *Pc*BMM-infected leaves (48hpi). p*81F2*::71*A13*/p*PEN2*::*PAD3* (black), *pen2 cyp71a12/13* (blue). The insert enlarges two earlier-eluting, low-abundant peaks at RT ≈ 11.8 and RT ≈ 13 min.

4.1.4. Double-gene p*81F2*::*71A13*/p*PEN2*::*PAD3* lines outperform single-gene lines for camalexin biosynthesis

To directly compare camalexin biosynthetic capacity in lines carrying the two-gene construct (p*81F2*::*71A13*/p*PEN2*::*PAD3*) with the reference single-gene transgenic plants (p*81F2*::*71A13*) under identical conditions, we assayed respective T_2 plants within the same experiment. As before, plants were treated with flg22 or inoculated with *Pc*BMM, and the obtained leaf extracts were analyzed by LC-FLD (Ex/Em = 318/386 nm). This analysis revealed that across *Pc*BMM inoculated plants, p*81F2*::*71A13*/p*PEN2*::*PAD3* lines accumulated clearly more camalexin than the single-gene transgenics (Fig. 4.1.7). Col-0 showed the highest camalexin accumulation, while in the *pen2 cyp71a12/13,* this phytoalexin was below the detection limit. Similarly, as in previous experiments, camalexin remained below the detection limit in samples obtained from mock and flg22-treated plants. Overall, these data indicate that co-expressing the committed entry enzyme (CYP71A13) with the terminal monooxygenase (PAD3) under epidermal promoters increases pathway output beyond that achieved by *CYP71A13* alone, where native *PAD3* is expressed predominantly in mesophyll cells.

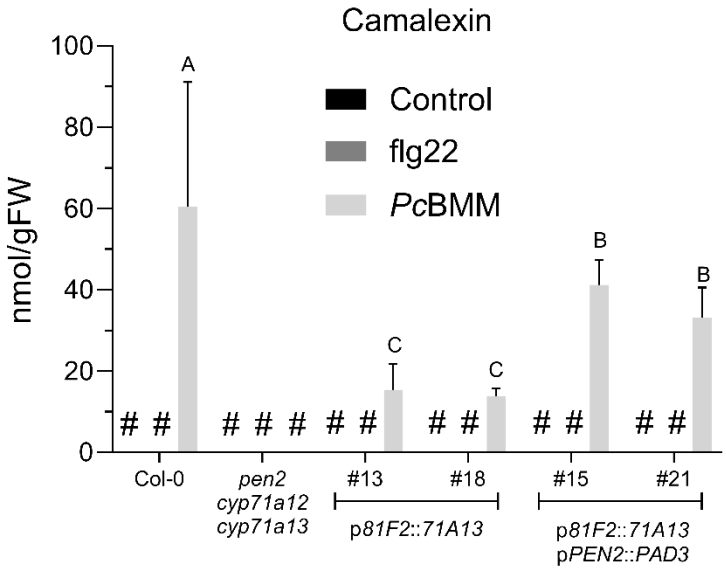

Fig. 4.1.7. LC-FLD quantification of camalexin accumulation in leaves of selected p*81F2*::*71A13* and p*81F2*::*71A13*/p*PEN2*::*PAD3* T_2 lines in response to flg22 treatment (24 hpi), and *Pc*BMM inoculation (48 hpi). Col-0 and *pen2 cyp71a12/13* lines included as positive and negative controls, respectively. Bars show mean ± SD of biological replicates (n = 6); "#", below

⟶ the detection limit; statistical groupings above bars indicate differences from one-way ANOVA with Tukey's post hoc test (α = 0.05).

In the same set of data, we inspected the earlier RTs of FLD chromatograms assigned above to HCX-hexosides (Fig. 4.1.6). Both compounds eluted at similar RTs as before (HCX-Hex #1 at 11.8 min; HCX-Hex #2 at 13 min). Their accumulation levels in *Pc*BMM-inoculated leaves mirrored the camalexin accumulation pattern; p*81F2*::*71A13*/p*PEN2*::*PAD3* lines accumulated higher levels of these camalexin derivatives as compared with the single-gene reference lines. Notably, unlike for camalexin, we detected respective signals in extracts from flg22-treated leaves. These were detectable only in Col-0 and the two-gene lines, but not in the single-gene transgenics. HCX-Hex #1 was less abundant in Col-0 than in p*81F2*::*71A13*/p*PEN2*::*PAD3* samples, while the abundance of isomer #2 was similar in these genotypes (Fig. 4.1.8).

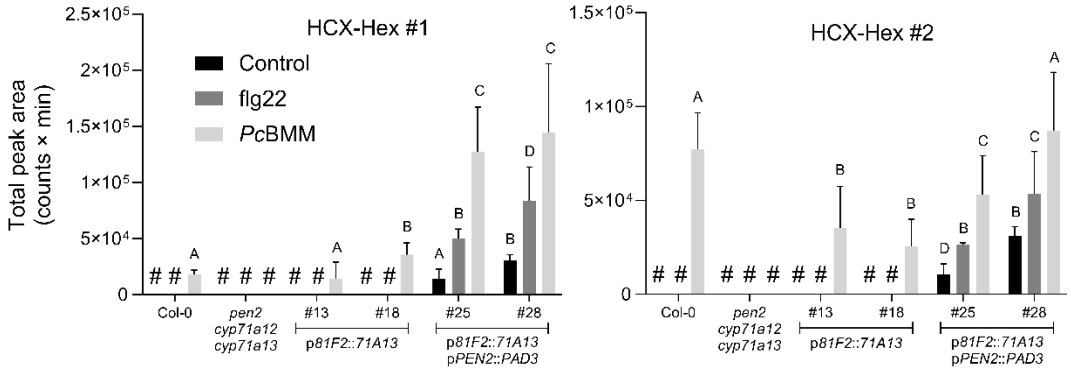

Fig. 4.1.8. LC-FLD quantification of HCX-Hex accumulation in leaves of selected p*81F2*::*71A13* and p*81F2*::*71A13*/p*PEN2*::*PAD3* T_2 lines in response to flg22 treatment (24 hpi), and *Pc*BMM inoculation (48 hpi). Col-0 and *pen2 cyp71a12/13* lines included as positive and negative controls, respectively. Bars show mean ± SD of biological replicates (n = 6); "#", below the detection limit; statistical groupings above bars indicate differences from two-way ANOVA with Tukey's post hoc test (α = 0.05).

4.1.5. Accumulation of camalexin pathway intermediates and derivatives in the obtained transgenic plants

Our targeted LC-FLD analysis indicated enhanced camalexin production in *Pc*BMM-inoculated p*81F2*::*71A13*/p*PEN2*::*PAD3* transgenic lines as compared with those of p*81F2*::*71A13*. To get a better insight into the re-engineered pathway, we prepared a new set of samples from *Pc*BMM infected plants (48hpi) including three independent p*81F2*::*71A13*/p*PEN2*::*PAD3* lines and respective control lines (Col-0 and *pen2 cyp71a12/13*). We reanalyzed this set of samples with targeted LC-MS/MS to quantify all reported intermediates and side products of camalexin pathway that we could not identify or detect during LC-UV/FLD analysis due to their low abundance and lack of respective standards.

We began with the IAOx precursor pool. This key intermediate is formed from Trp by the redundant CYP79B2 and CYP79B3 monooxygenases, and functions as the shared branch point leading to IGLs and camalexin, where it is converted by CYP71A13 to IAN (Fig. 4.1.9).

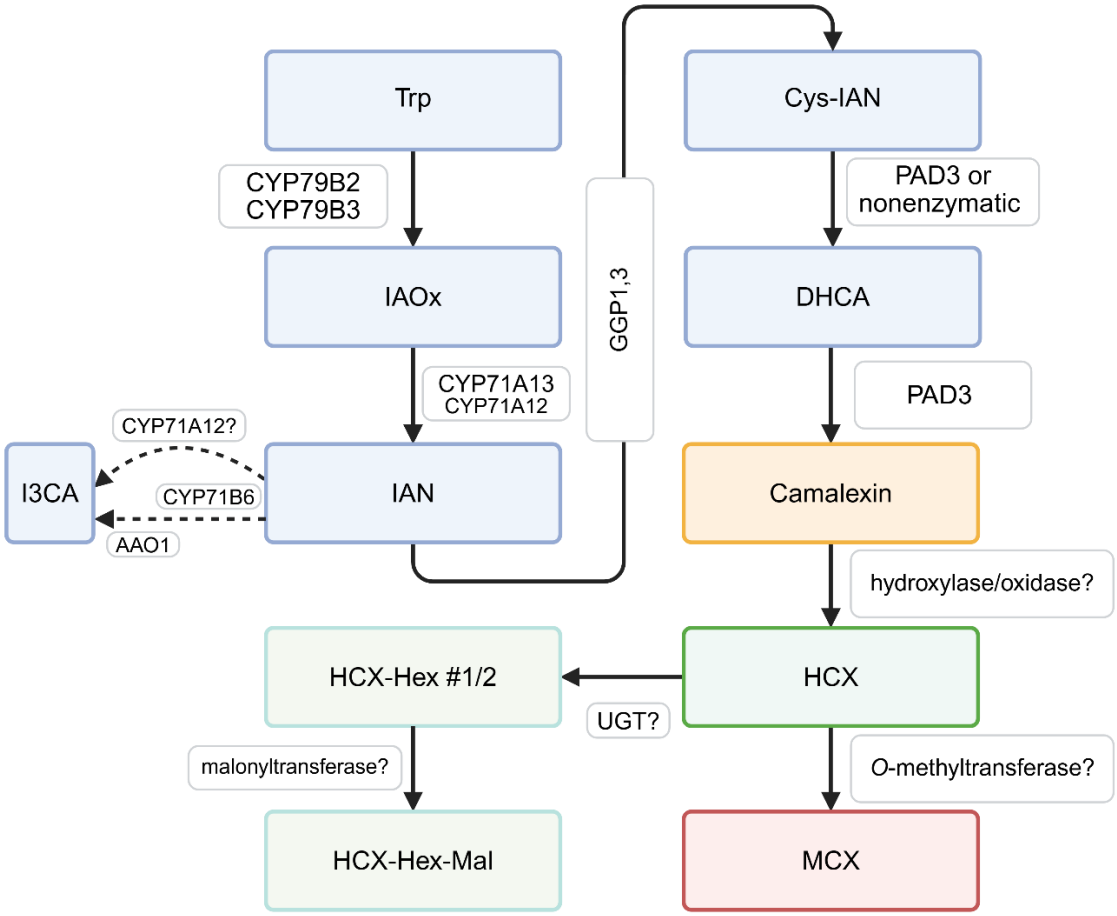

⟶ Fig. 4.1.9. Simplified scheme of camalexin biosynthesis and downstream metabolism depicting compounds detected in this study. Question marks indicate putative enzymatic steps.

Inspection of our LC-MS/MS data revealed a signal (*m/z* 175.08) corresponding to the molecular ion of IAOx (Fig. 4.1.10). In addition, we also observed MS/MS fragment ions fitted with the expected IAOx fragmentation pattern (Tab. 4.1).

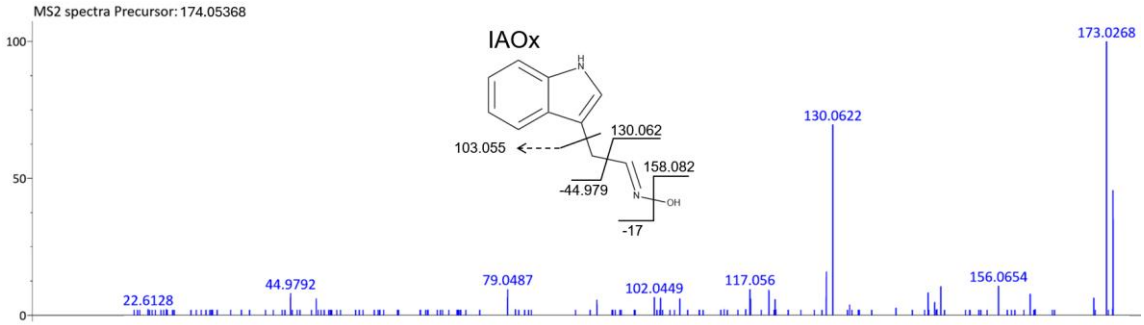

Fig. 4.1.10. LC-MS/MS spectrum of signal assigned to IAOx recorded in positive ionization mode. The precursor ion $[M+H]^+$ at *m/z* 175.083, and the observed fragment pattern matches characteristic fragments for IAOx.

Abundances of the putative molecular ion signal differed among analyzed genotypes (Fig. 4.1.11). The highest mean signal has been recorded for the *pen2 cyp71a12/13* samples, which fits with the deficiency in CYP71A12 and CYP71A13 that are IAOx-converting enzymes. This elevated accumulation was reduced back to the WT levels in p*81F2*::*71A13*/p*PEN2*::*PAD3* line #15. The other two transgenic lines revealed intermediate IAOx accumulation levels, which may indicate partial inefficiency of CYP71A13. In any case, our results indicated that introduced CYP71A13 at least partially metabolizes the excess of IAOx. This metabolization was further confirmed with the significantly elevated abundance of IAN-corresponding signal detected at *m/z* 157.076 in extracts from all three p*81F2*::*71A13*/p*PEN2*::*PAD3* lines as compared with Col-0 and the *pen2 cyp71a12/13* extracts (Fig. 4.1.11).

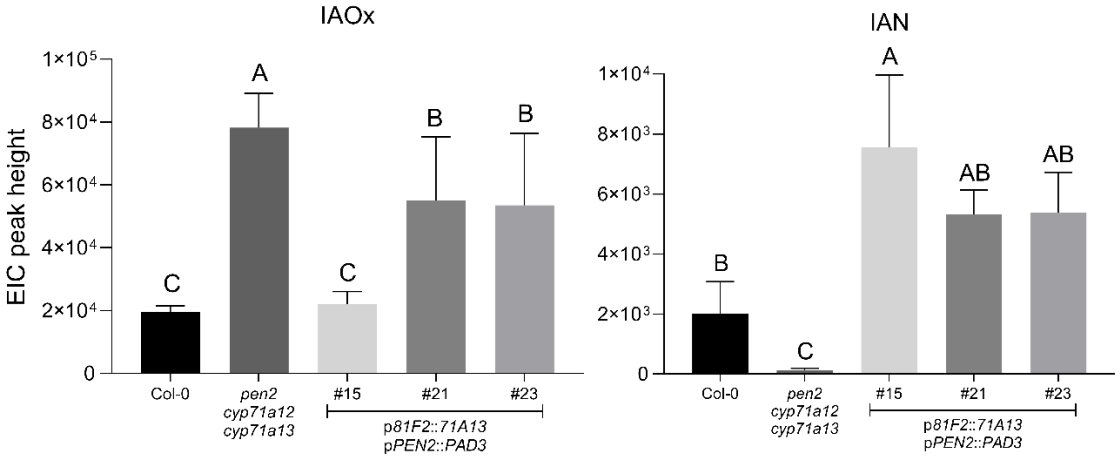

Fig. 4.1.11. LC-MS/MS quantification of IAOx and IAN accumulation in leaves of selected p*81F2*::*71A13*/p*PEN2*::*PAD3* T_2 lines in response to *Pc*BMM inoculation (48 hpi). Col-0 and *pen2 cyp71a12/13* lines included as controls. Bars show mean ± SD of biological replicates (n = 6); statistical groupings above bars indicate differences from one-way ANOVA with Tukey's post hoc test (α = 0.05).

The identity of IAN was validated with fragmentation pattern matching library spectra of this compound (Tab. 4.1) (Fig. 4.1.12).

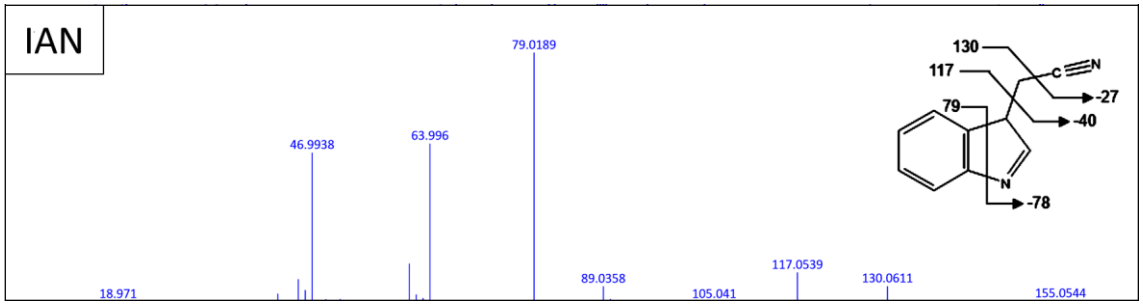

Fig. 4.1.12. Positive-ion LC-MS/MS spectrum of IAN used as the reference for compound identification. The precursor ion is $[M+H]^+$ at *m/z* 157.076, and the observed fragment pattern matches characteristic fragments for IAN.

Table 4.1. List of metabolites identified during LC/MS analysis of leaf extracts from lines expressing p*81F2*::*71A13*/p*PEN2*::*PAD3* construct.

No.	Retention time [min]	Ionization	Compound name	Molecular formula	Exact ion mass		Error [ppm]	Fragmentation
					Measured	Calculated		
1	7.88	$[M+H]^+$	IAOx (indole-3-acetaldoxime)	$C_{10}H_{10}N_2O$	175.08615	175.08659	-2.49	**175**, 158, 130. 103
2	12.369	$[M+H]^+$	IAN (indole-3-acetonitrile)	$C_{10}H_8N_2$	157.07600	157.07602	-0.16	**157**, 130, 117, 79
3	8.928	$[M+H]^+$	Cys-IAN (cysteine-IAN conjugate)	$C_{13}H_{13}N_3O_2S$	276.07978	276.08012	-1.23	**276**, 173, 155, 128
4	8.625	$[M+H]^+$	DHCA (dihydrocamalexic acid)	$C_{12}H_{10}N_2O_2S$	247.05368	247.05358	0.43	**247**, 201, 143, 58
5	14.864	$[M+H]^+$	Camalexin	$C_{11}H_8N_2S$	201.04867	201.04810	2.84	**201**, 160, 142, 116, 89, 58
6	9.185	$[M+H]^+$	HCX (hydroxy-camalexin)	$C_{11}H_8N_2OS$	217.04293	217.04301	-0.39	**217**, 199, 189, 172,
7	7.969/8.34	$[M+H]^+$	HCX-Hex (hydroxy-camalexin-*O*-hexoside) #1/#2	$C_{17}H_{18}N_2O_6S$	379.09751	379.09583	-0.84	**379**, 217, 200, 164, 103
8	10.134	$[M+H]^+$	HCX-Hex-Mal (*O*-malonyl-hydroxycamalexin hexoside)	$C_{20}H_{20}N_2O_9S$	465.09632	465.09623	4.43	**465**, 379, 217, 189, 162
9	11.984	$[M+H]^+$	MCX (methoxy-camalexin)	$C_{12}H_{10}N_2OS$	231.05885	231.05866	0.82	**231**, 201, 116
10	7.334	$[M+H]^+$	I3CA (indole-3-carboxylic acid)	$C_9H_7NO_2$	162.05496	162.05495	-1.58	**162**, 144, 130

We next identified the *m/z* 276.079 signal (Tab. 4.1), which corresponds to Cys-IAN, the cysteine adduct of IAN that locates immediately upstream of the PAD3 step. Identity of this compound was further supported with respective MS/MS fragment ions (Fig. 4.1.13).

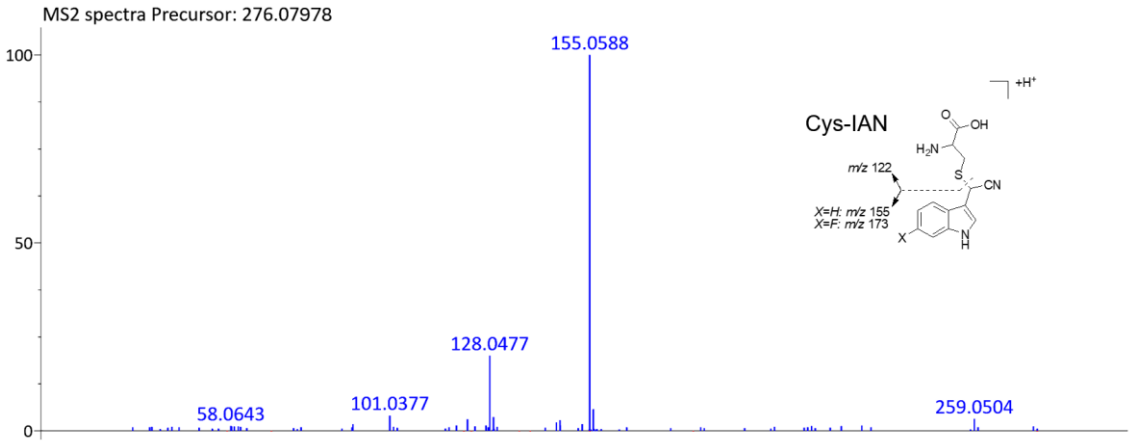

Fig. 4.1.13. Positive-ion LC-MS/MS spectrum of Cys-IAN used as the reference for compound identification. The precursor ion is $[M+H]^+$ at *m/z* 276.079, and the observed fragment pattern matches characteristic fragments for Cys-IAN.

The highest accumulation of Cys-IAN was observed in p*81F2*::*71A13*/p*PEN2*::*PAD3* lines (Fig. 4.1.14). Among these, line #15 accumulated less than the other transgenic lines. The *pen2 cyp71a12/13* were near the detection limit, below the accumulation level observed for Col-0 plants.

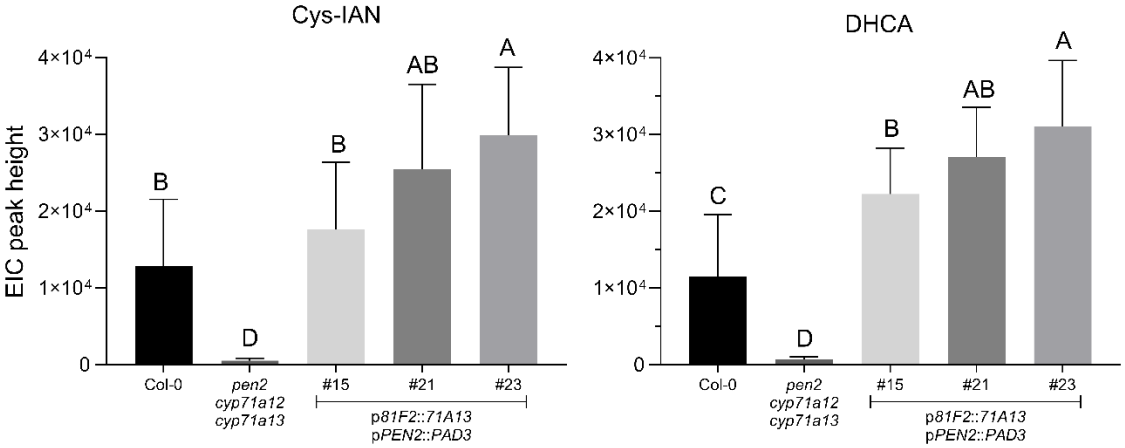

Fig. 4.1.14. LC-MS/MS quantification of Cys-IAN and DHCA accumulation in leaves of selected p*81F2*::*71A13*/p*PEN2*::*PAD3* T_2 lines in response to *Pc*BMM inoculation (48 hpi). Col-0 and *pen2 cyp71a12/13* lines included as controls. Bars show mean ± SD of biological replicates (n =

⟶ 6); statistical groupings above bars indicate differences from one-way ANOVA with Tukey's post hoc test (α = 0.05).

Continuing downstream of Cys-IAN, we identified a signal corresponding to the molecular weight of DHCA (*m/z* 247.053) (Tab. 4.1), the PAD3-proximal intermediate immediately preceding camalexin. The observed corresponding fragment ions matched the database fragmentation pattern (Fig. 4.1.15). Accumulation of this compound in the investigated lines followed the pattern observed for Cys-IAN, with the highest signal abundance observed in line #23 and the lowest in #15 plants (Fig. 4.1.14).

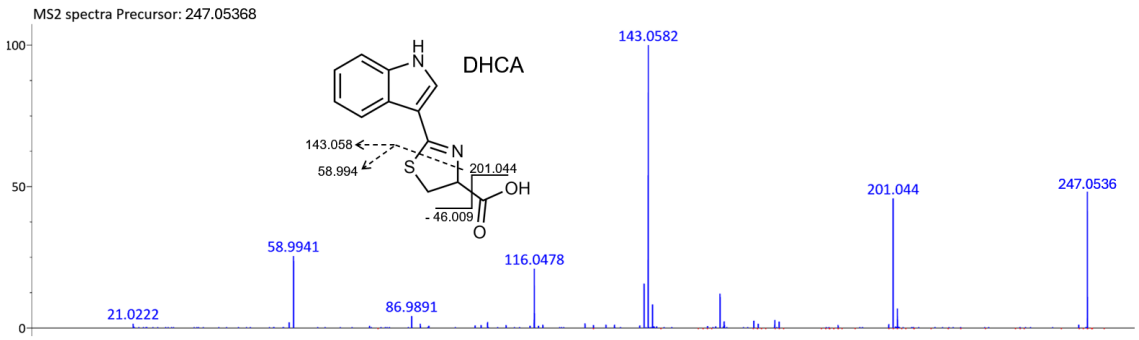

Fig. 4.1.15. Positive-ion LC-MS/MS spectrum of DHCA used as the reference for compound identification. The precursor ion is $[M+H]^+$ at *m/z* 247.053, and the observed fragment pattern matches characteristic fragments for DHCA.

We next quantified camalexin accumulation levels based on the respective single ion MS chromatograms. Identification of respective peak was based on the available camalexin standard and its characteristic fragmentation spectra (Fig. 4.1.16, Tab. 4.1).

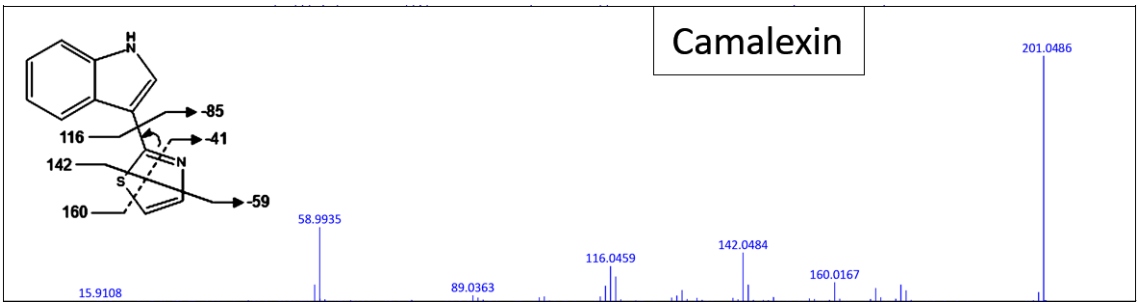

Fig. 4.1.16. LC-MS/MS spectrum of camalexin standard recorded in the positive ion mode. This spectrum was used as a reference for compound identification.

Quantitative analysis has been performed based on the chromatogram corresponding to the molecular ion (*m/z* 201.048). Line #15 samples revealed WT-like levels of camalexin signal, while signal abundance in samples from the two remaining lines was lower; however, still significantly higher than in *pen2 cyp71a12/a13* extracts (Fig. 4.1.17).

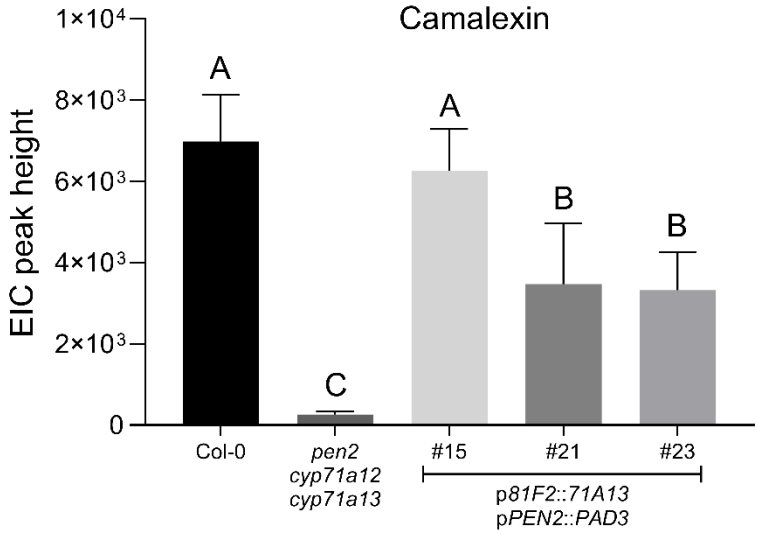

Fig. 4.1.17. LC-MS/MS quantification of camalexin accumulation in leaves of selected p*81F2*::*71A13*/p*PEN2*::*PAD3* T_2 lines in response to *Pc*BMM inoculation (48 hpi). Col-0 and *pen2 cyp71a12/13* lines included as controls. Bars show mean ± SD of biological replicates (n = 6); statistical groupings above bars indicate differences from one-way ANOVA with Tukey's post hoc test (α = 0.05).

We next checked for ions corresponding to putative camalexin derivatives. Processing of our LC-MS/MS data revealed presence of a signal matching HCX spectrum (molecular ion at *m/z* 217.042) (Fig. 4.1.18).

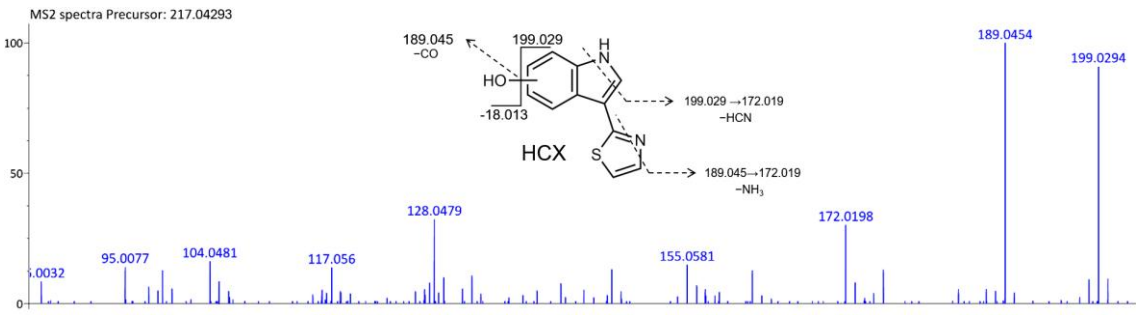

⟶ Fig. 4.1.18. Positive-ion LC-MS/MS spectrum of HCX used as the reference for compound identification. The precursor ion is $[M+H]^+$ at *m/z* 217.042, and the observed fragment pattern matches characteristic fragments for HCX.

Abundance of the HCX molecular ion mirrored camalexin accumulation, with Col-0-like levels in line #15 and intermediate accumulation in lines #21 and #23 (Fig. 4.1.19).

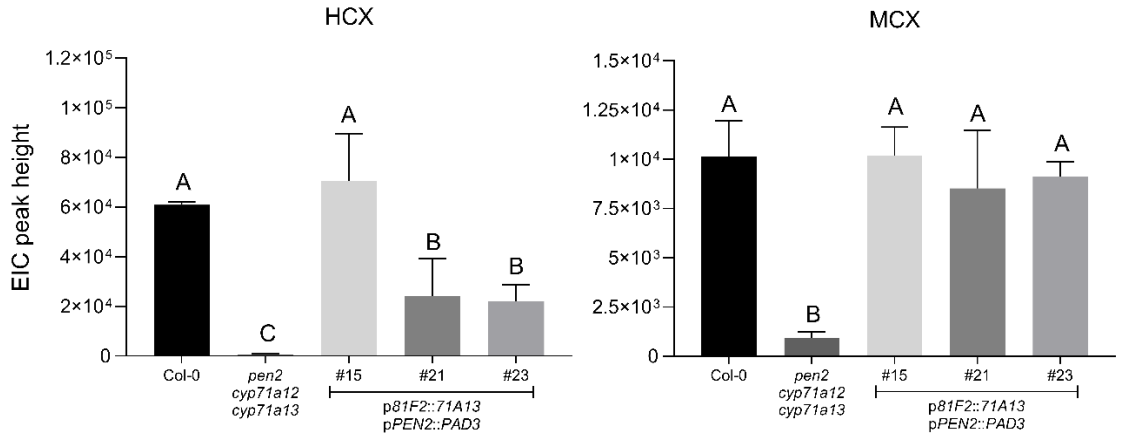

Fig. 4.1.19. LC-MS/MS quantification of HCX and MCX accumulation in leaves of selected p*81F2*::*71A13*/p*PEN2*::*PAD3* T_2 lines in response to *Pc*BMM inoculation (48 hpi). Col-0 and *pen2 cyp71a12/13* lines included as controls. Bars show mean ± SD of biological replicates (n = 6); statistical groupings above bars indicate differences from one-way ANOVA with Tukey's post hoc test (α = 0.05).

We next identified a signal corresponding to the direct derivative of HCX - MCX (molecular ion at *m/z* 231.058) (Fig. 4.1.20). Despite the differences between individual p*81F2*::*71A13*/p*PEN2*::*PAD3* lines in HCX levels, accumulation of MCX has been restored from the background to the Col-0-like levels in all three transgenic lines (Fig. 4.1.19).

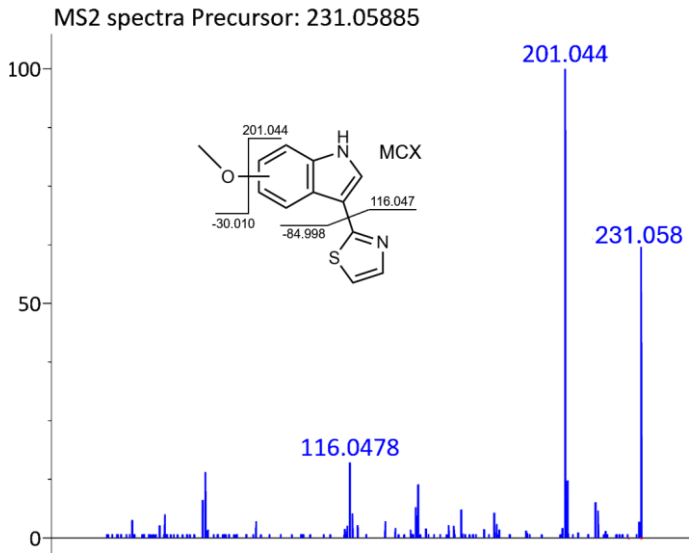

Fig. 4.1.20. Positive-ion LC-MS/MS spectrum of MCX used as the reference for compound identification. The precursor ion is $[M+H]^+$ at *m/z* 231.058, and the observed fragment pattern matches characteristic fragments for MCX.

We next checked for ions corresponding to HCX-Hex conjugates that we analyzed earlier with LC-FLD. Two respective LC-MS/MS features (*m/z* 379.097) were resolved by their retention times and by their fragmentation pattern (Fig. 4.1.21, tab. 4.1). It should be noted that for HCX-Hex the *O*-linkage position on the indole ring cannot be assigned unambiguously by MS/MS.

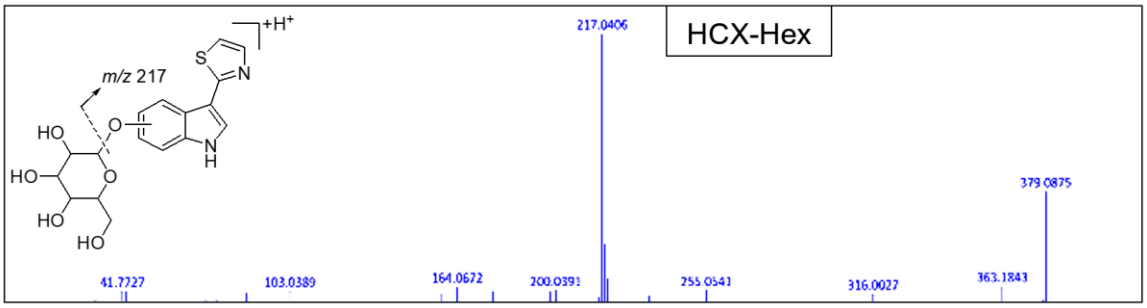

Fig. 4.1.21. Positive-ion LC-MS/MS spectrum of HCX-Hex #1 used as the reference for compound identification. The precursor ion is $[M+H]^+$ at *m/z* 379.097, and the observed fragment pattern matches characteristic fragments for HCX-Hex.

We used the respective molecular ion chromatograms to quantify the abundances of both Hex-conjugates. According to the obtained results conjugate #1 accumulated at much higher levels, as compared with Col-0, in all transgenic lines, while accumulation of conjugate #2 exceeded slightly Col-0 levels only in lines #15 and #23 (Fig. 4.1.22).

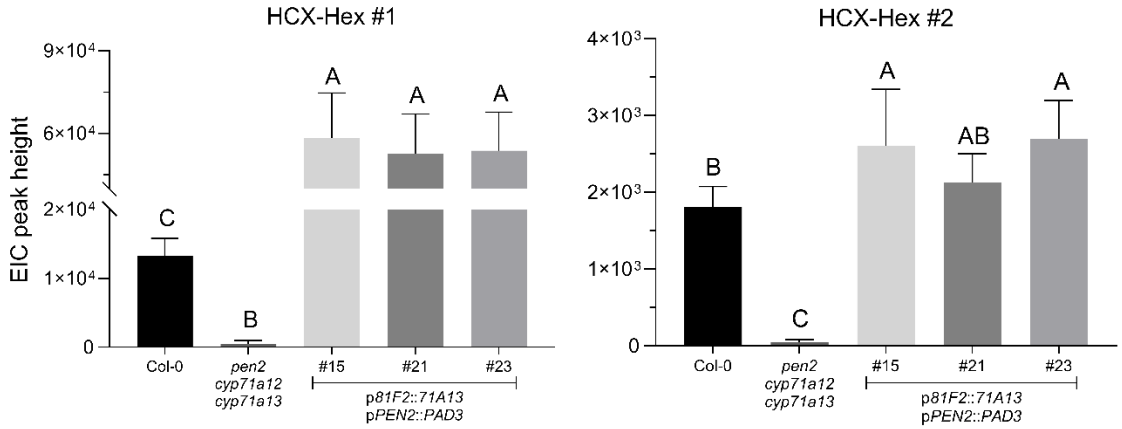

Fig. 4.1.22. LC-MS/MS quantification of HCX-Hex #1/#2 in leaves of selected p*81F2*::*71A13*/p*PEN2*::*PAD3* T_2 lines in response to *Pc*BMM inoculation (48 hpi). Col-0 and *pen2 cyp71a12/13* lines included as controls. Bars show mean ± SD of biological replicates (n = 6); statistical groupings above bars indicate differences from one-way ANOVA with Tukey's post hoc test ($\alpha = 0.05$).

Finally, we checked for a signal corresponding to the molecular ion of HCX-Hex-Mal (*m/z* 465.096), which is malonylated form of HCX-Hex (Fig. 4.1.9). Respective signal ion was present in our samples and accompanied by the expected MS/MS fragment ions at *m/z* 379, 217 and 189 (Tab. 4.1). Our transgenic lines were characterized by accumulation of these conjugates restored to (line #15), or slightly exceeding (lines #21 & 23) accumulation levels measured for Col-0 plants (Fig. 4.1.23).

In addition to camalexin intermediates and derivatives, we also measured accumulation of indol-3-carboxylic acid (I3CA), which constitutes another metabolic branch starting from IAN (Fig. 4.1.10). In case of this metabolite, we used authentic standard to perform identification. Precursor ion signal with *m/z* 162.054 along with characteristic fragments *m/z* 144, 130 confirmed the assignment. Our quantitative analysis (Fig. 4.1.23) revealed elevated accumulation of this compound in two of our transgenic lines (#15 and #23). However, this increase was rather moderate, suggesting only a small sub-fraction of IAN pool is redirected to the I3CA metabolic branch in the generated p*81F2*::*71A13*/p*PEN2*::*PAD3* lines.

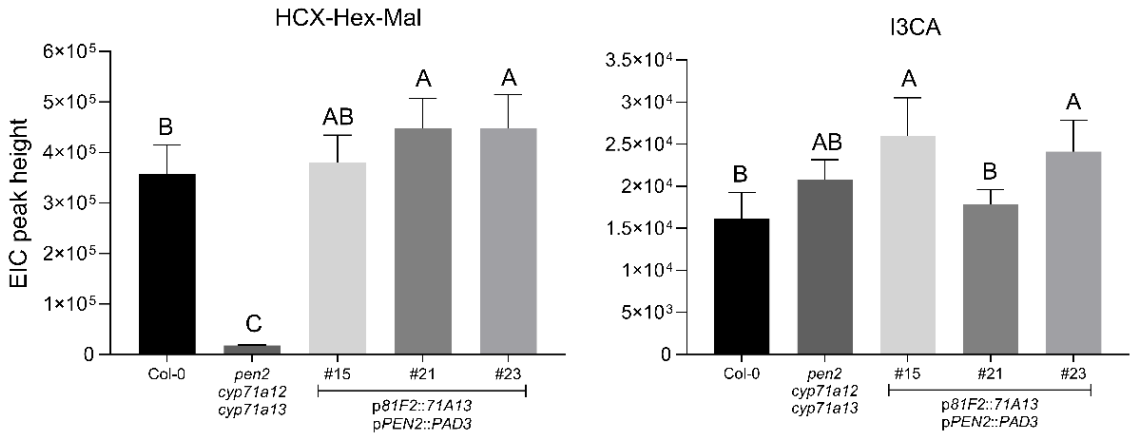

Fig. 4.1.23. LC-MS/MS quantification of HCX-Hex-Mal and I3CA in leaves of selected p*81F2*::*71A13*/p*PEN2*::*PAD3* T_2 lines in response to *Pc*BMM inoculation (48 hpi). Col-0 and *pen2 cyp71a12/13* lines included as controls. Bars show mean ± SD of biological replicates (n = 6); statistical groupings above bars indicate differences from one-way ANOVA with Tukey's post hoc test (α = 0.05).

4.1.6. Translating engineered camalexin pathway output into disease control

Having shown that our epidermal two-gene module is capable of restoring total camalexin accumulation to Col-0–like levels, we next asked whether this translates into reduced pathogen growth *in planta*. To that end, we applied qPCR to measure the amounts of fungal *β-tubulin* upon *Pc*BMM infection (5 dpi). This method can be used to quantify fungal biomass in infected tissue and has already been used by our group for evaluating susceptibility of *A. thaliana* lines toward *P. cucumerina* (Pastorczyk et al., 2020) (Fig. 4.1.24). Based on our metabolomics analysis we selected two best-performing p*81F2*::*71A13*/p*PEN2*::*PAD3* lines (#15 and #23) for the *Pc*BMM assays. As expected, the triple *pen2 cyp71a12/a13* mutant showed *Pc*BMM load significantly higher than Col-0, confirming its reported high susceptibility. Both engineered lines displayed significantly lower fungal biomass than the background genotype, demonstrating a clear reduction of pathogen proliferation. Yet fungal biomass in the transgenic lines remained above the values recorded for Col-0. Thus, the re-engineered camalexin module confers a partial, but not complete, rescue at the level of pathogen growth.

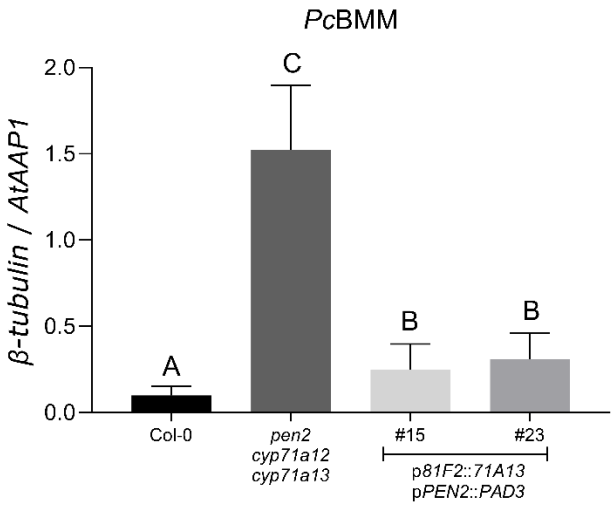

Fig. 4.1.24. *Pc*BMM fungal biomass estimated by qPCR in leaves of Col-0, *pen2 cyp71a12/a13* and p*81F2*::*71A13*/p*PEN2*::*PAD3* lines at 5 dpi; values are the ratio of *Pc*BMM *β-tubulin* to *A. thaliana AAP1*; bars show mean ± SD; uppercase letters indicate one-way ANOVA with Tukey's HSD groupings (α = 0.05).

4.2. Engineering of brassinin biosynthetic pathway in *A. thaliana*

Engineering of the brassinin pathway aimed at testing its immune function. Although the biosynthetic steps from IGLs to this phytoalexin and the downstream branches to cyclobrassinin and spirobrassinin have been characterized in *B. rapa* (Klein and Sattely, 2015, 2017), the contribution of these metabolites to pre-/post-invasive resistance has not been addressed yet. To engineer brassinin, we decided to use exactly the same mutant background (*pen2 cyp71a12/13*) and the same promoter set (*CYP81F2* and *PEN2*) as for camalexin engineering.

Based on the published results, we decided that the minimal brassinin construct should include two genes: *BABG.a* and *DTC-MT.a.* BABG is a myrosinase to convert I3G, the isothiocyanate intermediate, while DTC-MT *S*-methylates the resulting DTC to brassinin (Klein and Sattely, 2017). Arabidopsis provides in the infected epidermal cells the conserved IGL enzyme core set to produce I3G (Hunziker et al., 2020), which is the BABG substrate. Moreover, the IGL pathway enzymes GGP1/3 and SUR1 contribute again to the steps between isothiocyanate and DTC. We fused *BABG.a* with *PEN2*-promoter (both genes encode myrosinases) and *DTC-MT.a* with *CYP81F2* promoter to generate p*81F2*::*MT*/p*PEN2*::*BABG* plasmid.

As *A. thaliana* provides PEN2-mediated IGL-specific myrosinase activity in pathogen inoculated epidermal cells, we also asked whether this activity would be sufficient to substitute for BABG and drive brassinin biosynthesis. For this reason, we also decided to generate and test a single-gene construct *prom*$_{CYP81F2}$::*DTC-MT.a* (p*81F2*::*MT*). Because, according to our hypothesis, the function of this construct could depend on PEN2 activity, it would not be reasonable to transform it into the *pen2* mutant background. For this reason, we decided to transform this particular construct in the *cyp81f2 cyp71a12/13* triple mutant, which possesses PEN2 activity, but is defective in the IGL-dependent pre-invasive immunity due to the mutation in the *CYP81F2* gene (Fig. 1.7).

Table 4.2. List of detected brassinin-related metabolites in leaf extracts from lines expressing p*81F2*::*MT* and p*81F2*::*MT*/p*PEN2*::*BABG* constructs.

No.	RT [min]	Ionization	Compound name	Molecular formula	Exact ion mass		Error [ppm]	Fragmentation
					Measured	Calculated		
1	13.4	$[M-H]^-$	Brassinin	$C_{11}H_{12}N_2S_2$	235.03729	235.036914	1.60	**235**, 188, 159, 116, 57, 46
2	14.5	$[M+H]^+$	Cyclobrassinin	$C_{11}H_{10}N_2S_2$	235.0358	235.035817	-0.07	**235**, 187, 162, 128, 118
3	12.1	$[M+H]^+$	Spirobrassinin	$C_{11}H_{10}N_2OS_2$	251.0308	251.030731	0.27	**251**, 203, 178, 160, 145, 117
4	11.5	$[M-H]^-$	Hydroxybrassinin	$C_{11}H_{12}N_2OS_2$	251.03189	251.03183	0.24	**251**, 233, 207, 179, 161
5	9.6	$[M-H]^-$	Hydroxybrassinin-Hex	$C_{17}H_{22}N_2O_6S_2$	413.08398	413.08465	-1.62	**413**, 251, 233, 207, 179, 161
6	7.3	$[M+H]^+$	4-*O*-β-D-glucosyl-indol-3-yl formamide (4OGlcI3F)	$C_{15}H_{18}N_2O_7$	339.10062	339.10168	-3.13	**339**, 177, 149
7	9.1	$[M-H]^-$	I3M-DTC-Glc	$C_{16}H_{20}N_2O_5S_2$	383.07501	383.07409	2.40	**383**, 221, 187, 175
8	10.3	$[M+H]^+$	4MI3M-DTC-Glc	$C_{17}H_{22}N_2O_6S_2$	415.0864	415.09975	-32.17	**415**, 253, 176, 162

4.2.1. DTC-MT-mediated brassinin biosynthesis in *A. thaliana*

To test whether a single *DTC-MT*-gene module can already support brassinin formation, we transformed p*81F2*::*MT* in the *cyp81f2 cyp71a12/13* mutant. We quantified *DTC-MT* transcript levels in independent T_1 p*81F*2::*MT* plants obtained after glufosinate selection (Fig. 4.2.1). Our RT-qPCR analysis did not reveal any *DTC-MT*-related signal in the control *cyp81f2 cyp71a12/13* line, while all transgenic plants had detectable expression of this gene. Based on this analysis, we selected three T_1 plants (#1, #3 and #5) with relatively high *DTC-MT* expression to obtain T_2 seeds.

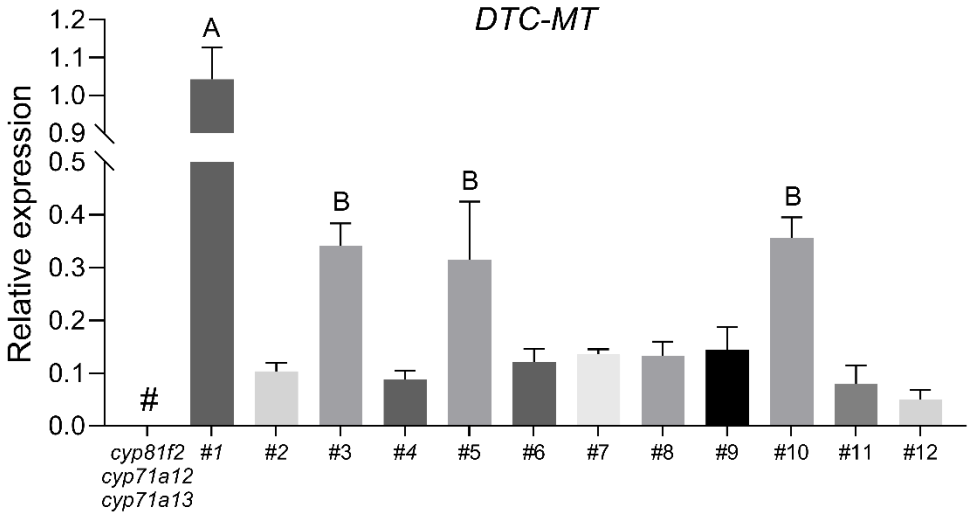

Fig. 4.2.1. RT-qPCR of *DTC-MT* in *Pc*BMM-inoculated leaves (72 hpi) of T_1 plants carrying p*81F2*::*MT* construct. Expression was normalized to the reference gene *Actin*; bars show mean ± SD of biological replicates (n = 3); letters above bars denote homogeneous groups from one-way ANOVA with Tukey's post hoc test (α = 0.05); Col-0 (WT) included as a reference.

We next checked if the obtained p*81F2*::*MT* T_2 lines are capable of producing brassinin. To this end, we grew respective lines, together with Col-0 and *cyp81f2 cyp71a12/13* plants, inoculated them with *Pc*BMM, and applied LC-MS/MS technique to detect this phytoalexin in respective extracts. Compound identity was supported by LC–MS/MS of the commercial brassinin standard. During analysis of samples from our transgenic plants, we detected in negative MS mode the deprotonated ion $[M–H]^-$ of brassinin at *m/z* 235.03729. When this ion was subjected to CID, the product-ion spectrum showed the characteristic fragmentation of dithiocarbamate/thio–type phytoalexins described for brassinin-class molecules (Fig. 4.2.2; Tab. 4.2) (Pedras et al., 2006; Bekešová et al., 2007). The same *m/z* signal was absent in samples prepared from Col-0

and *cyp81f2 cyp71a12/13* leaves, confirming its strict dependence on the introduced *DTC-MT* gene.

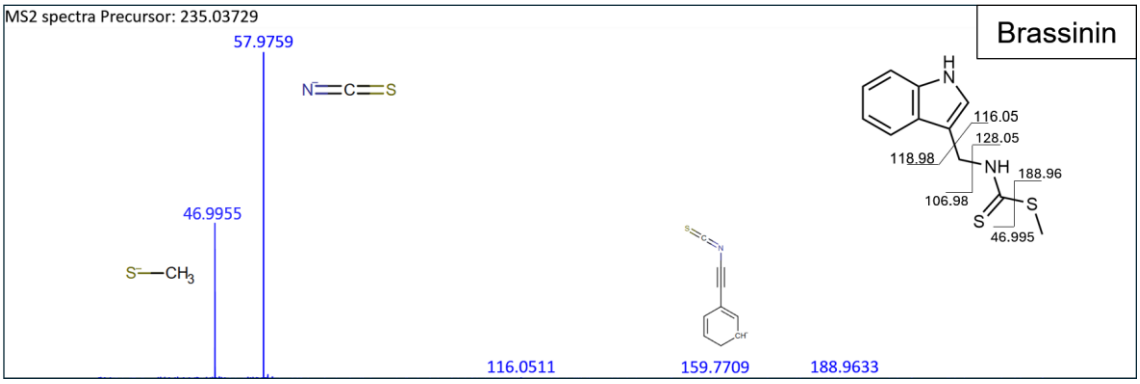

Fig. 4.2.2. LC-MS/MS spectrum of brassinin standard registered in negative-ion mode used as the reference for compound identification.

We used the single ion chromatograms representing brassinin to quantify the abundance of this phytoalexin in our samples as peak height (Fig. 4.2.3). This revealed that among the selected transgenic plants expressing p*81F2*::*MT* construct, line #5 is characterized with the highest brassinin accumulation levels. Overall, these results proved that the introduction of DTC-MT is sufficient to obtain brassinin biosynthesis in *A. thaliana*. Strikingly, we also found that brassinin accumulation in our lines did not correlate with gene expression levels, where line #1 revealed the highest values (Fig. 4.2.1). This could suggest that in the absence of BABG, the I3G hydrolysis constitutes a bottleneck in the pathway (Fig. 4.2.1).

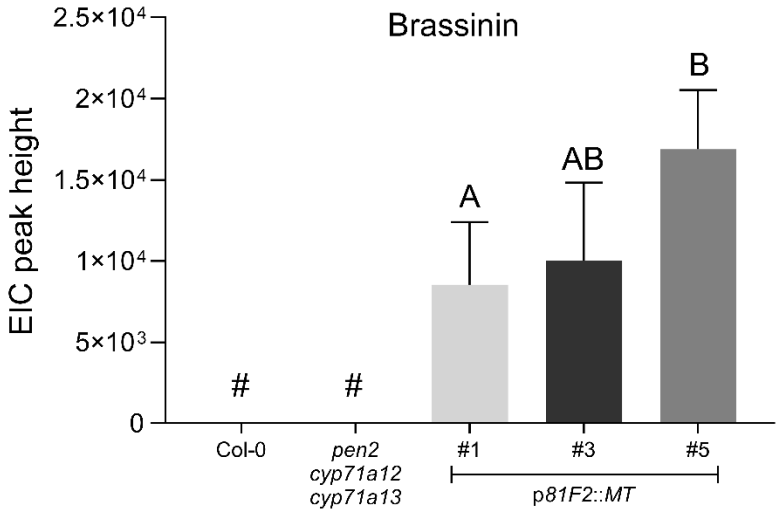

Fig. 4.2.3. LC-MS/MS quantification of brassinin in leaves of selected p*81F2*::*MT* T_2 lines in response to *Pc*BMM inoculation (72 hpi). Col-0 and *cyp81f2 cyp71a12/13* lines included as

negative controls. Bars show mean ± SD of biological replicates (n = 6); "#", below the detection limit; statistical groupings above bars indicate differences from one-way ANOVA with Tukey's post hoc test (α = 0.05).

4.2.2. Impact of BABG on brassinin biosynthesis in *A. thaliana*

To see if the introduction of the dedicated myrosinase, BABG, can increase brassinin accumulation, we transformed *pen2 cyp71a12/13* plants with p*81F2*::*MT*/p*PEN2*::*BABG* construct. We screened detached leaves of T_1 plants that survived glufosinate-treatment for accumulation of brassinin upon *Pc*BMM challenge using LC-MS/MS. We detected the respective *m/z* signal at 235.037 in the majority of samples analyzed. Quantification of this signal indicated leaves from T_1 plants #1, #3 and #9 accumulated brassinin at the highest concentrations (Fig. 4.2.4). These plants were selected for propagation and detailed testing in the T_2 generation.

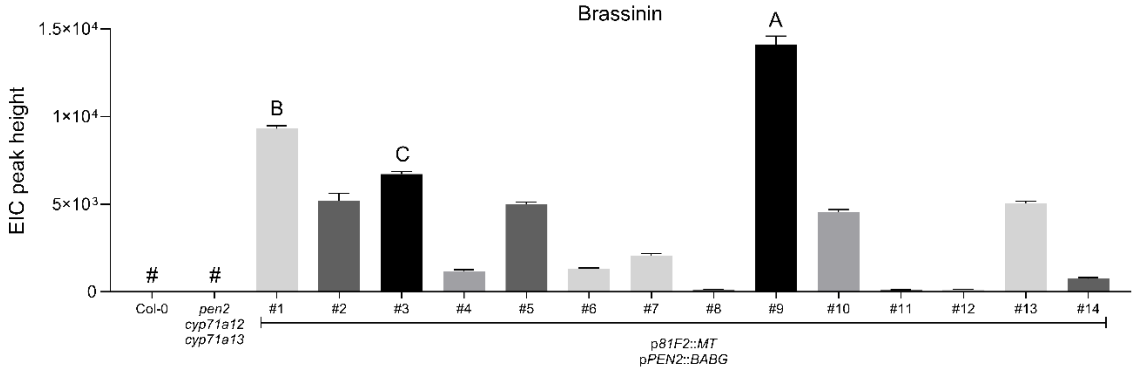

Fig. 4.2.4. LC-MS/MS quantification of brassinin in leaves of selected p*81F2*::*MT*/p*PEN2*::*BABG* T_2 lines in response to *Pc*BMM inoculation (72 hpi). Col-0 and *pen2 cyp71a12/13* lines included as negative controls. Bars show mean ± SD of biological replicates (n = 6); "#", below the detection limit; statistical groupings above bars indicate differences from one-way ANOVA with Tukey's post hoc test (α = 0.05).

We next grew the respective T_2 plants together with p*81F2*::*MT* #5, as a BABG-deficient reference line, and inoculated them with *Pc*BMM. We analyzed extracts obtained from leaves of these plants with LC-MS/MS to detect and quantify brassinin. Integration of respective single ion chromatograms revealed that two of our p*81F2*::*MT*/p*PEN2*::*BABG* lines (#1 and #9) accumulated significantly more brassinin than the p*81F2*::*MT* line (Fig. 4.2.5). The third two-gene line (#3) revealed brassinin

accumulation levels similar to these observed in the single gene line #5. Overall, this indicated that BABG is more potent than the native *A. thaliana* myrosinases in brassinin biosynthesis.

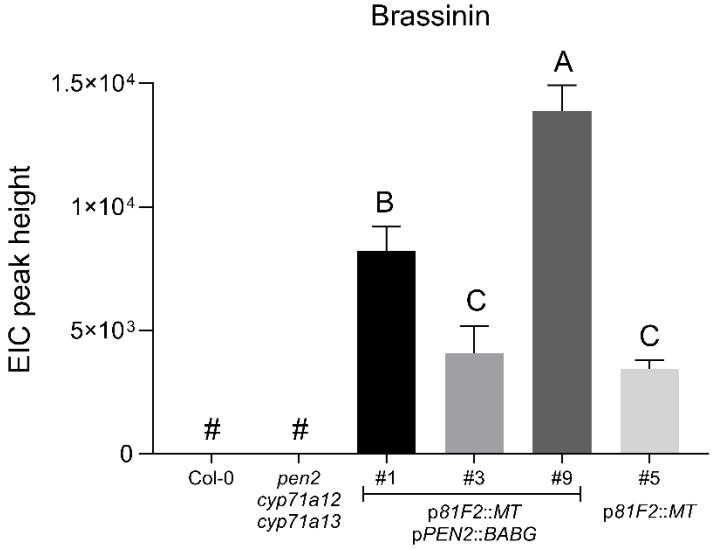

Fig. 4.2.5. LC-MS/MS quantification of brassinin in leaves of selected p*81F2*::*MT* and p*81F2*::*MT*/p*PEN2*::*BABG* T_2 lines in response to *Pc*BMM inoculation (72 hpi). Col-0 and *pen2 cyp71a12/13* lines included as negative controls. Bars show mean ± SD of biological replicates (n = 6); "#", below the detection limit; statistical groupings above bars indicate differences from one-way ANOVA with Tukey's post hoc test (α = 0.05).

We next checked for the presence of I3M-DTC-Glc, a side product obtained from I3M-DTC that was reported to accumulate in *N. benthamiana* leaves with engineered brassinin biosynthesis. This metabolite has been proposed to accumulate when DTC-MT-catalyzed final *S*-methylation of the I3M-DTC intermediate to brassinin is inefficient (Klein and Sattely, 2017). For this reason, this particular side product can be considered as a benchmark for efficiency of the DTC-MT-catalyzed step in the engineered brassinin pathway. Processing of our LC-MS/MS data revealed an *m/z* signal at 383.075 corresponding to the respective molecular ion. We also observed predicted fragmentation pattern for this ion (m/z 221, 187, 175) (Tab. 4.2). This signal was present in samples from leaves of Col-0 and our transgenic lines, but not from *pen2 cyp71A12/13* leaves (Fig. 4.2.6). This indicated that I3M-DTC formation requires either PEN2 or BABG myrosinase. Overall, the distribution of this metabolite across transgenic plants broadly resembled the pattern observed for brassinin (Fig. 4.2.5). In the transgenic lines, I3M-DTC-Glc-related signal was higher than in Col-0, but still relatively low-abundant,

indicating that the introduced DTC-MT enzyme supported efficient conversion of the I3M-DTC intermediate to brassinin.

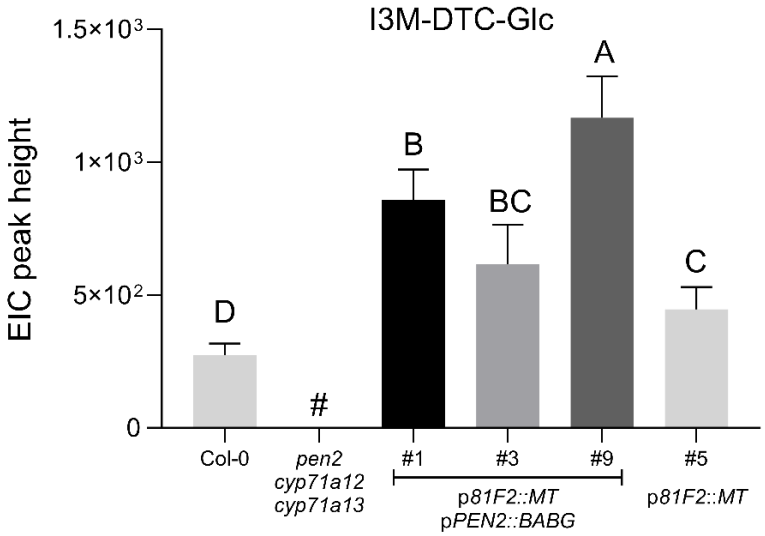

Fig. 4.2.6. LC-MS/MS quantification of I3M-DTC-Glc in leaves of selected p*81F2*::*MT* and p*81F2*::*MT*/p*PEN2*::*BABG* T_2 lines in response to *Pc*BMM inoculation (72 hpi). Col-0 and *pen2 cyp71a12/13* lines included as negative controls. Bars show mean ± SD of biological replicates (n = 6); "#", below the detection limit; statistical groupings above bars indicate differences from one-way ANOVA with Tukey's post hoc test ($\alpha = 0.05$).

Prompted by the identification of I3M-DTC-Glc in our samples, we also asked a question if other IGLs are processed by PEN2 and/or BABG to such conjugates. To address this, we searched for ions corresponding to hydroxy- and methoxy-I3M-DTC-Glc that could be derived from 4OHI3G and 1M- or 4MI3G. We were not able to identify any ions corresponding to the *m/z* of 4OH-I3M-DTC-Glc (calculated $[M-H]^-$ at 399.069). However, we found a *m/z* feature at 415.086 $[M+H]^+$ that we tentatively assigned as molecular ion of methoxy-I3M-DTC-Glc (Fig. 4.2.7). Identification of this product was further supported by the dominant fragmentation ions at *m/z* 253 and 176 (Tab. 4.2). However, MS analysis did not enable us to discriminate between the position 1- or 4- of the methoxy group on the indole core. Quantification of the abundance of the molecular ion revealed that this product is already present in Col-0 and its accumulation decreases with mutation in the *PEN2* gene.

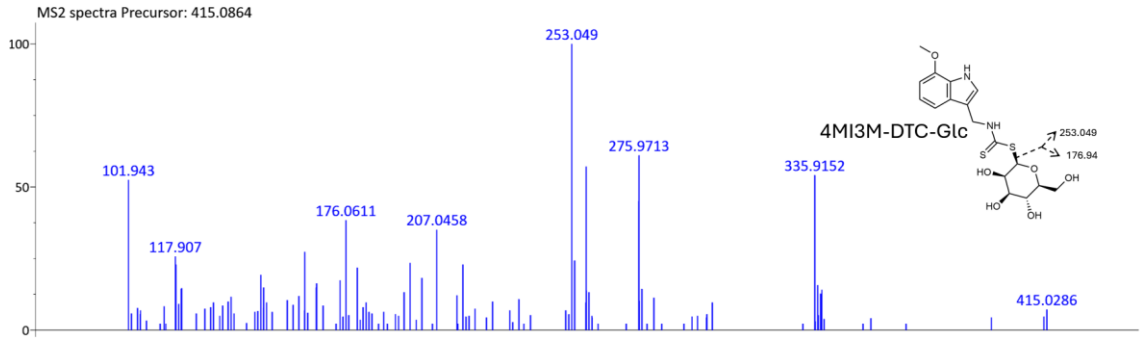

Fig. 4.2.7. LC-MS/MS spectrum of signal assigned to 4MI3M-DTC-Glc recorded in positive ionization mode. The precursor ion $[M+H]^+$ at *m/z* 415.0864, and the observed fragment ions matches predicted fragmentation pattern.

Our analysis also indicated that the introduction of the p*81F2*::*MT*/p*PEN2*::*BABG* construct increased the accumulation of methoxy-DTC-Glc. Interestingly, the abundance of the respective *m/z* signal in samples from the single transgenic line, generated in the *cyp81f2 cyp71a12/13* mutant background, was clearly lower than in Col-0 samples (Fig. 4.2.8). This indicated that the observed derivative originates from 4MI3G, whose accumulation is strongly reduced with the mutation in the *CYP81F2* gene. For this reason, we refer to this metabolite as 4MI3M-DTC-Glc.

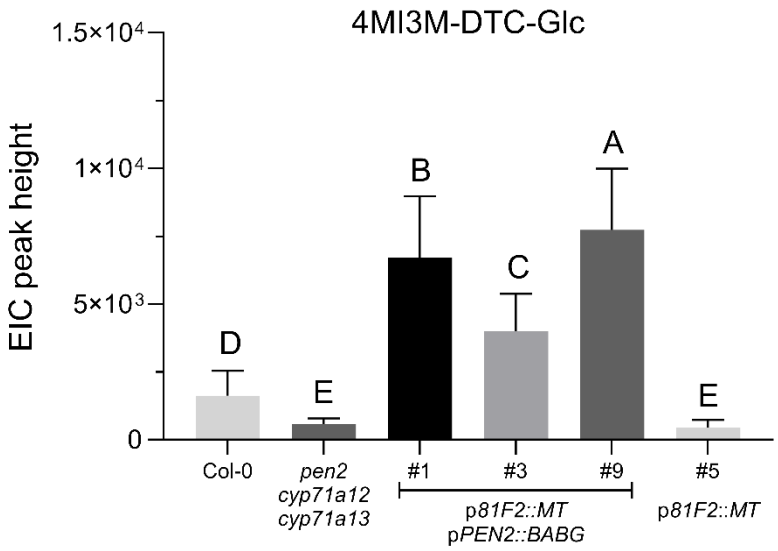

Fig. 4.2.8. LC-MS/MS quantification of 4MI3M-DTC-Glc in leaves of selected p*81F2*::*MT* and p*81F2*::*MT*/p*PEN2*::*BABG* T_2 lines in response to *Pc*BMM inoculation (72 hpi). Col-0 and *pen2 cyp71a12/13* lines included as negative controls. Bars show mean ± SD of biological replicates (n = 6); statistical groupings above bars indicate differences from one-way ANOVA with Tukey's post hoc test ($\alpha = 0.05$).

Similar to analysis of our camalexin producing lines, we also searched our LC-MS/MS data for signals that could represent putative brassinin derivatives. We first checked for ions that are exclusively present in samples from *Pc*BMM inoculated leaves of our transgenic plants and were not detectable or low-abundant in samples from Col-0 and *pen2 cyp71a12/13* lines. Later on, we checked if the selected *m/z* values could be assigned to brassinin derivatives. With this approach, we identified *m/z* signal at 251.031. The difference in molecular weight between this signal and the molecular ion of brassinin indicates that it can represent hydroxybrassinin (Tab. 4.2). This assignment was additionally supported by the respective fragmentation pattern (Tab. 4.2; Fig. 4.2.9).

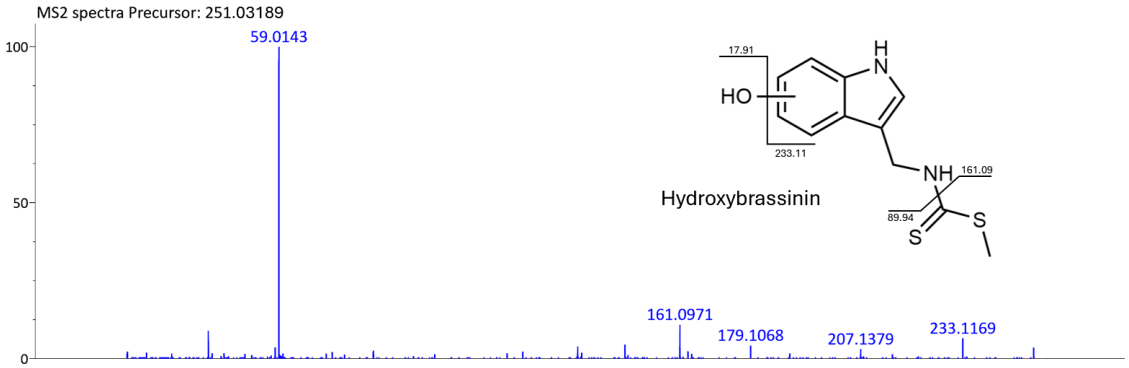

Fig. 4.2.9. LC-MS/MS spectrum of signal assigned to hydroxybrassinin recorded in negative ionization mode. The precursor ion is $[M-H]^-$ at m/z 251.031, and the observed fragment ions matches predicted fragmentation pattern.

Quantification of the abundance of this ion in our samples indicated that, in contrast to brassinin, which reached its highest level in transgenic line #9 (Fig. 4.2.5), hydroxy-brassinin accumulated most strongly in line #5 (Fig. 4.2.10). This pattern suggests line-specific differences in the conversion of brassinin to hydroxybrassinin. According to our initial selection criterion, the respective signal remained below the detection limit in Col-0 and in the *pen2 cyp71a12/13* triple mutant.

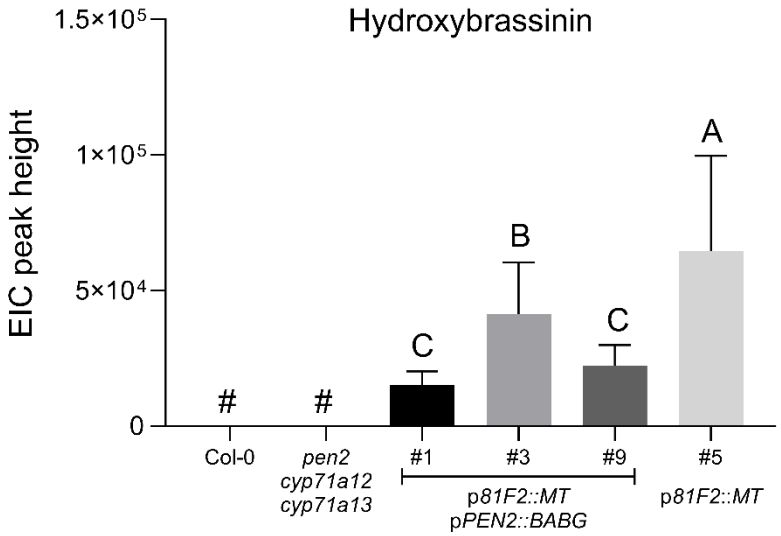

Fig. 4.2.10. LC-MS/MS quantification of hydroxybrassinin in leaves of selected p*81F2*::*MT* and p*81F2*::*MT*/p*PEN2*::*BABG* T_2 lines in response to *Pc*BMM inoculation (72 hpi). Col-0 and *pen2 cyp71a12/13* lines included as controls. Bars show mean ± SD of biological replicates (n = 6); "#", below the detection limit; statistical groupings above bars indicate differences from one-way ANOVA with Tukey's post hoc test (α = 0.05).

After detecting hydroxybrassinin, we asked whether this metabolite could be further conjugated with hexose, as reported for hydroxylated camalexin in *A. thaliana*. In accordance with this assumption, our screen for brassinin derivatives revealed signal at *m/z* 413.08, which corresponded to the molecular weight of hydroxybrassinin conjugated with a hexose and yielded expected fragment ions at *m/z* 251, 233, 207 (Tab. 4.2). Our quantitative analysis revealed that accumulation of this putative hexoside of hydroxybrassinin resembled that of hydroxybrassinin, with the highest level in the single gene line #5 and lower accumulation in the p*81F2*::*MT*/p*PEN2*::*BABG* plants (Fig. 4.2.11). This metabolite remained below the detection limit in Col-0 and in the *pen2 cyp71a12/13* plants.

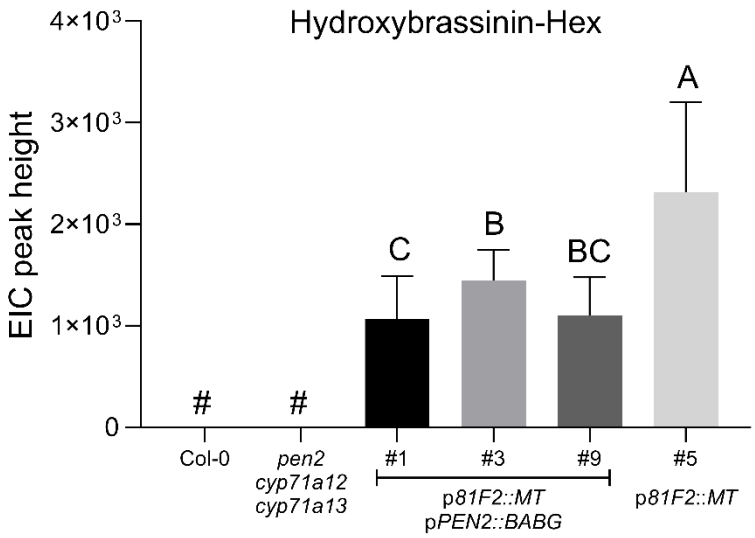

Fig. 4.2.11. LC-MS/MS quantification of hydroxybrassinin-Hex in leaves of selected p*81F2*::*MT* and p*81F2*::*MT*/p*PEN2*::*BABG* T_2 lines in response to *Pc*BMM inoculation (72 hpi). Col-0 and *pen2 cyp71a12/13* lines included as controls. Bars show mean ± SD of biological replicates (n = 6); "#", below the detection limit; statistical groupings above bars indicate differences from one-way ANOVA with Tukey's post hoc test ($\alpha = 0.05$).

Strikingly, our search for brassinin derivatives did not reveal any $[M+H]^+$ ions at *m/z* 267.062 corresponding to the calculated molecular ion 4M-brassinin. We expected the presence of such a compound based on the detection of 4MI3M-DTC-Glc in our samples (Tab. 4.2; Fig. 4.2.8). The fact that we did not identify the respective ion suggests 4MI3M-DTC is not accepted as a substrate by DTC-MT and the whole pool of this compound is glycosylated.

Finally, we checked if brassinin can be converted by any of the native *A. thaliana* enzymes to spirobrassinin or cyclobrassinin, which are known to accumulate in *B. rapa*. However, despite a careful search, we were not able to identify $[M+H]^+$ signals at *m/z* 251.030 and 235.035, which would correspond to molecular ions of spirobrassinin and cyclobrassinin, respectively.

4.2.3. Impact of BABG expression on GLs metabolism in p*81F2*::*MT*/p*PEN2*::*BABG* plants

We asked the question whether BABG is specific for brassinin pathway or if it can also contribute to the formation of other IGL-derived products, e.g., those formed in the PEN2 pathway (Fig. 1.7). To test this, we checked the extracts from *Pc*BMM-infected

leaves of our transgenic plants for accumulation of two such compounds, I3A and 4OGlcI3F. Due to the availability of the I3A standard as well as its strong fluorescence, we used LC-FLD to specifically detect and quantify this compound. Our analysis revealed enhanced accumulation of I3A in samples from transgenic lines relative to Col-0 and the *pen2 cyp71a12/13* controls (Fig. 4.2.12). This indicated that BABG significantly contributes to the hydrolysis of I3G in our transgenic plants.

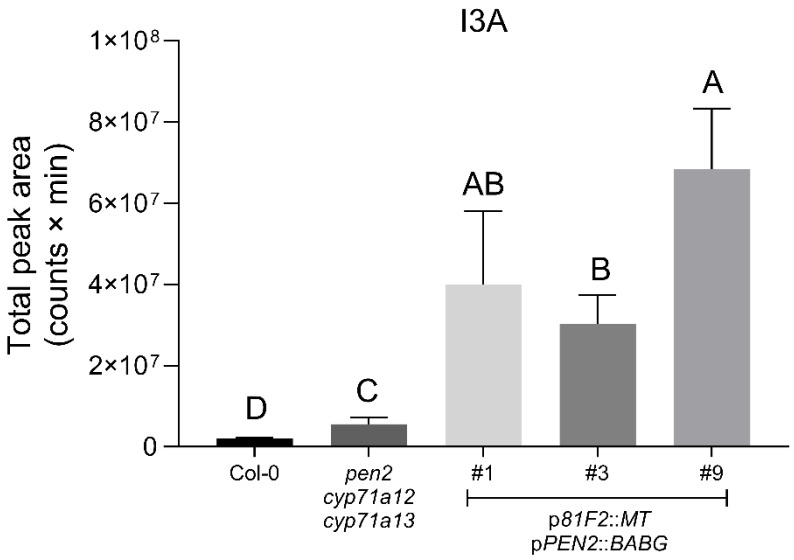

Fig. 4.2.12. LC-FLD quantification of I3A in leaves of selected p*81F2*::*MT*/p*PEN2*::*BABG* T_2 lines in response *Pc*BMM inoculation (72 hpi). Col-0 and *pen2 cyp71a12/13* lines included as controls. Bars show mean ± SD of biological replicates (n = 6); statistical groupings above bars indicate differences from one-way ANOVA with Tukey's post hoc test (α = 0.05).

For detection and quantification of 4OGlcI3F, we used LC-MS/MS supported with the respective synthetic standard. The presence of this compound in our samples was confirmed with the detection of its molecular ion (*m/z* 339.100) at the respective RT. Additionally, we verified its characteristic fragmentation pattern (Fig. 4.2.13).

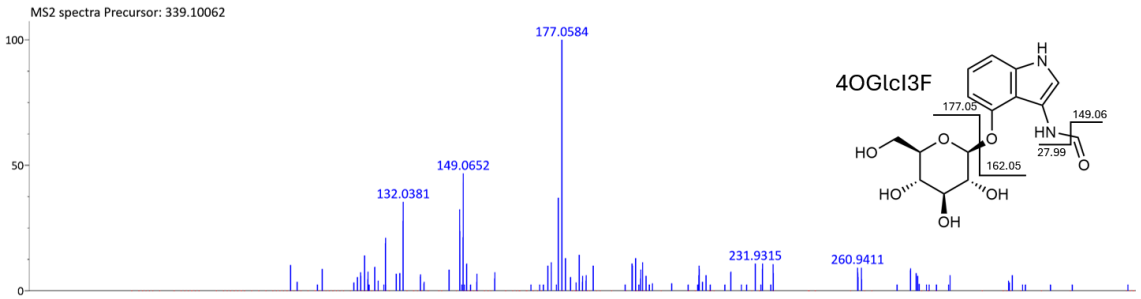

⟶ Fig. 4.2.13. LC-MS/MS spectrum of 4OGlcI3F standard recorded in the positive ion mode. This spectrum was used as a reference for compound identification.

Quantification of this signal revealed that 4OGlcI3F accumulated most strongly in Col-0, remained detectable in the p*81F2*::*MT*/p*PEN2*::*BABG* plants, and was not detected in the *pen2 cyp71a12/13* and in samples derived from line #5. (Fig. 4.2.14). This absence can be attributed to the lack of PEN2 and CYP81F2 enzymes that are necessary for the formation of 4OGlcI3F. Reduced accumulation of this metabolite in the two gene transgenic plants as compared with Col-0 suggests that PEN2 is more efficient in the hydrolysis of 4MI3G as compared with BABG.

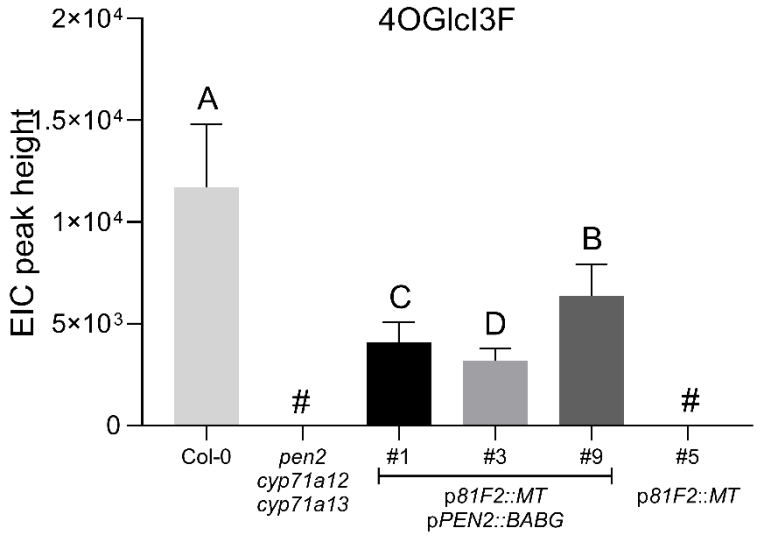

Fig. 4.2.14. LC-MS/MS quantification of 4OGlcI3F in leaves of selected p*81F2*::*MT* and p*81F2*::*MT*/p*PEN2*::*BABG* T_2 lines in response to *Pc*BMM inoculation (72 hpi). Col-0 and *pen2 cyp71a12/13* lines included as controls. Bars show mean ± SD of biological replicates (n = 6); "#", below the detection limit; statistical groupings above bars indicate differences from one-way ANOVA with Tukey's post hoc test ($\alpha = 0.05$).

Our quantitative analysis of I3A and 4OGlcI3F indicated that *BABG* expression under *PEN2* promoter leads to enhanced hydrolysis of IGLs. Reduction in the accumulation of these compounds could affect plant fitness due to their important physiological functions, which are not limited to plant immunity. On the other hand, the reported *de novo* epidermal IGL synthesis during infection could buffer such a drain; however, this is not clear. Similarly, we wondered if BABG is IGL specific or if it can also metabolize AGLs, affecting their accumulation in our transgenic plants. To address

these issues, we compiled a targeted LC-MS/MS search and quantification of IGL and AGL-related signals in samples from *Pc*BMM infected leaves of *pen2 cyp71a12/13* background, and p*81F2*::*MT*/pPEN2::*BABG* transgenic lines. Identification followed standard GL practice: comparison of exact ion masses and diagnostic GL fragments in negative ionization mode at *m/z* 97, 195, 241, 259, and 275 together with subclass-specific neutral losses and side-chain-derived product ions (Table 4.3). This approach allowed us to identify signals corresponding to GLs.

Table 4.3. List of detected GLs in leaf extracts from lines expressing p*81F2*::*MT*/p*PEN2*::*BABG* constructs.

No.	RT [min]	Ionization	Compound name	Molecular formula	Exact ion mass		Error [ppm]	Fragmentation
					Measured	Calculated		
1	5	$[M-H]^-$	indol-3-ylmethyl GL (I3G)	$C_{16}H_{20}N_2O_9S_2$	447.053612	447.053746	-0.30	**447**, 394, 313, 259, 205, 152, 97
2	8.7	$[M-H]^-$	N-methoxyindol-3-ylmethyl GL (1MI3G)	$C_{17}H_{22}N_2O_{10}S_2$	477.065217	477.064311	1.90	**477**, 446, 421, 365, 341, 315, 259, 97
3	2.1	$[M-H]^-$	4-hydroxyindol-3-ylmethyl GL (4OHI3G)	$C_{16}H_{20}N_2O_{10}S_2$	463.047596	463.048661	-2.30	**463**, 374, 221, 157, 97
4	7	$[M-H]^-$	4-methoxyindol-3-ylmethyl GL (4MI3G)	$C_{17}H_{22}N_2O_{10}S_2$	477.064597	477.064311	0.60	**477**, 425, 373, 345, 307, 259, 205, 97
5	1.8	$[M-H]^-$	3-(methylsulfinyl)propyl GL	$C_{11}H_{21}NO_{10}S_3$	422.024723	422.025483	-1.80	**422**, 358, 196, 97
6	1.81	$[M-H]^-$	4-(methylsulfinyl) GL	$C_{12}H_{23}NO_{10}S_3$	436.041656	436.041133	1.20	**436**, 372, 195, 97
7	2.68	$[M-H]^-$	4-(methylsulfinyl)butyl GL	$C_{12}H_{23}NO_{10}S_3$	436.040828	436.041133	-0.70	**436**, 372, 178, 97
8	1.86	$[M-H]^-$	5-(methylsulfinyl)pentyl GL	$C_{13}H_{25}NO_{10}S_3$	450.057863	450.056783	2.40	**450**, 386, 285, 194, 97
9	1.94	$[M-H]^-$	6-(methylsulfinyl)hexyl GL	$C_{14}H_{27}NO_{10}S_3$	464.071412	464.072433	-2.20	**464**, 400, 274, 229, 149, 97
10	1.98	$[M-H]^-$	7-(methylsulfinyl)heptyl GL	$C_{15}H_{29}NO_{10}S_3$	478.089183	478.088083	2.30	**478**, 414, 252, 97
11	2.48	$[M-H]^-$	8-(methylsulfinyl)octyl GL	$C_{16}H_{31}NO_{10}S_3$	492.102798	492.103733	-1.90	**492**, 428, 234, 97
12	7.2	$[M-H]^-$	8-(methylsulfonyl)octyl GL	$C_{16}H_{31}NO_{11}S_3$	508.099969	508.098648	2.60	**508**, 444, 328, 275, 204, 97

13	7.8	$[M-H]^-$	9-(methylsulfinyl)nonyl GL	$C_{17}H_{33}NO_{10}S_3$	506.118017	506.119383	-2.70	**506**, 442, 248, 97
14	8.73	$[M-H]^-$	6-(methylthio)hexyl GL	$C_{14}H_{27}NO_9S_3$	448.078773	448.077519	2.80	**448**, 363, 243, 141, 97
15	9.78	$[M-H]^-$	7-(methylthio)heptyl GL	$C_{15}H_{29}NO_9S_3$	462.091829	462.093169	-2.90	**462**, 382, 275, 220, 97
16	10.6	$[M-H]^-$	8-(methylthio)octyl GL	$C_{16}H_{31}NO_9S_3$	476.110009	476.108819	2.50	**476**, 275, 259, 195, 97
17	11.4	$[M-H]^-$	9-(methylthio)nonyl GL	$C_{17}H_{33}NO_9S_3$	490.123194	490.124469	-2.60	**490**, 275, 241, 195, 97

First, we focused on IGLs and compared their accumulation across tested genotypes. Our analysis showed that expression of our construct leads to reduced accumulation of I3G, which corresponds with the elevated formation of I3A observed in the same lines (Fig. 4.2.15). Unlike I3G, accumulation levels of 4OHI3G and 4MI3G remained unaffected in the p*81F2*::*MT*/p*PEN2*::*BABG* lines. Strikingly, we observed an elevated 1MI3G signal in samples from transgenic plants as compared with *pen2 cyp71a12/13* samples. Overall, our analysis did not reveal any drastic reduction in the total IGL accumulation caused by BABG activity.

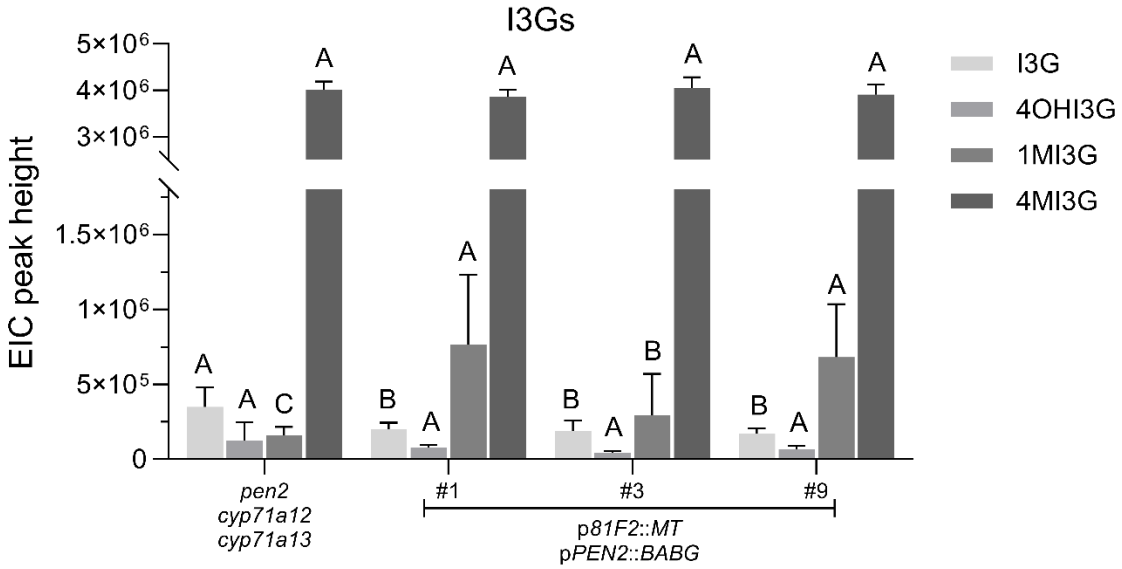

Fig. 4.2.15. LC-MS/MS quantification of I3Gs in leaves of selected p*81F2*::*MT*/p*PEN2*::*BABG* T_2 lines in response to *Pc*BMM inoculation (72 hpi). *pen2 cyp71a12/13* line included as reference. Bars show mean ± SD of biological replicates (n = 6); statistical groupings above bars indicate differences within each metabolite from one-way ANOVA with Tukey's post hoc test ($\alpha = 0.05$).

Next, we compared the accumulation of the identified representatives of the methylthio (MT)-alkyl class of AGLs. Overall, we did not note any consistent changes in the accumulation of these compounds among our transgenic lines as compared with the *pen2 cyp71a12/13* background line (Fig. 4.2.16).

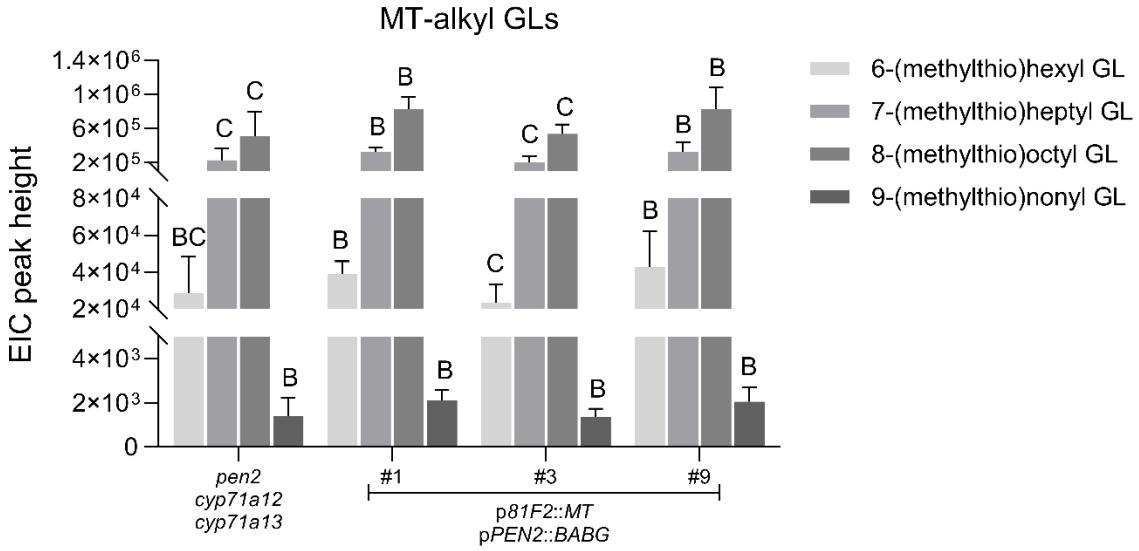

Fig. 4.2.16. LC-MS/MS quantification of MT-alkyl GLs in leaves of selected p*81F2*::*MT*/p*PEN2*::*BABG* T_2 lines in response to *Pc*BMM inoculation (72 hpi). *pen2 cyp71a12/13* line included as reference. Bars show mean ± SD of biological replicates (n = 6); statistical groupings above bars indicate differences within each metabolite from one-way ANOVA with Tukey's post hoc test (α = 0.05).

We also compared the accumulation of methylsulfinyl (MSO)-alkyl AGLs across genotypes. Our p*81F2*::*MT*/p*PEN2*::*BABG* lines showed line-specific shifts in accumulation of particular members of this GLs sub-class rather than a uniform trend, with some MSO species matching or exceeding the *pen2 cyp71a12/13* levels and others decreased (Fig. 4.2.17).

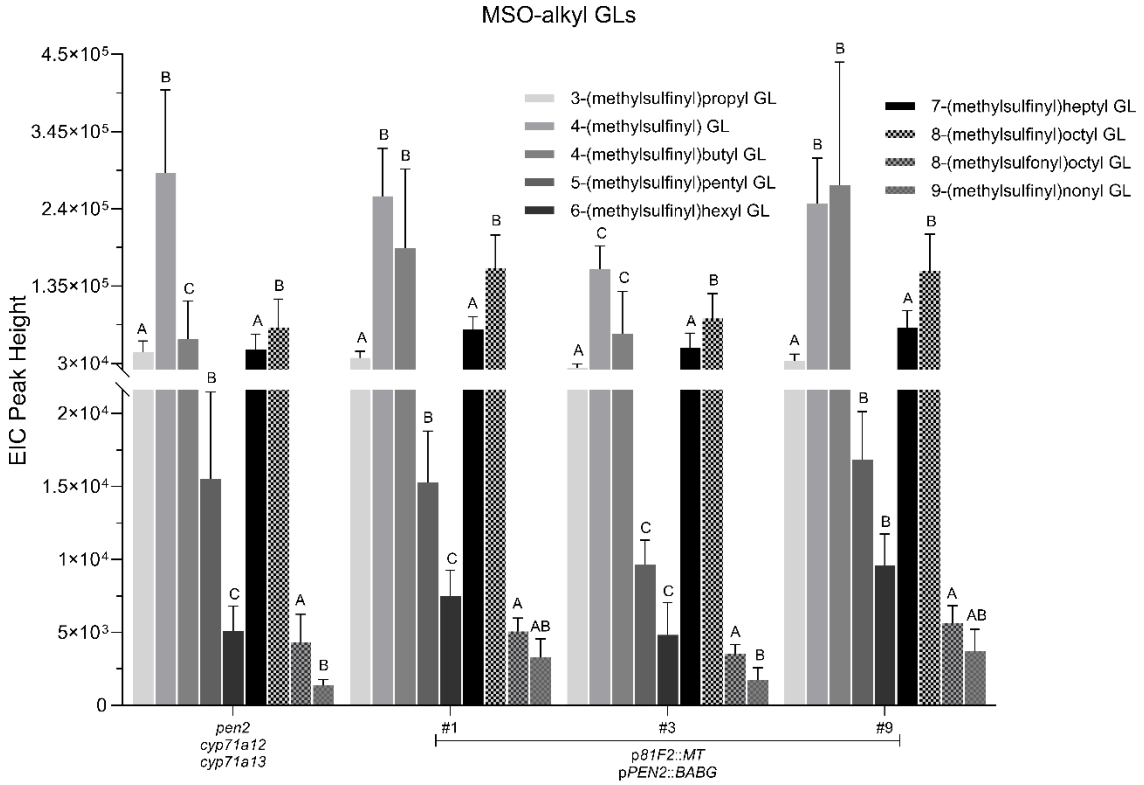

Fig. 4.2.17. LC-MS/MS quantification of MSO-alkyl GLs in leaves of selected p*81F2*::*MT*/p*PEN2*::*BABG* T_2 lines in response to *Pc*BMM inoculation (72 hpi). *pen2 cyp71a12/13* line included as reference. Bars show mean ± SD of biological replicates (n = 6); statistical groupings above bars indicate differences within each metabolite from one-way ANOVA with Tukey's post hoc test (α = 0.05).

Overall, our analysis of GL accumulation revealed that BABG has a moderate impact on I3G and 1MI3G accumulation. The reduced I3G levels matched with elevated I3A accumulation (Fig. 4.2.15, 4.2.16, 4.2.17), while an increase in 1MI3G accumulation was, in a sense, unexpected. In contrast to IGLs, the accumulation of AGLs was not reproducibly affected in the transgenic lines investigated.

4.2.4. Pathogen resistance of p*81F2*::*MT*/p*PEN2*::*BABG* transgenic plants

Having confirmed successful brassinin biosynthesis in our p*81F2*::*MT*/p*PEN2*::*BABG* lines, we next tested whether this output translates into reduced pathogen proliferation. To address this, we inoculated these plants, together with Col-0 and *pen2 cyp71a12/13* control plants, with spores of *Pc*BMM. Leaf samples were collected, and *Pc*BMM biomass was quantified at 5 dpi by qPCR as the ratio of fungal *β-tubulin* to the plant reference *AtAAP1* in total DNA samples (Fig. 4.2.18). In line with the

reported susceptible phenotype of the *pen2 cyp71a12/13* plants, fungal biomass was clearly higher in this line as compared with Col-0. All three independent p*81F2*::*MT*/p*PEN2*::*BABG* lines displayed a significant reduction in *Pc*BMM biomass relative to *pen2 cyp71a12/13*. Among these, line #3 remained above Col-0 (group B), while lines #1 and #9 fell into an intermediate group (AB) that was not statistically distinguishable from either Col-0 or line #3. Overall, engineering the brassinin module suppressed *Pc*BMM proliferation in the susceptible *pen2 cyp71a12/13* background, with variation consistent with differences in brassinin output.

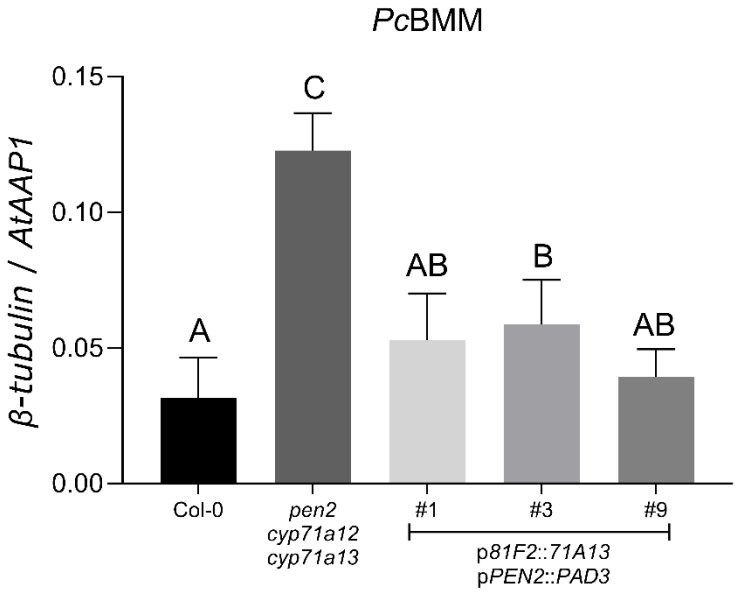

Fig. 4.2.18. *Pc*BMM biomass estimated by qPCR in leaves of indicated genotypes at 5 dpi; values are the ratio of *Pc*BMM *β-tubulin* to *A. thaliana AAP1*; bars show mean ± SD; uppercase letters indicate one-way ANOVA with Tukey's HSD groupings (α = 0.05).

4.2.5. Introducing cyclobrassinin and spirobrassinin biosynthesis in *A. thaliana*

After evaluating and confirming brassinin biosynthesis in our transgenic p*81F2*::*MT*/p*PEN2*::*BABG* lines, we selected line #9, which showed the highest relative brassinin production, which correlated with reduced *Pc*BMM biomass abundance, to additionally engineer cyclobrassinin and spirobrassinin biosynthesis. To convert brassinin into these downstream sulfur-containing indole phytoalexins, we decided to additionally introduce *B. rapa CYP71CR1* or *CYP71CR2* genes, encoding two cytochrome P450 enzymes reported to catalyze alternative *S*-heterocyclizations on the

brassinin scaffold that diversify the pathway toward spiro- and cyclo-derivatives (Klein and Sattely, 2015, 2017). To make these genes co-expressed with *DTC-MT,* we decided to drive their expression with the same *CYP81F2* promoter. As the parental p*81F2*::*MT*/p*PEN2*::*BABG* #9 line carries the glufosinate-resistance marker, we used CYP71CR-transformation vectors carrying a kanamycin resistance gene. To keep nomenclature explicit and traceable, we refer to the resulting plant variants as p*81F2*::*71CR1* and p*81F2*::*71CR2*.

To verify whether adding either *CYP71CR1* or *CYP71CR2* is sufficient to extend the previously introduced brassinin cassette towards downstream phytoalexins, we inoculated detached leaves of kanamycin-resistant individual T_1 plants derived from the parental p*81F2*::*MT*/p*PEN2*::*BABG* line #9 transformed with *CYP71CR1* or *CYP71CR2* constructs with *Pc*BMM spores. We collected the leaves 72 hpi and screened the obtained extracts with LC-MS/MS for the appearance of the expected brassinin-conversion products. Because ionization efficiency differs across crucifer phytoalexins, we checked for spirobrassinin and cyclobrassinin primarily in positive-ion mode, while brassinin was monitored in negative-ion mode, as in previous analyses. Positive-ion mode sensitivity for many crucifer phytoalexins has been reported previously, supporting this acquisition strategy (Pedras et al., 2006).

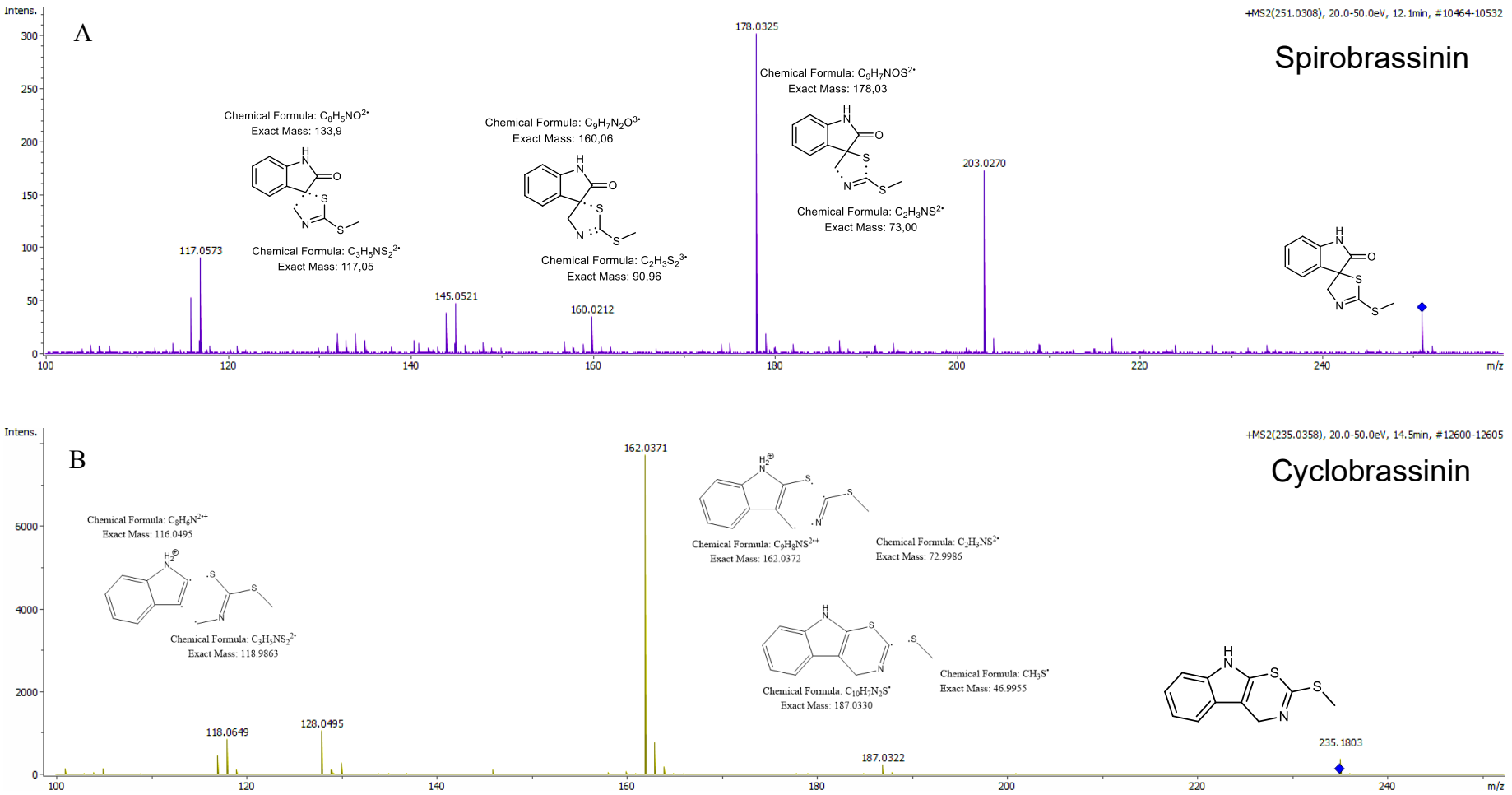

Fig. 4.2.19. LC-MS/MS spectra recorded in positive ionization mode for spirobrassinin (A) and cyclobrassinin (B) molecular ions $[M+H]^+$. Precursor molecular ions marked with blue diamonds. Main product-ions represented by respective structures.

We started our analysis with p*81F2*::*71CR1* plants. We detected the expected spirobrassinin molecular ion $[M+H]^+$ at *m/z* 251.0308 across samples from independent T_1 individuals, (Fig. 4.2.19A, 4.2.20A; Tab. 4.2). This signal yielded reproducible MS/MS fragment ions that were consistent with the postulated fragmentation scheme, including a dominant product ion at *m/z* 178.03, alongside the additional structure-informative fragments (for example *m/z* 160.06 and 117.05) (Pedras et al., 2006). The presence of this ion pattern in the same chromatographic peak as the precursor provides direct MS/MS support that the detected feature corresponds to spirobrassinin rather than an isobaric interference. In contrast, the parental p*81F2*::*MT*/p*PEN2*::*BABG* #9 line did not show this spirobrassinin-associated signal above the applied detection threshold in the same analytical run, supporting that the signal arises from the introduced CYP71CR1-dependent conversion step rather than from background.

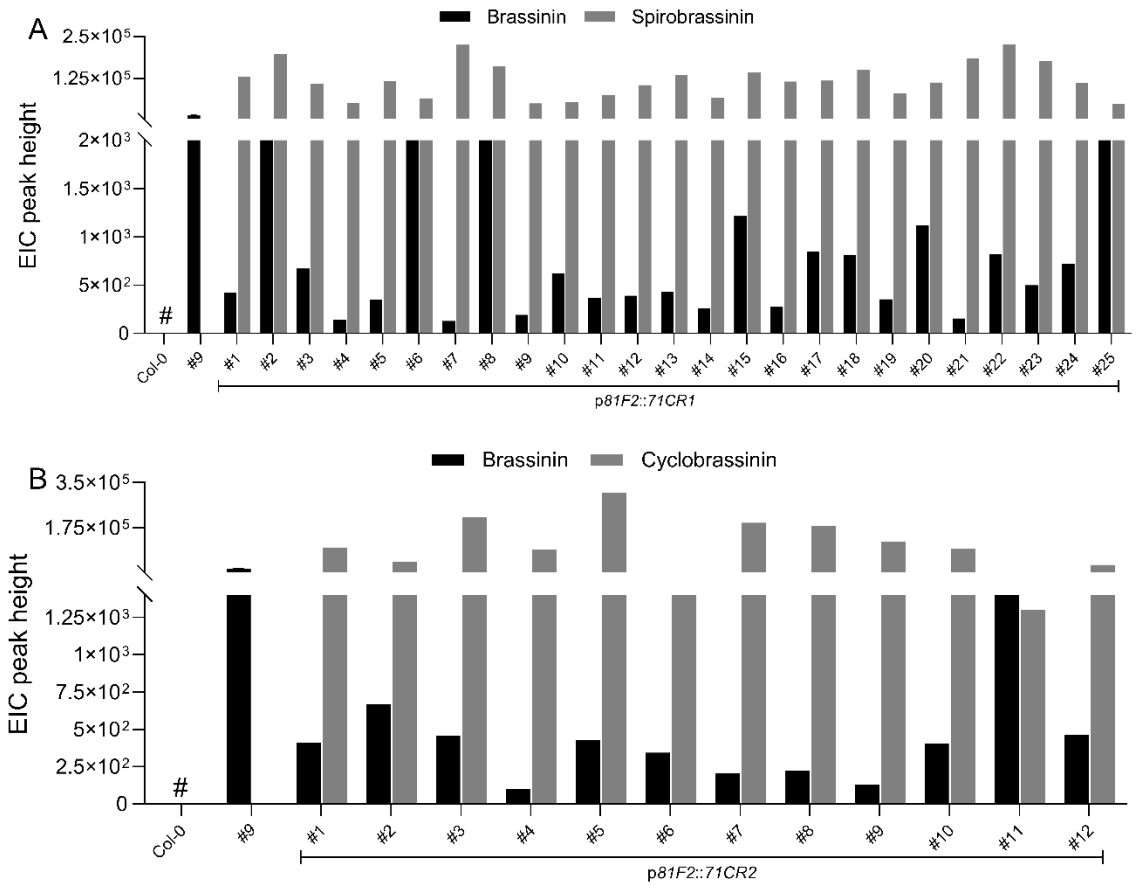

Fig. 4.2.20. LC-MS/MS-based quantification of brassinin and spirobrassinin (A) or cyclobrassinin (B), in leaves of *Pc*BMM inoculated (72hpi) T_1 p*81F2*::*71CR1* and p*81F2*::*71CR2* plants, respectively. Col-0 and parental p*81F2*::*MT*/p*PEN2*::*BABG* line #9 were used as controls.

Similarly, in samples from infected p*81F2*::*71CR2* leaves we detected, using positive-ion mode, a clear signal corresponding to cyclobrassinin-associated molecular ion $[M+H]^+$ (measured *m/z* 235.0358), whereas the parental #9 line lacked this signal under the same acquisition and processing settings (Fig. 4.2.20B; Tab. 4.2). Moreover, this putative molecular ion signal was accompanied by the expected fragmentation pattern reported for this crucifer phytoalexin, including ions at *m/z* 187, 162, 128 (Pedras et al., 2006; Klein and Sattely, 2015) (Fig. 4.2.19B; Tab. 4.2). Overall, this confirmed the expected CYP71CR2-dependent brassinin cyclization *in planta*.

In both types of lines, samples from multiple independent T_1 individuals displayed a spirobrassinin-associated or cyclobrassinin-associated signal while maintaining clearly detectable brassinin accumulation (Fig. 4.2.20). The concurrent presence of brassinin indicates that the production efficiency of this phytoalexin exceeds the metabolic capacity of the introduced CYP71CR enzymes.

DISCUSSION

5.1. Rationale for epidermal, pathogen-inducible pathway engineering

The biological effectiveness of defense metabolites is determined not only by their chemical properties but also by the spatial and temporal context of their accumulation. In *A. thaliana*, this principle is well illustrated by the PEN2-dependent branch of IGL metabolism, in which IGL hydrolysis, GSH conjugation, and product export occur locally at pathogen contact sites within epidermal cells, coordinated through the infection-triggered relocalization of PEN2 and the ABC transporter PEN3 (Lipka et al., 2005; Stein et al., 2006; Bednarek et al., 2009). These observations indicate that the defense contribution of IGL-derived metabolites is strictly dependent on their site of production.

This principle guided the engineering strategy applied in this study. Two Trp-metabolic defense branches, the native camalexin pathway and the foreign brassinin pathway originating from *B. rapa*, were reconstructed using the pathogen-inducible, epidermis-active *CYP81F2* and *PEN2* promoters. The *pen2 cyp71a12/13* triple mutant was selected as the primary engineering background because it is deficient in two major Trp-derived defense branches: PEN2-dependent IGL activation and CYP71A12/CYP71A13-dependent IAOx metabolism. This sensitized background was considered advantageous for two reasons. First, metabolic products of the introduced pathways could be detected and quantified without interference from the corresponding endogenous activities. Second, the elevated susceptibility of this mutant to fungal pathogens, particularly *Pc*BMM, provided a defined resistance baseline against which defense contributions of the engineered branches could be assessed (Sanchez-Vallet et al., 2010; Pastorczyk et al., 2020)

5.2. Camalexin engineering

5.2.1. *CYP71A13* expression reopens the camalexin branch

To test the pathway design, *CYP71A13* was reintroduced first as a single transgene under the *CYP81F2* promoter. This allowed the contribution of the branch entry step to

be assessed independently before the terminal enzyme was added. In *Pc*BMM-inoculated p*81F2*::*71A13* plants, camalexin accumulated significantly above the background level observed in *pen2 cyp71a12/13*, which remained below the detection limit (Fig. 4.1.3). This is consistent with the established role of CYP71A13 in converting IAOx to IAN during camalexin biosynthesis as well as with the presence of other required enzymes, including PAD3 in *pen2 cyp71a12/13* background (Nafisi et al., 2007). flg22-treated transgenics did not accumulate detectable camalexin. This distinction between *Pc*BMM and flg22 responses suggests that additional signals or co-substrates generated during *Pc*BMM colonization are needed to drive the branch beyond the entry step. Whether this reflects the involvement of infection-specific co-factors, stronger induction kinetics, or differences in precursor availability between the two treatments was not resolved.

Of note, camalexin concentrations in the p*81F2*::*71A13* plants remained clearly below those recorded in Col-0 under the same infection conditions (Fig. 4.1.3). This indicated that restoring the entry step alone was not sufficient for efficient camalexin formation. In these plants, the terminal biosynthetic step still depended on the endogenous *PAD3* locus, whose expression was variable among the selected transgenic lines (Fig. 4.1.2). In addition, camalexin biosynthesis in *A. thaliana* has been reported to involve mesophyll-localized metabolon-like association of the participating P450 enzymes at the ER membrane, with physical interaction between CYP71A13 and PAD3 contributing to efficient substrate channeling (Mucha et al., 2019). It is therefore conceivable that epidermal *CYP71A13* expression, in the absence of locally co-expressed *PAD3*, was insufficient to reconstitute efficient channeling of intermediates through the late part of the pathway. These observations provided the rationale for testing whether co-expression of *PAD3* under an epidermal promoter could improve local pathway completion.

5.2.2. Epidermal co-expression of *PAD3* increases camalexin accumulation

The limited camalexin output in the p*81F2*::*71A13* plants indicated that restoring the branch entry step alone was not sufficient for efficient product formation. To test whether reinforcement of the terminal biosynthetic step could improve pathway completion at the infection site, *PAD3* was introduced under the *PEN2* promoter alongside with *CYP71A13*. In the resulting p*81F2*::*71A13*/p*PEN2*::*PAD3* plants, camalexin was clearly induced in response to *Pc*BMM, whereas it remained below the

detection limit after flg22 treatment (Fig. 4.1.4, 4.1.5). Addition of PAD3 enzyme therefore did not change the requirement for pathogen infection.

Direct comparison of p*81F2*::*71A13*/p*PEN2*::*PAD3* and p*81F2*::*71A13* lines under *Pc*BMM infection revealed consistently higher camalexin accumulation in the two-gene plants (Fig. 4.1.7). In both genotypes, camalexin remained below the detection limit in mock- and flg22-treated samples, whereas *Pc*BMM inoculation triggered clear accumulation of this phytoalexin. Col-0 showed the highest camalexin levels and the *pen2 cyp71a12/13* mutant remained below the detection limit, preserving the expected reference pattern. The observation that adding *PAD3* under an epidermal promoter substantially increased camalexin levels argues against a model in which the sole limitation in the single-gene plants was at branch entry. If the bottleneck had been confined to the CYP71A13 step, reinforcement of the terminal reaction would not be expected to produce such a clear effect. Instead, the data supposedly indicate that in the p*81F2*::*71A13* plants, intermediates generated at the infection site were not efficiently converted to camalexin because the terminal step depended on the endogenous *PAD3*, whose expression occurred mostly in mesophyll cells, contrary with the introduced *CYP71A13*. Co-expression of both enzymes under epidermal, pathogen-inducible promoters likely increased the probability that intermediates formed locally were channeled through the late part of the pathway rather than accumulating as incompletely processed precursors (Schuhegger et al., 2006).

5.2.3. Intermediate profiles support efficient camalexin biosynthesis in generated transgenic lines.

In response to *Pc*BMM inoculation, the two-gene lines reduced the excess IAOx present in the mutant background and accumulated elevated mounts of IAN, confirming that the introduced CYP71A13 was functionally connected to the native precursor pool (Fig. 4.1.11). However, IAOx and IAN accumulation levels alone do not reveal whether intermediates were efficiently channeled through the late biosynthetic segment. The route from IAN to camalexin is not a direct transfer to PAD3 but involves a GSH-dependent activation and peptide-processing segment. GSTF6 catalyzes GSH conjugation of IAN, GGP1/3 process the resulting conjugate, and PAD3 acts at the two final Cys-IAN to camalexin steps (Nafisi et al., 2007; Su et al., 2011; Geu-Flores et al., 2011). Cys-IAN and DHCA, which are positioned within this late segment, therefore provide a more

informative measure of pathway progression than IAN itself does. Both intermediates accumulated to slightly higher levels in the p*81F2*::*71A13*/p*PEN2*::*PAD3* plants as compared with Col-0 (Fig. 4.1.14). This marginal difference in accumulation indicates that co-expression of *PAD3* is sufficient to mediate conversion of IAN-derived intermediates through the committed camalexin-biosynthetic segment relatively efficiently.

Strikingly, the line-by-line comparison revealed a dissociation between upstream and late-pathway performance. Line #15 showed the clearest CYP71A13-dependent conversion signature, reducing excess IAOx almost to Col-0 levels while reaching the highest IAN abundance in the two-gene set (Fig. 4.1.11). Yet this upstream advantage did not translate into the largest Cys-IAN or DHCA pools, which were higher in lines #21 and #23 (Fig. 4.1.14). Line #15 nevertheless reached the strongest camalexin accumulation (Fig. 4.1.17). This pattern indicates that the critical determinant of camalexin production was not how much IAN was generated, but how efficiently this intermediate was captured by the GSH-dependent camalexin route and processed through to the final product.

The distinction between IAN and Cys-IAN is important to this interpretation. IAN can feed both camalexin biosynthesis and I3CA formation, whereas Cys-IAN appears only after the nitrile has entered the GSH-dependent segment committed to camalexin (Su et al., 2011; Böttcher et al., 2014). It should be noted, however, that elevated Cys-IAN accumulation does not necessarily indicate efficient camalexin formation, it may also reflect a rate-limiting step farther downstream. Taken together, these intermediate profiles indicate that the transgenic lines differed not in their capacity to reopen the camalexin branch, but in how efficiently they channeled IAN-derived intermediates through the late biosynthetic segment toward camalexin (Fig. 4.1.11, 4.1.14, 4.1.17).

5.2.4. Camalexin and its derivatives

The observed accumulation of free camalexin confirmed that the reintroduced branch was functional. However, free camalexin levels alone do not reveal how the newly formed product was handled by the native *A. thaliana* metabolic network. This is relevant because camalexin in *A. thaliana* is subject to a sequential modification cascade involving hydroxylation, *O*-glycosylation, and malonylation, which channels the phytoalexin toward less reactive, more polar forms (Böttcher et al., 2009; Kruszka et al., 2020).

Analysis of downstream derivatives therefore addressed not only whether the restored branch reached camalexin, but whether the product entered the same endogenous modification route observed in Col-0. The first indication that camalexin was processed differently in the engineered lines came from our initial LC-FLD analysis. Upon *Pc*BMM inoculation, the two-gene plants accumulated free camalexin, whereas flg22 treatment yielded mainly the HCX-Hex (Fig. 4.1.7, 4.1.8). This indicated that flg22 was sufficient to activate the branch but did not deliver it to the same product balance as infection. The sharper contrast, however, emerged from the comparison with Col-0 plants. Although this genotype reached the highest free camalexin accumulation level after *Pc*BMM inoculation, this did not coincidence with abundance of HCX-Hex #1 signal, respective peak was more abundant in the p*81F2*::*71A13*/p*PEN2*::*PAD3* transgenics. HCX-Hex #2 peak height remained comparable between samples from Col-0 and transgenic plants (Fig. 4.1.7, 4.1.8). This divergence between the parent compound and its downstream derivatives suggests that the engineered lines did not simply reproduce the Col-0 camalexin profile but fed newly formed camalexin into a quantitatively different metabolic context. In *A. thaliana*, HCX-Hex formation follows the established sequence of hydroxylation and *O*-glycosylation, and such glycosylation is commonly associated with partial detoxification of reactive small molecules (Böttcher et al., 2009; Wang et al., 2019). The highest HCX-Hex #1 concentration in the transgenic lines may therefore reflect a shift in the balance between local synthesis, export, and downstream conversion resulting from the epidermal re-localization of the pathway. One factor that was not addressed in this study is the export of newly formed metabolites from the producing cell. In *A. thaliana*, PEN3 was initially implicated in delivery of toxic PEN2-pathway products to attempted invasion sites, while later work showed that PEN3, together with PDR12 (Pleiotropic Drug Resistance 12) contributes to camalexin secretion during pathogen infection. In addition, ABCG34 has also been implicated in camalexin secretion to the leaf surface (Stein et al., 2006; Matern et al., 2019). Once *CYP71A13* and *PAD3* were re-established under epidermal promoters, spatial relationship between synthesis, export, and downstream conversion likely changed as well. It should be noted that line-specific differences in expression strength or substrate availability may also contribute to this pattern, and our data and other mentioned studies do not establish that epidermal localization alone is responsible for that kind of shifts (Fuchs et al., 2016).

LC-MS/MS analysis extended this observation by resolving additional individual downstream products. HCX largely followed the free camalexin accumulation pattern, line #15 reached Col-0-like levels of this compound, whereas lines #21 and #23 remained intermediate (Fig. 4.1.19). MCX, by contrast, did not fit the expected profile as this compound was not detected during the earlier studies in *A. thaliana* (Böttcher et al., 2009; Bednarek et al., 2011). Böttcher et al. (2009) emphasized that simple methoxycamalexins, although known from other camalexin-producing Camelineae plants (Browne et al., 1991; Jimenez et al., 2005; Böttcher et al., 2009), were surprisingly absent from *A. thaliana*, whose modification route was instead dominated by hydroxylated, hexosylated, and malonylated forms. The earlier studies on camalexin and its derivatives in *A. thaliana* utilized silver nitrate and *P. infestans* (Böttcher et al., 2009), or *B. cinerea* and *Blumeria graminis* (Bednarek et al., 2011) to induce camalexin biosynthesis. For this reason, MCX detected in our samples obtained from *Pc*BMM-inoculated leaves could be interpreted as a context-dependent side product rather than as a standard *A. thaliana* camalexin derivative comparable to HCX-Hex or HCX-Hex-Mal (Fig. 4.1.19). Alternatively, we cannot exclude that MCX has been not detected in these earlier studies due to some technical limitations of the respective LC/MS systems.

HCX-Hex-Mal, quantified by LC-MS/MS, matched Col-0-like concentrations in leaves of line #15 and slightly exceeded Col-0 in lines #21 and #23 (Fig. 4.1.23). Of note, HCX-Hex-Mal accumulation did not simply mirror the HCX-Hex pattern, and this difference may be informative. Böttcher et al. (2009) described the dominant *A. thaliana* camalexin modification leaf route as sequential hydroxylation, *O*-glycosylation, and malonylation, and noted that hydroxylation and glycosylation of camalexin had been identified as detoxification reactions in a pathogen, suggesting that a similar logic could apply *in planta* because camalexin has been shown to be toxic to *A. thaliana* cells in tissue culture, suggesting that its accumulation may require containment or export to limit self-toxicity (Rogers, 1996) (Fig. 4.1.9). More broadly, malonylation of glucosides is associated with altered transport behavior, vacuolar sequestration, and metabolite containment (Taguchi et al., 2010; Louveau and Osbourn, 2019). The appearance of HCX-Hex-Mal in the transgenic lines may therefore indicate that once the epidermally restored branch began to deliver camalexin efficiently, part of the product entered a containment route that shifts the phytoalexin toward a chemically less reactive, compartment-compatible form. This interpretation is consistent with the available

evidence, although the physiological role of HCX-Hex-Mal was not directly tested in this work.

5.2.5. I3CA biosynthesis is not strongly upregulated in p81F2::71A13/pPEN2::PAD3 plants.

Our analysis indicated that I3CA accumulated only modestly in *Pc*BMM-infected leaves, with a limited increase in its accumulation observed in lines #15 and #23 while line #21 remained closer to Col-0 (Fig. 4.1.23). Compared with the substantially stronger induction of biosynthesis of camalexin and HCX-derived products, the increase in I3CA accumulation was marginal. This suggests that the epidermal CYP71A13/PAD3 module redirected the majority of the available IAN pool toward camalexin. The enzymatic basis for this preferential routing is well characterized. *In vitro* pathway reconstitution has shown that CYP71A13 and CYP71A12, despite sharing 89.5% amino acid identity, produce strikingly different product ratios from IAOx. CYP71A13 generates predominantly Cys-IAN with only minor contribution of ICHO (indole-3-carbaldehyde), whereas CYP71A12 produces mainly ICHO with minimal amounts of Cys-IAN (Klein et al., 2013). Because Cys-IAN is the precursor for camalexin biosynthesis, while ICHO feeds into the I3CA route, the product distribution of CYP71A13 inherently favors camalexin over I3CA-related metabolism. These *in vitro* observations have been also confirmed *in planta* during studies with *cyp71a12* and *cyp71a13* mutants, which revealed that pathogen-triggered I3CA accumulation depends mainly on CYP71A12, whereas CYP71A13 does not contribute significantly to this branch (Müller et al., 2015; Pastorczyk et al., 2020). Conversely, *cyp71a12* mutants are not affected in camalexin accumulation, the contribution of CYP71A12 to camalexin biosynthesis was only observed in the *cyp71a13* background (Pastorczyk et al., 2020). Accordingly with these findings, restoring *CYP71A13*, but not *CYP71A12* in our engineered lines was expected to channel the enlarged IAOx-derived precursor pool preferentially toward camalexin rather than toward I3CA. This prediction was unambiguously confirmed with the obtained metabolite profiles.

5.2.6. Camalexin-branch reintroduction corresponds to partial *Pc*BMM restriction

Having established that adding *PAD3* after reintroducing *CYP71A13* increased throughput through the re-engineered branch and raised camalexin and its downstream products accumulation in response to *Pc*BMM inoculation (Fig. 4.1.8, 4.1.11-4.1.14, 4.1.21-4.1.23), the key question was whether this was sufficient to restrict the pathogen growth significantly. Our fungal biomass assay addressed this point at the whole-leaf level revealing the engineered two-gene plants showed significantly reduced *Pc*BMM DNA accumulation as compared with the highly susceptible *pen2 cyp71a12/13* background (Fig. 4.1.24). While the pathogen biomass was lower than in the background genotype, it remained slightly, but significantly, above Col-0, indicating a strong, yet incomplete, shift toward the resistant WT reference. Thus, re-engineering of the camalexin pathway reduced *Pc*BMM proliferation relative to the mutant plants, but it did not fully restore Col-0-like resistance.

This observed phenotype fits well with the genetic and metabolic logic of the system. The engineered lines possess a novel pathogen-inducible epidermal arm, but they did not rebuild the broader Trp-derived defense architecture that is present in WT plants. Pathogen-triggered Trp metabolism is not limited to camalexin alone but includes PEN2-dependent IGL-conversion route and CYP71A12-linked production of other indolics, particularly I3CA-related metabolites. These two sub-branches of Trp-metabolism that are absent in the *pen2 cyp71a12/13* background line have been shown to contribute significantly to *A. thaliana* resistance towards *Pc*BMM (Sanchez-Vallet et al., 2010; Pastorczyk et al., 2020). For this reason, re-engineering only the CYP71A13/PAD3 Trp-metabolic branch would be expected to produce a less pronounced phenotype rather than restoring full Col-0-like resistance.

In addition, the downstream camalexin-metabolite accumulation may help explain why proficient camalexin induction coincides with an intermediate resistance phenotype. Efficient camalexin production in our transgenic lines was accompanied by elevation, as compared with Col-0, hydroxylation and formation of more polar camalexin-related products (Fig. 4.1.21-4.1.23). This observation suggests that once the restored branch was strongly upregulated, a significant part of its output was entering downstream conversion to less active metabolites. Accordingly, the amounts of free camalexin detected in extracts should not be understood as the whole defensive capability of the branch, but as one

visible part of a dynamic balance between synthesis and subsequent processing during infection (Böttcher et al., 2009).

Overall, metabolite and pathogen biomass measurements in our transgenic lines support a constrained conclusion: reintroducing CYP71A13 and PAD3 in an inducible epidermal locus was sufficient to reduce *Pc*BMM proliferation relative to the chemically depleted background genotype, but, by itself, it did not rebuild the full Trp-derived defense capacity present in Col-0. Further studies with additional control lines deficient in particular branches of Trp-metabolism as well as with additional pathogens, are required to fully address the contribution of the re-engineered camalexin pathway to immunity, particularly to dissect its involvement in pre- and post-invasive immunity.

5.3. Brassinin biosynthesis in *A. thaliana*

Initially, engineering of brassinin biosynthesis in *A. thaliana* seemed to constitute a bigger challenge than re-engineering of camalexin pathway. Camalexin belongs to the native Trp-derived defense metabolism of this species, whereas brassinin does not. The question was therefore not only whether pathogen-inducible epidermal expression can support formation of a defense metabolite at the infection site, but also whether the metabolic background of *A. thaliana* can support formation of this foreign Brassicaceae phytoalexin.

Previous work on brassinin biosynthesis in *B. rapa* and its engineering in *N. benthamiana* indicated that only a limited number of pathway-specific activities is required for brassinin formation in an IGL-producing species. These include BABG hydrolyzing I3G and DTC-MT methylating the resulting I3M-DTC to brassinin (Fig. 1.9) (Klein and Sattely, 2017). Additionally, CYP71CR1 and CYP71CR2 can further convert brassinin to spirobrassinin and cyclobrassinin, respectively (Klein and Sattely, 2015). The remaining part of the pathway, including GPP1/3 and SUR1 was supposed to overlap with native *A. thaliana* IGL metabolism. For this reason, this system provided a suitable test whether a foreign indole-sulfur branch can be introduced into an already immune-active Trp-derived network rather than rebuilt from the beginning (Klein and Sattely, 2015, 2017).

5.3.1. *DTC-MT* is sufficient to produce brassinin in *A. thaliana*

Before testing p*81F2*::*MT*/p*PEN2*::*BABG* construct, we addressed the question of whether the *A. thaliana* metabolic background retains sufficient upstream activity to deliver the DTC intermediate to DTC-MT without a dedicated foreign myrosinase. To this end, the single-gene p*81F2*::*MT* construct was introduced into the *cyp81f2 cyp71a12/13* triple mutant. This background genotype kept native PEN2 activity in place while removing CYP81F2, which is required for 4-methoxylation of I3G and for the CYP81F2-dependent branch of PEN2-mediated pre-invasive immunity (Bednarek et al., 2009; Clay et al., 2009). The single-gene lines therefore, addressed the question whether I3M-ITC formed upon PEN2- or other myrosinase-initiated hydrolysis of I3G, followed by native GST-dependent processing, can be natively converted to I3M-DTC intermediate to support detectable brassinin formation by the introduced DTC-MT.

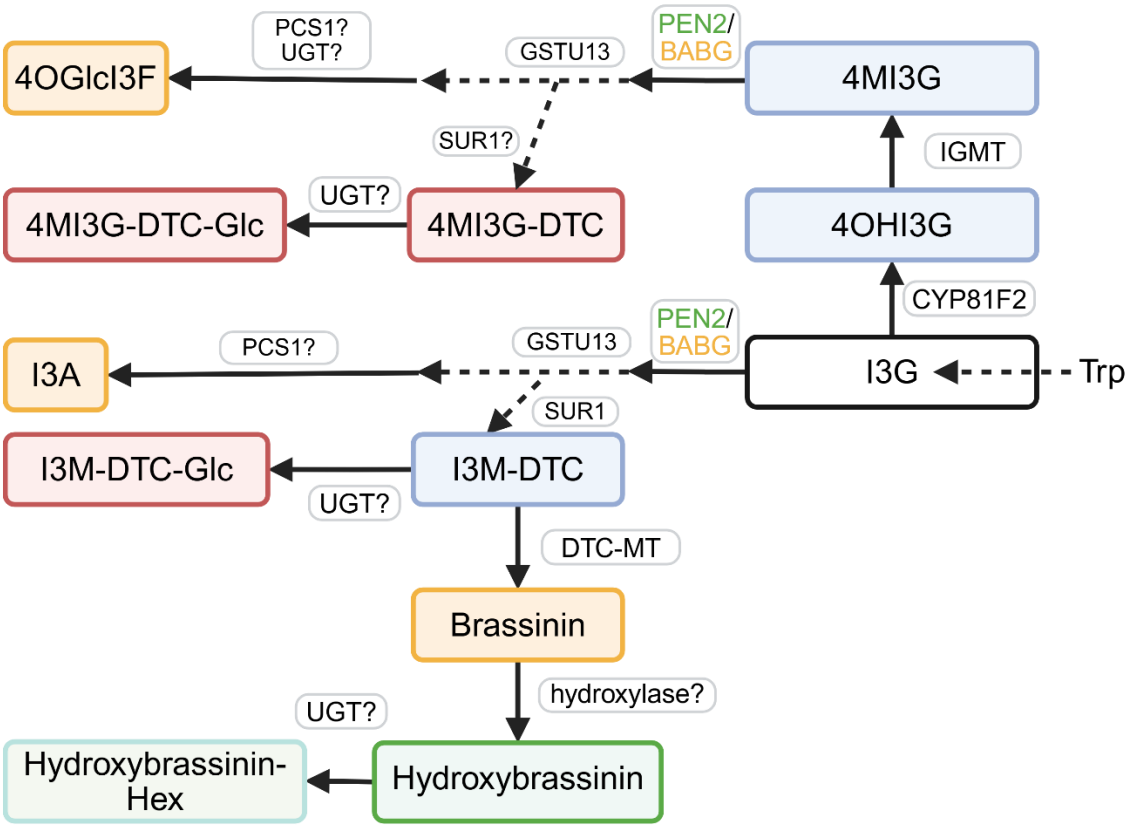

Fig. 5.1. Proposed model of native PEN2-dependent IGL turnover in *A. thaliana* and its engineered redirection toward brassinin biosynthesis by BABG and DTC-MT. Established and putative steps are shown based on the PEN2/GSTU13 pathway and the *B. rapa* brassinin pathway.

In *Pc*BMM-inoculated p*81F2*::*MT* plants, brassinin was clearly detectable by LC-MS/MS, whereas it remained below the detection limit in non-transgenic controls (Fig. 4.2.3). This result demonstrated that the *cyp81f2 cyp71a12/13* background possesses enough upstream hydrolytic and GST-conjugation activity to form I3M-ITC. Moreover, this indicated that apart from being converted to the already identified PEN2-pathway products (I3A, RA) I3M-ITC is also natively converted in *A. thaliana* to I3M-DTC, likely by GSTU13 and the natively induced in the epidermal cells GGP1/3 and SUR1 enzymes (Fig. 5.1, 4.2.6) (Fuchs et al., 2016; Piślewska-Bednarek et al., 2018). In accordance with this assumption, we were able to detect the presence of I3M-DTC in our samples from transgenic lines as well as Col-0 (Fig. 4.2.6). The introduced DTC-MT further converted this intermediate to brassinin. The important conclusion from these analyses is that the PEN2-proficient background maintained a residual metabolic connection to the foreign pathway even in the absence of a dedicated I3G-specific myrosinase.

Of note, brassinin accumulation across the independent p*81F2*::*MT* lines did not closely correspond to DTC-MT transcript levels (Fig. 4.2.1, 4.2.3). This weak correlation argues that DTC-MT expression itself was not the principal limiting factor. The stronger constraint was more likely upstream, at the level of I3G hydrolysis and conversion of I3M-ITC to I3M-DTC. In this context, the amount of I3M-DTC generated from I3G by PEN2/GSTU13-initiated processing would be expected to remain limited, which is in agreement with the low brassinin levels observed.

5.3.2. BABG introduction supports higher brassinin accumulation

Direct comparison of brassinin accumulation in p*81F2*::*MT* and p*81F2*::*MT*/p*PEN2*::*BABG* transgenic lines revealed a positive impact of BABG on biosynthesis of this phytoalexin. p*81F2*::*MT*/p*PEN2*::*BABG* lines #1 and #9 accumulated significantly more brassinin than the single-gene p*81F2*::*MT* reference line #5, whereas line #3 did not differ from it (Fig. 4.2.5). As all lines were analyzed under the same infection regime the divergence between them is best explained by line-specific effectiveness of BABG expression rather than by the two-gene genotype alone. Overall, these data indicate that addition of BABG was able to strengthen the engineered biosynthetic branch.

This result fits the expected role of BABG that was identified in *B. rapa* as a β-glucosidase associated with the I3G-to-brassinin route (Klein and Sattely, 2017). In the

single-gene configuration, DTC-MT action depended on native *A. thaliana* hydrolytic activities to generate the upstream precursor. Concluding from the analysis of the downstream products of the PEN2 pathway, I3A and RA (Bednarek et al., 2009), formation of I3M-ITC is almost completely dependent on the PEN2 activity. This has been confirmed with our analysis of I3M-DTC accumulation. This I3M-ITC-derived intermediate was present in Col-0, but its accumulation was strongly reduced in *pen2 cyp71a12/a13* mutant (Fig. 4.2.6). Regarding this, the simplest interpretation of differences in brassinin accumulation between both types of lines is that the upstream limitation in the single-gene system resulted from differences in substrate specificity and activity between PEN2 and BABG. This hypothesis has been recently confirmed in our parallel study, which revealed BABG hydrolyzes I3G *in planta* more efficiently than PEN2 (Agrawal et al., unpublished). Apart from differences in activity, another potential issue could be linked with sub-cellular localization of both myrosinases. PEN2 is anchored in peroxisomal and mitochondrial membranes (Fuchs et al., 2016), which can limit its co-localization with the introduced putatively cytoplasmic DTC-MT. Notably, BABG is also predicted to be a cytoplasmic enzyme, for this reason possibly better suited to cooperate with DTC-MT.

An important issue in metabolic engineering is redirection of intermediates into undesired side products (Pickens et al., 2011). It has been reported that during engineering of brassinin pathway in *N. benthamiana* a sub-fraction of I3M-DTC was conjugated with glucose by an endogenous glucosyl-transferase to form I3M-DTC-Glc (Fig. 4.2.6) (Pickens et al., 2011). Our LC-MS/MS analysis confirmed presence of this particular dead end metabolic sub-branch product in our samples. I3M-DTC-Glc accumulated clearly in all lines that possessed either PEN2 or BABG myrosinase activity, but not in the *pen2 cyp71a12/13* triple mutant (Fig. 4.2.6). Because formation of this compound is competitive with DTC-MT-mediated conversion of I3M-DTC to brassinin, its accumulation pattern serves as an indirect gauge of DTC-MT efficiency, if the methylation step were severely limiting, I3M-DTC-Glc should dominate over brassinin. Instead, the conjugate remained relatively low abundant even in the two-gene lines characterized with high brassinin accumulation, consistent with efficient DTC-MT-mediated conversion. This agrees with the *N. benthamiana* pathway reconstitution, where I3M-DTC-Glc was similarly interpreted as a minor overflow product rather than a major branch point (Klein and Sattely, 2017).

Of note, we also putatively detected a methoxy-I3M-DTC-Glc on the basis of its molecular ion *m/z* and fragmentation pattern (Fig. 4.2.7, 4.2.8). This compound was present in Col-0, while its accumulation increased with BABG expression in the two-gene lines. Conversely, in tissue concentration dropped below the Col-0 levels in the *CYP81F2*-deficient single-gene transgenic line (Fig. 4.2.6). This CYP81F2-dependence indicates that it originates from 4MI3G, confirming that both PEN2 and BABG can hydrolyze this IGL (Fig. 5.1). Strikingly, the corresponding methoxy-brassinin was not detected in any sample, even though 4MI3M-DTC-Glc was clearly present. The simplest interpretation is that DTC-MT does not accept the methoxylated I3M-DTC intermediate as a substrate, so the entire pool is diverted toward glycosylation (Fig. 5.1). This reveals a potential and previously uncharacterized substrate restriction of DTC-MT, while the enzyme efficiently methylates the unsubstituted I3M-DTC, the additional methoxy group on the indole ring appears to prevent effective substitution. This observation may also explain the fact that methoxylated brassinin forms have so far not been reported in *Brassica* spp. (Pedras et al., 2011).

5.3.3. *A. thaliana* modifies brassinin through a native hydroxylation–glycosylation route

Free brassinin levels alone do not reveal how *A. thaliana* handles a foreign phytoalexin once it has been formed. The metabolic fate of brassinin matters for two reasons, it determines which fraction of the engineered product remains bioactive, and it exposes whether native modification enzymes recognize this compound at all. Our LC-MS/MS profiling addressed both questions by tracking putative brassinin derivatives across the transgenic and control lines (Fig. 4.2.6–4.2.11; Tab. 4.2). Beyond pathway intermediates, our analysis uncovered signals corresponding to two putative brassinin derivatives, hydroxybrassinin and hydroxybrassinin-Hex, which were exclusively present in transgenic lines and absent in both Col-0 and *pen2 cyp71a12/13* (Fig. 4.2.10, 4.2.11). These two metabolites, therefore arise from brassinin itself rather than from the native Trp-derived network. Their detection shows that *A. thaliana* recognizes brassinin as a substrate for endogenous modification enzymes despite having no evolutionary history with this compound.

The modification sequence, hydroxylation followed by glycosylation, closely parallels the established route by which *A. thaliana* processes camalexin toward less

reactive, more polar forms (Böttcher et al. 2009). This modification sequence was also observed in our lines with re-engineered camalexin biosynthesis. The appearance of an analogous hydroxylation–glycosylation series on brassinin suggests that *A. thaliana* applies a conserved detoxification logic to reactive indole-sulfur compounds, irrespective of whether they belong to the native metabolic repertoire (Böttcher et al., 2009).

An interesting discordance emerged between brassinin and hydroxybrassinin accumulation patterns across lines. Whereas brassinin reached its highest level in the two-gene line #9, hydroxybrassinin was most abundant in the single-gene line #5 (Fig. 4.2.5, 4.2.10). Hydroxybrassinin-Hex mirrored this inverted pattern. This dissociation may reflect line-specific differences in the activity or inducibility of the hydroxylation step, possibly driven by variation in the expression of the responsible cytochrome P450 or other oxidative enzyme(s). It may also indicate that the ratio of free brassinin to its hydroxylated derivatives depends on pathway throughput. When brassinin production is modest, the hydroxylation capacity may keep pace, shifting a larger proportion of the total pool toward the modified form. In either case, the result shows that free brassinin concentration alone does not fully represent the total metabolic investment into the hydroxybrassinin branch.

5.3.4. Extending the brassinin branch toward cyclobrassinin and spirobrassinin

Despite careful screening of our LC/MS data, we found no signals corresponding to spirobrassinin or cyclobrassinin in any of the investigated brassinin-producing lines (Tab. 4.2). This negative result was not surprising given that these heterocyclization reactions have been shown to require specific cytochrome P450 enzymes (CYP71CRs) that are absent from the *A. thaliana* genome (Klein and Sattely, 2015). Our results confirm that the native *A. thaliana* metabolic network does not possess enzymatic capacity to close the brassinin scaffold into either the spiro- or cyclo-ring system. This raised the question whether the brassinin pool generated in the p*81F2*::*MT*/p*PEN2*::*BABG* plants could be converted to respective derivatives upon introduction of respective CYP71CRs that catalyze alternative *S*-heterocyclizations on the brassinin scaffold *in planta*. To address this, line #9 characterized by the highest brassinin accumulation and the strongest *Pc*BMM restriction, was supertransformed with p*81F2*::*71CR1* or p*81F2*::*71CR2* constructs (Klein and Sattely, 2015, 2017)

LC-MS/MS analysis of *Pc*BMM-inoculated T_1 leaves confirmed the presence of spirobrassinin in p*81F2*::*71CR1* plants and cyclobrassinin in p*81F2*::*71CR2* plants, in each case supported by diagnostic fragmentation patterns consistent with published reference spectra (Fig. 4.2.19, 4.2.20; Tab. 4.2) (Pedras et al., 2006). This result has a straightforward but important implication; Brassinin, produced by the upstream BABG/DTC-MT module, is spatially and temporally accessible to subsequently introduced cytochrome P450 enzymes expressed under the *CYP81F2* promoter, which was also used to drive *DTC-MT* expression. The co-induction of *DTC-MT* and *CYP71CR1* or *CYP71CR2* under this shared pathogen-responsive epidermal promoter, therefore appears sufficient to connect sequential biosynthetic steps within the same cell, without requiring additional scaffolding or deliberate co-localization strategies. This is consistent with the observation by Klein and Sattely (2017) that the brassinin pathway enzymes do not appear to form an obligate metabolon in *B. rapa*, and that individual steps can be functionally reconstituted by transient expression in *N. benthamiana*.

In both p*81F2*::*71CR1* and p*81F2*::*71CR2* plants, brassinin remained clearly detectable alongside the newly formed heterocyclic product (Fig. 4.2.20). The concurrent presence of brassinin indicates that the upstream module generates this phytoalexin at levels that exceed the conversion capacity of the introduced CYP71CR enzymes. This is not unexpected for a T_1 generation analysis, where CYP71CR expression levels will vary with insertion site and copy number and are unlikely to be optimized. Selecting high-expressing lines in subsequent generations and potentially adjusting promoter strength or introducing both CYP71CR genes simultaneously could shift the balance further toward the downstream products.

From a pathway-design perspective, the incomplete conversion is informative rather than limiting. It demonstrates that the brassinin branch operates with sufficient throughput to supply a downstream extension step, which is the prerequisite for any further elaboration of the introduced metabolic network. At the same time, the residual brassinin pool means that the T_1 plants effectively accumulate a mixture of brassinin and its spiro- or cyclo-derivative, a situation that may itself have defense relevance. In this context, it should also be noted that *Brassica* spp. also accumulate mixtures of brassinin and its derivatives, so also in the native system, conversion of brassinin to its derivatives is not complete (Pedras et al., 2011).

It should be noted that the present analysis is restricted to the T_1 and tested for their individual contributions to pathogen restriction. Establishing whether these

downstream phytoalexins confer additional defense beyond what brassinin alone provides will require stable homozygous lines, dose-response comparisons, and infection assays that are beyond the scope of this study. Nevertheless, the successful detection of both heterocyclic products in *Pc*BMM-challenged leaves demonstrates that the *A. thaliana* Trp-derived metabolic network can support a multi-step foreign phytoalexin pathway when the necessary enzymatic activities are supplied under appropriate spatiotemporal control.

5.3.5. Engineered brassinin biosynthesis restricts *Pc*BMM proliferation in the susceptible background.

Our metabolite profiling established that the p*81F2*::*MT*/p*PEN2*::*BABG* module generates brassinin and a series of related products upon *Pc*BMM challenge. The remaining question was whether this newly introduced metabolic branch translates into a measurable restriction of pathogen growth. To address this, *Pc*BMM biomass was quantified by qPCR in leaves of the three independent p*81F2*::*MT*/p*PEN2*::*BABG* transgenic lines alongside Col-0 and the *pen2 cyp71a12/13* background at 5 dpi (Fig. 4.2.18).

All tested transgenic lines displayed significantly reduced fungal biomass relative to the *pen2 cyp71a12/13* mutant (Fig. 4.2.18). This ranking broadly corresponded to the brassinin accumulation levels recorded across the same lines. Lines #1 and #9, which accumulated highest brassinin levels, showed the strongest reduction in *Pc*BMM biomass, while line #3, which did not significantly exceed the single-gene reference in brassinin production, displayed a weaker, though still significant, restriction of pathogen growth (Fig. 4.2.5). This correlation between brassinin accumulation and fungal biomass reduction supports the interpretation that brassinin itself, or its downstream metabolic products, contributes to the observed defense phenotype.

It is worth noting, however, that the resistance conferred by the brassinin module was partial rather than WT-like, even the best-performing lines did not fully restore Col-0-like resistance (Fig. 4.2.18). This outcome parallels the result obtained with the camalexin-branch re-engineering, where two-gene p*81F2*::*71A13*/p*PEN2*::*PAD3* plants also showed significant but incomplete rescue. In both cases, the engineered lines introduced a single inducible metabolic arm into a background that lacks a broader set of Trp-derived defense components, including the PEN2-dependent pre-invasive pathway

and CYP71A12-linked metabolism. The resistance towards *P. cucumerina* in *A. thaliana* involves defense responses that depend on multiple Trp-derived branches acting in concert (Sanchez-Vallet et al., 2010; Pastorczyk et al., 2020), and reconstitution of a single branch, whether camalexin or brassinin, cannot be expected to replace the full chemical defense architecture of WT plants. The more informative comparison is therefore not between the transgenic lines and Col-0, but between the transgenic lines and the *pen2 cyp71a12/13* background from which they were derived. Viewed in this context, the result demonstrates that a foreign phytoalexin that does not occur in *A. thaliana*, can be produced at sufficient levels in epidermal cells during infection to measurably limit pathogen proliferation. This establishes a functional link between engineered brassinin biosynthesis and disease restriction in a heterologous host.

An additional consideration is that the effective defense output of the brassinin module may not be limited to brassinin itself. As discussed before, the transgenic lines also accumulated hydroxybrassinin and hydroxybrassinin-Hex. Whether these co-products contribute to pathogen restriction alongside brassinin remains an open question. In *B. rapa*, brassinin and its derivatives are known to accumulate coordinately during infection, and antimicrobial activity has been reported for several members of the DTC family (Pedras et al., 2011). The defense phenotype observed in our transgenic lines may therefore reflect the combined action of multiple metabolic products generated by the engineered branch rather than brassinin alone.

5.3.6. BABG cross-feeds the native PEN2 branch and selectively reshapes the IGL pool

The brassinin pathway branches off from the native *A. thaliana* IGL pathway at the level of I3G hydrolysis. An important follow-up question was therefore whether introduced BABG activity remains confined to the brassinin route or whether it also feeds intermediates into endogenous IGL-processing pathways, particularly the PEN2-dependent branch that generates end products such as I3A and 4OGlcI3F (Bednarek et al., 2009; Lu et al., 2015) (Fig. 1.8). If this is the case, the enhanced resistance of p*81F2*::*MT*/p*PEN2*::*BABG* could at least partially result from production of some of these products. A related concern was whether BABG-mediated IGL hydrolysis depletes the pool of these compounds to an extent that could compromise other aspects of plant fitness.

Our LC-FLD analysis showed that I3A, one of the markers of PEN2 activity, accumulated at higher levels in all three p*81F2*::*MT*/p*PEN2*::*BABG* lines than in *pen2 cyp71a12/13* plants (Fig. 4.2.12). This result indicates that GS-I3M-DTC formed upon BABG-mediated I3G hydrolysis is not only channeled to brassinin, but also processed to I3A (Fig. 1.8, 5.1) (Piślewska-Bednarek et al., 2018). The ratio of these products is presumably determined by the relative local abundance and affinity of the competing enzymes. Interestingly, despite using the native *PEN2* promoter, I3A accumulation levels in the BABG-expressing lines exceeded those observed in Col-0 (Fig. 4.2.12) suggesting BABG is more efficient in hydrolyzing I3G as compared with PEN2.

In addition to driving I3A accumulation, expression of BABG restored accumulation of the other marker end product of PEN2 pathway, 4OGlcI3F in the *pen2 cyp71a12/13* background (Fig. 4.2.14). This indicates BABG can hydrolyze 4MI3G, generating the respective ITC intermediate that native downstream enzymes convert to 4OGlcI3F (Fig. 5.1). This is consistent with the detection of 4MI3M-DTC-Glc in the same lines (Fig. 4.2.8). However, unlike I3A, accumulation of 4OGlcI3F was only partially restored in p*81F2*::*MT*/p*PEN2*::*BABG* lines as compared with Col-0 (Fig. 4.2.14). In contrast to the results for I3G, these findings indicate that BABG has lower activity toward 4MI3G compared with PEN2. This preference of BABG towards I3G correlated with accumulation of particular IGLs. I3G *in planta* concentrations were reduced while those of 4MI3G were unaffected in p*81F2*::*MT*/p*PEN2*::*BABG* lines as compared with *pen2 cyp71a12/13* mutant (Fig. 4.2.15). This striking difference in substrate specificity towards particular IGLs between BABG and PEN2 is in accordance with results of our study directly comparing activities of selected myrosinases *in planta* (Agrawal et al., unpublished). In addition, it should be noted that PEN2 is anchored in mitochondrial and peroxisomal membranes (Fuchs et al., 2016), while BABG is supposed to be cytoplasmic. These differential subcellular localizations can expose both enzymes to different pools of I3G/4MI3G, which additionally can affect the efficiency of hydrolysis of particular IGLs.

Despite the molecular basis of this difference in substrate specificity, it should be noted that PEN2 contributes to plant immunity exclusively through hydrolysis of 4OH/4MI3G while formation of I3A, even in elevated amounts, is without any significance for pathogen invasion (Bednarek et al., 2009). In addition, it has been shown that association of PEN2 with mitochondria, which is not the case for BABG, is indispensable for its immune function (Fuchs et al., 2016). Consequently, we may assume

that the enhanced resistance of p*81F2*::*MT*/p*PEN2*::*BABG* plants to *Pc*BMM results mainly from brassinin biosynthesis, rather than from functional reactivation of PEN2 pathway by BABG.

In addition to the reduced I3G concentrations, 1MI3G accumulated at higher levels in the transgenic plants than in the background genotype (Fig. 4.2.15). This unexpected increase cannot be readily explained by direct BABG activity. One possibility is that enhanced I3G turnover triggers a compensatory transcriptional response in the IGL biosynthetic pathway. Such feedback would be consistent with the established regulatory circuitry in which MYB transcription factors adjust pathway activity in response to perturbation of IGL homeostasis (Frerigmann and Gigolashvili, 2014; Czerniawski et al., 2023). If activated, this feedback could selectively enrich IGL species that are not efficiently processed by BABG, such as 1MI3G. In any case, the increase in the accumulation of this modified IGL at least partially compensates for the reduced I3G accumulation. For these reasons, it seems rather unlikely that sustained BABG expression in our brassinin–producing lines could compromise IGL-dependent physiological processes beyond immunity, including sulfur storage and developmental signaling (Aghajanzadeh et al., 2014).

Despite changes in IGL profile, our GL analysis revealed no significant consistent changes in AGL accumulation in the transgenic lines. The absence of a systematic effect on AGL accumulation indicates that BABG activity in these lines is largely restricted to IGL substrates. This could reflect either BABG substrate specificity or cell-specific accumulation of AGLs. These compounds are produced in cells surrounding the phloem and xylem, and it is not clear if they are abundant in epidermal cells (Nintemann et al., 2018).

CONCLUSIONS

1. Camalexin biosynthesis can be reconstructed in epidermal cells with the expression of *CYP71A13* and *PAD3* genes. Remaining required activities of GST and GGP1/3 are induced in epidermal cells with infection.
2. The relative proportions of HCX, HCX-Hex, HCX-Hex-Mal, and MCX between Col-0 and transgenic lines indicate that in the epidermis, camalexin undergoes elevated detoxification processes as compared with its native biosynthetic site.
3. As evidenced by restricted *Pc*BMM biomass, in the novel epidermal localization, camalexin is still able to restrict pathogen proliferation.
4. I3M-DTC and 4MI3M-DTC are additional side products of the PEN2 pathway formed in *A. thaliana* upon pathogen recognition.
5. The core of brassinin biosynthesis from I3G to I3M-DTC is conserved between *A. thaliana* and *B. rapa*, and possibly among other Brassicaceae species. For this reason, expression of *DTC-MT* alone is sufficient to produce brassinin in *A. thaliana*.
6. BABG is more efficient in brassinin biosynthesis than PEN2, possibly due to its substrate preference towards I3G and/or its cytoplasmic localization.
7. DTC-MT is not capable to *S*-methylate 4MI3M-DTC.
8. Brassinin is functional in the alien *A. thaliana* background and can contribute to pathogen restriction. Moreover, it can be detoxified by native *A. thaliana* enzymes, including hydroxylation and subsequent glycosylation.
9. Formation of spirobrassinin and cyclobrassinin from brassinin is not supported by the native *A. thaliana* enzymatic activity and requires *B. rapa* CYP71CR1 or CYP71CR2, respectively.

ABSTRACT

Tryptophan-derived specialized metabolites are among central components of Brassicaceae immunity, yet the extent to which their defense function depends on their biochemical activity rather than on the spatial and temporal context of their accumulation remains unclear. To address this question, two indole phytoalexin pathways have been re-engineered in the susceptible to infection *Arabidopsis thaliana pen2 cyp71a12 cyp71a13* triple mutant background, which is deficient in camalexin production and lacks the pre-invasive indole glucosinolate-based defense. The introduced genes were placed under the control of the pathogen-inducible, epidermis-active *PENETRATION 2* (*PEN2*) and *CYP81F2* promoters, and the resulting lines were challenged with the necrotrophic fungus *Plectosphaerella cucumerina*.

The native camalexin branch was re-engineered to change its cellular localization. Expression of *CYP71A13*, encoding the first camalexin-specific enzyme, alone supported only modest camalexin accumulation. Combined epidermal expression of *CYP71A13* and *Phytoalexin Deficient 3*, encoding the last enzyme on camalexin branch, markedly improved pathway completion upon infection, indicating that the remaining required glutathione *S*-transferase and γ-glutamyl peptidase activities are induced locally and can be recruited without additional engineering. Of note, the pools of camalexin hydroxylation and glycosylation products in the transgenic lines were clearly enriched relative to wild-type plants, indicating that relocation of this phytoalexin to the epidermis exposes it to elevated detoxification activity as compared with its native mesophyll site. Despite this partial diversion, the engineered branch significantly restricted *P. cucumerina* proliferation relative to the background mutant, demonstrating that camalexin retains its defense function in a non-native cellular compartment.

The foreign brassinin pathway from *Brassica rapa* was introduced into the same mutant background. Strikingly, expression of the *B. rapa dithiocarbamate S-methyltransferase* gene alone was sufficient to yield brassinin in the PEN2 background activity, indicating that the core route from the indole glucosinolate pool to the dithiocarbamate intermediate is conserved between the two species and does not strictly depend on a *Brassica*-specific glucosinolate-hydrolyzing enzyme. Co-expression of the *B. rapa brassinin-associated β-thioglucoside glucohydrolase* gene (*BABG*) further enhanced brassinin accumulation, identifying it as a more efficient contributor to indol-

3-ylmethyl-dithiocarbamate formation than the native *A. thaliana* enzymes. In the engineered background, brassinin was further processed by native hydroxylation and glycosylation activities, whereas formation of cyclobrassinin and spirobrassinin required additional expression of *B. rapa CYP71CR1* and *CYP71CR2*, respectively. As in the case of camalexin, the brassinin-producing lines displayed a significant restriction of *P. cucumerina* proliferation.

Together, these results show that both a native and a foreign indole phytoalexin can be functionally reconstituted in pathogen-challenged epidermal cells of a susceptible *A. thaliana* background, where they significantly restrict fungal proliferation. This supports the interpretation that the immune function of tryptophan-derived metabolites is shaped mainly by their chemical identity and not so much dependent on cellular localization of their production. This also highlights BABG as a particularly effective glucosinolate-hydrolyzing enzyme for engineering foreign indolic phytoalexins in *A. thaliana*.

STRESZCZENIE

Wyspecjalizowane metabolity pochodzące od tryptofanu stanowią jeden z centralnych komponentów odporności roślin Brassicaceae na infekcję, jednak nadal nie jest jasne, w jakim stopniu ich funkcja obronna zależy od aktywności biochemicznej, a nie od przestrzennego i czasowego kontekstu ich akumulacji. Aby odpowiedzieć na to pytanie, zrekonstruowano dwa szlaki biosyntezy fitoaleksyn indolowych w podatnym na infekcję potrójnym mutancie *Arabidopsis thaliana pen2 cyp71a12 cyp71a13*, który posiada defekt w biosyntezie kamaleksyny i pozbawiony jest przed-inwazyjnej gałęzi obrony opartej na glukozynolanach indolowych. Wprowadzone geny kodujące enzymy wybranych szlaków umieszczono pod kontrolą indukowalnych przez patogena, aktywnych w epidermie promotorów *PENETRATION 2* (*PEN2*) oraz *CYP81F2*, a uzyskane linie poddano infekcji nekrotroficznym grzybem *Plectosphaerella cucumerina*.

W pierwszej kolejności przekonstruowano natywny szlak kamaleksyny aby zmienić jej komórkową lokalizację. Ekspresja samego genu *CYP71A13*, kodującego pierwszy enzym szlaku, wspierała jedynie niewielką akumulację kamaleksyny. Z kolei równoległa epidermalna ekspresja *CYP71A13* i *Phytoalexin Deficient 3*, kodującego ostatni enzym szlaku, wyraźnie poprawiała domknięcie szlaku w odpowiedzi na infekcję, co wskazuje, że pozostałe wymagane aktywności transferazy *S*-glutationowej oraz γ-glutamylowej peptydazy są indukowane lokalnie i mogą zostać wykorzystane bez dodatkowej inżynierii. Co istotne, ilość produktów hydroksylacji i glikozylacji kamaleksyny w liniach transgenicznych była wyraźnie zwiększona względem roślin typu dzikiego, co wskazuje, że przeniesienie tej fitoaleksyny do epidermy naraża ją na wyższą aktywność detoksykacyjną niż w natywnym miejscu biosyntezy w mezofilu. Pomimo tego częściowego przekierowania, zrekonstruowana gałąź istotnie ograniczała proliferację *P. cucumerina* w porównaniu z mutantem wyjściowym, wykazując, że kamaleksyna zachowuje swoją funkcję obronną w nienatywnym przedziale komórkowym.

Używając tego samego tła genetycznego wprowadzono do *A. thaliana* obcy szlak brassininy z *Brassica rapa*. Co ciekawe, sama ekspresja genu kodującego *S-metylotransferazę ditiokarbaminianową* z *B. rapa* była wystarczająca do wytworzenia brassininy w tle z aktywnym PEN2, co wskazuje, że zasadnicza droga od puli glukozynolanów indolowych do pośredniego ditiokarbaminianu jest zachowana między

tymi dwoma gatunkami i nie zależy bezwzględnie od swoistego dla *B. rapa* enzymu hydrolizującego glukozynolany. Ko-ekspresja genu kodującego *β-tioglukozydową glukohydrolazę związana z brassininą* w *B. rapa* (*BABG*) dodatkowo zwiększała akumulację brassininy, wskazując, że enzym ten wydajniej uczestniczy w tworzeniu indol-3-ylometylo-ditiokarbaminianu niż natywne enzymy *A. thaliana*. W otrzymanych liniach transgenicznych brassinina była dalej przetwarzana przez natywne enzymy katalizujace hydroksylację i glikozylację. Z kolei tworzenie cyklobrassininy i spirobrassininy wymagało dodatkowej ekspresji odpowiednio *CYP71CR1* i *CYP71CR2* z *B. rapa*. Podobnie jak w przypadku kamaleksyny, linie produkujące brassininę wykazywały istotne ograniczenie proliferacji *P. cucumerina*.

Łącznie wyniki te pokazują, że zarówno natywna, jak i obca indolowa fitoaleksyna mogą zostać funkcjonalnie odtworzone w poddanych infekcji komórkach epidermy podatnego tła *A. thaliana*, gdzie w znaczący sposób ograniczają proliferację patogenu. Wspiera to interpretację, że funkcja odpornościowa metabolitów pochodzących od tryptofanu jest kształtowana głównie przez ich aktywność biochemiczną, a nie przez komórkową lokalizację ich wytwarzania. Dodatkowo nasze wyniki wskazują na BABG jako szczególnie efektywny enzym hydrolizujący glukozynolany do zastosowań w inżynierii fitoaleksyn indolowych u *A. thaliana*.

BIBLIOGRAPHY

1. Adrian, M., Jeandet, P., Veneau, J., Weston, L.A., Bessis, R., *Biological Activity of Resveratrol, a Stilbenic Compound from Grapevines, Against Botrytis cinerea, the Causal Agent for Gray Mold.* Journal of Chemical Ecology, 1997. 23: 1689-1702. DOI: 10.1023/B:JOEC.0000006444.79951.75

2. Aghajanzadeh, T., Hawkesford, M.J., De Kok, L.J., *The significance of glucosinolates for sulfur storage in Brassicaceae seedlings.* Frontiers in Plant Science, 2014. 5. DOI: 10.3389/fpls.2014.00704

3. Aharoni, A., Galili, G., *Metabolic engineering of the plant primary-secondary metabolism interface.* Current Opinion in Biotechnology, 2011. 22: 239-244. DOI: 10.1016/j.copbio.2010.11.004

4. Ahuja, I., De Vos, R.C.H., Rohloff, J., Stoopen, G.M., Halle, K.K., Ahmad, S.J.N., Hoang, L., Hall, R.D., Bones, A.M., *Arabidopsis myrosinases link the glucosinolate-myrosinase system and the cuticle.* Scientific Reports, 2016. 6: 38990. DOI: 10.1038/srep38990

5. Alonso, J.M., Ecker, J.R., *Moving forward in reverse: genetic technologies to enable genome-wide phenomic screens in Arabidopsis.* Nature Reviews Genetics, 2006. 7: 524-536. DOI: 10.1038/nrg1893

6. Andersson, D., Chakrabarty, R., Bejai, S., Zhang, J., Rask, L., Meijer, J., *Myrosinases from root and leaves of Arabidopsis thaliana have different catalytic properties.* Phytochemistry, 2009. 70: 1345-1354. DOI: 10.1016/j.phytochem.2009.07.036

7. Bai, Y., Fernández-Calvo, P., Ritter, A., Huang, A.C., Morales-Herrera, S., Bicalho, K.U., Karady, M., Pauwels, L., Buyst, D., Njo, M., Ljung, K., Martins, J.C., Vanneste, S., Beeckman, T., Osbourn, A., Goossens, A., Pollier, J., *Modulation of Arabidopsis root growth by specialized triterpenes.* New Phytologist, 2021. 230: 228-243. DOI: 10.1111/nph.17144

8. Bak, S., Feyereisen, R., *The involvement of two P450 enzymes, CYP83B1 and CYP83A1, in auxin homeostasis and glucosinolate biosynthesis.* Plant Physiology, 2001. 127: 108-118. DOI: 10.1104/pp.127.1.108

9. Bednarek, P., Piślewska-Bednarek, M., Svatoš, A., Schneider, B., Doubský, J., Mansurova, M., Humphry, M., Consonni, C., Panstruga, R., Sanchez-Vallet, A., Molina, A., Schulze-Lefert, P., *A Glucosinolate Metabolism Pathway in Living Plant Cells Mediates Broad-Spectrum Antifungal Defense.* Science, 2009. 323: 101-106. DOI: 10.1126/science.1163732

10. Bednarek, P., Piślewska-Bednarek, M., Ver Loren Van Themaat, E., Maddula, R.K., Svatoš, A., Schulze-Lefert, P., *Conservation and clade-specific diversification of pathogen-inducible tryptophan and indole glucosinolate metabolism in Arabidopsis thaliana relatives.* New Phytologist, 2011. 192: 713-726. DOI: 10.1111/j.1469-8137.2011.03824.x

11. Bekešová, S., Kováčik, V., Tvaroška, I., Čurillová, Z., Škultéty, Ľ., Řehulka, P., *Elimination of Isocyanate and Isothiocyanate Molecules at the Electrospray Ionization Ion Trap, Electrospray Ionization Quadrupole Time-of-Flight and Matrix-Assisted Laser Desorption/Ionization Time-of-Flight Tandem Mass Spectrometry Fragmentation of Sodium Cationized Brassitin, Brassinin and Their Glycosides.* European Journal of Mass Spectrometry, 2007. 13: 147-154. DOI: 10.1255/ejms.847

12. Block, A., Li, G., Fu, Z.Q., Alfano, J.R., *Phytopathogen type III effector weaponry and their plant targets.* Current Opinion in Plant Biology, 2008. 11: 396-403. DOI: 10.1016/j.pbi.2008.06.007

13. Bohlmann, J., Keeling, C.I., *Terpenoid biomaterials.* The Plant Journal, 2008. 54: 656-669. DOI: 10.1111/j.1365-313X.2008.03449.x

14. Boller, T., Felix, G., *A Renaissance of Elicitors: Perception of Microbe-Associated Molecular Patterns and Danger Signals by Pattern-Recognition Receptors.* Annual Review of Plant Biology, 2009. 60: 379-406. DOI: 10.1146/annurev.arplant.57.032905.105346

15. Böttcher, C., Chapman, A., Fellermeier, F., Choudhary, M., Scheel, D., Glawischnig, E., *The Biosynthetic Pathway of Indole-3-Carbaldehyde and Indole-3-Carboxylic Acid Derivatives in Arabidopsis.* Plant Physiology, 2014. 165: 841-853. DOI: 10.1104/pp.114.235630

16. Böttcher, C., Westphal, L., Schmotz, C., Prade, E., Scheel, D., Glawischnig, E., *The Multifunctional Enzyme CYP71B15 (PHYTOALEXIN DEFICIENT3) Converts Cysteine-Indole-3-Acetonitrile to Camalexin in the Indole-3-Acetonitrile Metabolic*

Network of Arabidopsis thaliana. The Plant Cell, 2009. 21: 1830-1845. DOI: 10.1105/tpc.109.066670

17. Browne, L.M., Conn, K.L., Ayert, W.A., Tewari, J.P., *The camalexins: New phytoalexins produced in the leaves of Camelina sativa (Cruciferae).* Tetrahedron, 1991. 47: 3909-3914. DOI: 10.1016/S0040-4020(01)86431-0

18. Butelli, E., Titta, L., Giorgio, M., Mock, H.-P., Matros, A., Peterek, S., Schijlen, E.G.W.M., Hall, R.D., Bovy, A.G., Luo, J., Martin, C., *Enrichment of tomato fruit with health-promoting anthocyanins by expression of select transcription factors.* Nature Biotechnology, 2008. 26: 1301-1308. DOI: 10.1038/nbt.1506

19. Carrillo-Gavilán, A., Moreira, X., Zas, R., Gonzalez-Voyer, A., Vilà, M., Sampedro, L., *Phylogenetic and biogeographical patterns in defensive strategies and quantitative allocation to chemical defences in Palaearctic and Nearctic pine trees.* Journal of Biogeography, 2015. 42: 684-693. DOI: 10.1111/jbi.12444

20. Caruso, F., Mendoza, L., Castro, P., Cotoras, M., Aguirre, M., Matsuhiro, B., Isaacs, M., Rossi, M., Viglianti, A., Antonioletti, R., *Antifungal Activity of Resveratrol against Botrytis cinerea Is Improved Using 2-Furyl Derivatives.* PLOS ONE, 2011. 6: e25421. DOI: 10.1371/journal.pone.0025421

21. Chen, J., Zhang, X., Rathjen, J.P., Dodds, P.N., *Direct recognition of pathogen effectors by plant NLR immune receptors and downstream signalling.* Essays in Biochemistry, 2022. 66: 471-483. DOI: 10.1042/EBC20210072

22. Cheng, Q., Dong, L., Gao, T., Liu, T., Li, N., Wang, L., Chang, X., Wu, J., Xu, P., Zhang, S., *The bHLH transcription factor GmPIB1 facilitates resistance to Phytophthora sojae in Glycine max.* Journal of Experimental Botany, 2018. 69: 2527-2541. DOI: 10.1093/jxb/ery103

23. Chinchilla, D., Zipfel, C., Robatzek, S., Kemmerling, B., Nürnberger, T., Jones, J.D.G., Felix, G., Boller, T., *A flagellin-induced complex of the receptor FLS2 and BAK1 initiates plant defence.* Nature, 2007. 448: 497-500. DOI: 10.1038/nature05999

24. Chong, J., Baltz, R., Schmitt, C., Beffa, R., Fritig, B., Saindrenan, P., *Downregulation of a Pathogen-Responsive Tobacco UDP-Glc: Phenylpropanoid Glucosyltransferase Reduces Scopoletin Glucoside Accumulation, Enhances*

Oxidative Stress, and Weakens Virus Resistance. The Plant Cell, 2002. 14: 1093-1107. DOI: 10.1105/tpc.010436

25. Clay, N.K., Adio, A.M., Denoux, C., Jander, G., Ausubel, F.M., *Glucosinolate Metabolites Required for an Arabidopsis Innate Immune Response.* Science, 2009. 323: 95-101. DOI: 10.1126/science.1164627
26. Clough, S.J., Bent, A.F., *Floral dip: a simplified method for Agrobacterium-mediated transformation of Arabidopsis thaliana.* The Plant Journal, 1998. 16: 735-743. DOI: 10.1046/j.1365-313x.1998.00343.x
27. Contreras, M.P., Lüdke, D., Pai, H., Toghani, A., Kamoun, S., *NLR receptors in plant immunity: making sense of the alphabet soup.* EMBO Reports, 2023. 24: e57495. DOI: 10.15252/embr.202357495
28. Corwin, J.A., Subedy, A., Eshbaugh, R., Kliebenstein, D.J., *Expansive Phenotypic Landscape of Botrytis cinerea Shows Differential Contribution of Genetic Diversity and Plasticity.* Molecular Plant-Microbe Interactions, 2016. 29: 287-298. DOI: 10.1094/MPMI-09-15-0196-R
29. Cosme, M., Fernández, I., Van Der Heijden, M.G.A., Pieterse, C.M.J., *Non-Mycorrhizal Plants: The Exceptions that Prove the Rule.* Trends in Plant Science, 2018. 23: 577-587. DOI: 10.1016/j.tplants.2018.04.004
30. Costet, L., Fritig, B., Kauffmann, S., *Scopoletin expression in elicitor-treated and tobacco mosaic virus-infected tobacco plants.* Physiologia Plantarum, 2002. 115: 228-235. DOI: 10.1034/j.1399-3054.2002.1150208.x
31. Czerniawski, P., Piślewska-Bednarek, M., Piasecka, A., Kułak, K., Bednarek, P., *Loss of MYB34 Transcription Factor Supports the Backward Evolution of Indole Glucosinolate Biosynthesis in a Subclade of the Camelineae Tribe and Releases the Feedback Loop in This Pathway in Arabidopsis.* Plant and Cell Physiology, 2023. 64: 80-93. DOI: 10.1093/pcp/pcac142
32. Dahiya, J.S., Rimmer, S.R., *Phytoalexin accumulation in tissues of Brassica napus inoculated with Leptosphaeria maculans.* Phytochemistry, 1988. 27: 3105-3107. DOI: 10.1016/0031-9422(88)80009-8
33. Dangl, J.L., Jones, J.D.G., *Plant pathogens and integrated defence responses to infection.* Nature, 2001. 411: 826-833. DOI: 10.1038/35081161

34. Danzer, K., Currie, L.A., *Guidelines for calibration in analytical chemistry. Part I. Fundamentals and single component calibration (IUPAC Recommendations 1998).* Pure and Applied Chemistry, 1998. 70: 993-1014. DOI: 10.1351/pac199870040993

35. Denekamp, M., Smeekens, S.C., *Integration of Wounding and Osmotic Stress Signals Determines the Expression of the AtMYB102 Transcription Factor Gene.* Plant Physiology, 2003. 132: 1415-1423. DOI: 10.1104/pp.102.019273

36. Denoux, C., Galletti, R., Mammarella, N., Gopalan, S., Werck, D., De Lorenzo, G., Ferrari, S., Ausubel, F.M., Dewdney, J., *Activation of defense response pathways by OGs and Flg22 elicitors in Arabidopsis seedlings.* Molecular Plant, 2008. 1: 423-445. DOI: 10.1093/mp/ssn019

37. Devys, M., Barbier, M., Loiselet, I., Rouxel, T., Sarniguet, A., Kollmann, A., Bousquet, J.-F., *Brassilexin, a novel sulphur-containing phytoalexin from Brassica juncea L. (Cruciferae).* Tetrahedron Letters, 1988. 29: 6447-6448. DOI: 10.1016/S0040-4039(00)82369-2

38. Dodds, P.N., Rathjen, J.P., *Plant immunity: towards an integrated view of plant-pathogen interactions.* Nature Reviews Genetics, 2010. 11: 539-548. DOI: 10.1038/nrg2812

39. Duan, Y., Wang, S., Wang, R., Zhou, Y., Shi, A., Liu, X., Chu, J., Yao, X., *Growth, photosynthesis, redox homeostasis, secondary metabolism and metabolomic changes of Pinellia ternata under antibiotic stress: A comparative study of oxytetracycline, norfloxacin and sulfamethazine.* Plant Physiology and Biochemistry, 2025. 228: 110215. DOI: 10.1016/j.plaphy.2025.110215

40. Fahey, J.W., Zalcmann, A.T., Talalay, P., *The chemical diversity and distribution of glucosinolates and isothiocyanates among plants.* Phytochemistry, 2001. 56: 5-51. DOI: 10.1016/S0031-9422(00)00316-2

41. Felix, G., Duran, J.D., Volko, S., Boller, T., *Plants have a sensitive perception system for the most conserved domain of bacterial flagellin.* The Plant Journal, 1999. 18: 265-276. DOI: 10.1046/j.1365-313X.1999.00265.x

42. Feng, Z., Zhang, B., Ding, W., Liu, X., Yang, D.-L., Wei, P., Cao, F., Zhu, S., Zhang, F., Mao, Y., Zhu, J.-K., *Efficient genome editing in plants using a CRISPR/Cas system.* Cell Research, 2013. 23: 1229-1232. DOI: 10.1038/cr.2013.114

43. Fraenkel, G.S., *The Raison d'Être of Secondary Plant Substances.* Science, 1959. 129: 1466-1470. DOI: 10.1126/science.129.3361.1466

44. Frerigmann, H., Gigolashvili, T., *MYB34, MYB51, and MYB122 Distinctly Regulate Indolic Glucosinolate Biosynthesis in Arabidopsis thaliana.* Molecular Plant, 2014. 7: 814-828. DOI: 10.1093/mp/ssu004

45. Frerigmann, H., Piślewska-Bednarek, M., Sánchez-Vallet, A., Molina, A., Glawischnig, E., Gigolashvili, T., Bednarek, P., *Regulation of Pathogen-Triggered Tryptophan Metabolism in Arabidopsis thaliana by MYB Transcription Factors and Indole Glucosinolate Conversion Products.* Molecular Plant, 2016. 9: 682-695. DOI: 10.1016/j.molp.2016.01.006

46. Frey, M., Schullehner, K., Dick, R., Fiesselmann, A., Gierl, A., *Benzoxazinoid biosynthesis, a model for evolution of secondary metabolic pathways in plants.* Phytochemistry, 2009. 70: 1645-1651. DOI: 10.1016/j.phytochem.2009.05.012

47. Fuchs, R., Kopischke, M., Klapprodt, C., Hause, G., Meyer, A.J., Schwarzländer, M., Fricker, M.D., Lipka, V., *Immobilized Subpopulations of Leaf Epidermal Mitochondria Mediate PENETRATION2-Dependent Pathogen Entry Control in Arabidopsis.* The Plant Cell, 2016. 28: 130-145. DOI: 10.1105/tpc.15.00887

48. Garba Mikail, H., Mohammed, M., Danmalam Umar, H., Musa Suleiman, M., *Secondary Metabolites: The Natural Remedies.* In: Vijayakumar, R., Selvapuram Sudalaimuthu Raja, S. (Eds.), Secondary Metabolites - Trends and Reviews. IntechOpen, 2022. DOI: 10.5772/intechopen.101791

49. Geu-Flores, F., Møldrup, M.E., Böttcher, C., Olsen, C.E., Scheel, D., Halkier, B.A., *Cytosolic γ-Glutamyl Peptidases Process Glutathione Conjugates in the Biosynthesis of Glucosinolates and Camalexin in Arabidopsis.* The Plant Cell, 2011. 23: 2456-2469. DOI: 10.1105/tpc.111.083998

50. Glawischnig, E., *Camalexin.* Phytochemistry, 2007. 68: 401-406. DOI: 10.1016/j.phytochem.2006.12.005

51. Glawischnig, E., Hansen, B.G., Olsen, C.E., Halkier, B.A., *Camalexin is synthesized from indole-3-acetaldoxime, a key branching point between primary and secondary metabolism in Arabidopsis.* Proceedings of the National Academy of Sciences, 2004. 101: 8245-8250. DOI: 10.1073/pnas.0305876101

52. Gómez-Gómez, L., Boller, T., *FLS2: an LRR receptor-like kinase involved in the perception of the bacterial elicitor flagellin in Arabidopsis.* Molecular Cell, 2000. 5: 1003-1011. DOI: 10.1016/s1097-2765(00)80265-8

53. Grubb, C.D., Zipp, B.J., Kopycki, J., Schubert, M., Quint, M., Lim, E., Bowles, D.J., Pedras, M.S.C., Abel, S., *Comparative analysis of Arabidopsis UGT74 glucosyltransferases reveals a special role of UGT74C1 in glucosinolate biosynthesis.* The Plant Journal, 2014. 79: 92-105. DOI: 10.1111/tpj.12541

54. Halkier, B.A., Gershenzon, J., *Biology and biochemistry of glucosinolates.* Annual Review of Plant Biology, 2006. 57: 303-333. DOI: 10.1146/annurev.arplant.57.032905.105228

55. Hanschen, F.S., Lamy, E., Schreiner, M., Rohn, S., *Reactivity and Stability of Glucosinolates and Their Breakdown Products in Foods.* Angewandte Chemie International Edition, 2014. 53: 11430-11450. DOI: 10.1002/anie.201402639

56. Hansen, B.G., Kliebenstein, D.J., Halkier, B.A., *Identification of a flavin-monooxygenase as the S-oxygenating enzyme in aliphatic glucosinolate biosynthesis in Arabidopsis.* The Plant Journal, 2007. 50: 902-910. DOI: 10.1111/j.1365-313X.2007.03101.x

57. Harborne, J.B., *Twenty-five years of chemical ecology.* Natural Product Reports, 2001. 18: 361-379. DOI: 10.1039/b005311m

58. Harborne, J.B., *Introduction to Ecological Biochemistry.* Academic Press, London, 1977.

59. Haruta, M., Major, I.T., Christopher, M.E., Patton, J.J., Constabel, C.P., *A Kunitz trypsin inhibitor gene family from trembling aspen (Populus tremuloides Michx.): cloning, functional expression, and induction by wounding and herbivory.* Plant Molecular Biology, 2001. 46: 347-359. DOI: 10.1023/A:1010654711619

60. Hasegawa, M., Mitsuhara, I., Seo, S., Imai, T., Koga, J., Okada, K., Yamane, H., Ohashi, Y., *Phytoalexin Accumulation in the Interaction Between Rice and the Blast Fungus.* Molecular Plant-Microbe Interactions, 2010. 23: 1000-1011. DOI: 10.1094/MPMI-23-8-1000

61. Hématy, K., Lim, M., Cherk, C., Piślewska-Bednarek, M., Sanchez-Rodriguez, C., Stein, M., Fuchs, R., Klapprodt, C., Lipka, V., Molina, A., Grill, E., Schulze-Lefert,

P., Bednarek, P., Somerville, S., *Moonlighting Function of Phytochelatin Synthase1 in Extracellular Defense against Fungal Pathogens.* Plant Physiology, 2020. 182: 1920-1932. DOI: 10.1104/pp.19.01393

62. Hiruma, K., Fukunaga, S., Bednarek, P., Piślewska-Bednarek, M., Watanabe, S., Narusaka, Y., Shirasu, K., Takano, Y., *Glutathione and tryptophan metabolism are required for Arabidopsis immunity during the hypersensitive response to hemibiotrophs.* Proceedings of the National Academy of Sciences, 2013. 110: 9589-9594. DOI: 10.1073/pnas.1305745110

63. Hiruma, K., Onozawa-Komori, M., Takahashi, F., Asakura, M., Bednarek, P., Okuno, T., Schulze-Lefert, P., Takano, Y., *Entry Mode-Dependent Function of an Indole Glucosinolate Pathway in Arabidopsis for Nonhost Resistance against Anthracnose Pathogens.* The Plant Cell, 2010. 22: 2429-2443. DOI: 10.1105/tpc.110.074344

64. Hopkins, R.J., Van Dam, N.M., Van Loon, J.J.A., *Role of Glucosinolates in Insect-Plant Relationships and Multitrophic Interactions.* Annual Review of Entomology, 2009. 54: 57-83. DOI: 10.1146/annurev.ento.54.110807.090623

65. Huang, A.C., Jiang, T., Liu, Y.-X., Bai, Y.-C., Reed, J., Qu, B., Goossens, A., Nützmann, H.-W., Bai, Y., Osbourn, A., *A specialized metabolic network selectively modulates Arabidopsis root microbiota.* Science, 2019. 364: eaau6389. DOI: 10.1126/science.aau6389

66. Hunziker, P., Ghareeb, H., Wagenknecht, L., Crocoll, C., Halkier, B.A., Lipka, V., Schulz, A., *De novo indol-3-ylmethyl glucosinolate biosynthesis, and not long-distance transport, contributes to defence of Arabidopsis against powdery mildew.* Plant, Cell & Environment, 2020. 43: 1571-1583. DOI: 10.1111/pce.13766

67. Jacobs, A.K., Lipka, V., Burton, R.A., Panstruga, R., Strizhov, N., Schulze-Lefert, P., Fincher, G.B., *An Arabidopsis Callose Synthase, GSL5, Is Required for Wound and Papillary Callose Formation.* The Plant Cell, 2003. 15: 2503-2513. DOI: 10.1105/tpc.016097

68. Jahan, M.A., Harris, B., Lowery, M., Infante, A.M., Percifield, R.J., Kovinich, N., *Glyceollin Transcription Factor GmMYB29A2 Regulates Soybean Resistance to Phytophthora sojae.* Plant Physiology, 2020. 183: 530-546. DOI: 10.1104/pp.19.01293

69. Jensen, L.M., Halkier, B.A., Burow, M., *How to discover a metabolic pathway? An update on gene identification in aliphatic glucosinolate biosynthesis, regulation and transport.* Biological Chemistry, 2014. 395: 529-543. DOI: 10.1515/hsz-2013-0286

70. Jiang, Q.-W., Chen, M.-W., Cheng, K.-J., Yu, P.-Z., Wei, X., Shi, Z., *Therapeutic Potential of Steroidal Alkaloids in Cancer and Other Diseases.* Medicinal Research Reviews, 2016. 36: 119-143. DOI: 10.1002/med.21346

71. Jimenez, L.D., Ayer, W.A., Tewari, J.P., *Phytoalexins produced in the leaves of Capsella bursa-pastoris (shepherd's purse).* Phytoprotection, 2005. 78: 99-103. DOI: 10.7202/706124ar

72. Jones, J.D.G., Dangl, J.L., *The plant immune system.* Nature, 2006. 444: 323-329. DOI: 10.1038/nature05286

73. Kabera, J.N., Semana, E., Mussa, A.R., He, X., *Plant Secondary Metabolites: Biosynthesis, Classification, Function and Pharmacological Properties.* Journal of Pharmacy and Pharmacology, 2014. 2(7): 377-392.

74. Kim, J.H., Jander, G., *Myzus persicae (green peach aphid) feeding on Arabidopsis induces the formation of a deterrent indole glucosinolate.* The Plant Journal, 2007. 49: 1008-1019. DOI: 10.1111/j.1365-313X.2006.03019.x

75. Kim, W., Prokchorchik, M., Tian, Y., Kim, S., Jeon, H., Segonzac, C., *Perception of unrelated microbe-associated molecular patterns triggers conserved yet variable physiological and transcriptional changes in Brassica rapa ssp. pekinensis.* Horticulture Research, 2020. 7: 186. DOI: 10.1038/s41438-020-00410-0

76. Kishi-Kaboshi, M., Okada, K., Kurimoto, L., Murakami, S., Umezawa, T., Shibuya, N., Yamane, H., Miyao, A., Takatsuji, H., Takahashi, A., Hirochika, H., *A rice fungal MAMP-responsive MAPK cascade regulates metabolic flow to antimicrobial metabolite synthesis.* The Plant Journal, 2010. 63: 599-612. DOI: 10.1111/j.1365-313X.2010.04264.x

77. Klein, A.P., Anarat-Cappillino, G., Sattely, E.S., *Minimum Set of Cytochromes P450 for Reconstituting the Biosynthesis of Camalexin, a Major Arabidopsis Antibiotic.* Angewandte Chemie International Edition, 2013. 52: 13625-13628. DOI: 10.1002/anie.201307454

78. Klein, A.P., Sattely, E.S., *Biosynthesis of cabbage phytoalexins from indole glucosinolate.* Proceedings of the National Academy of Sciences, 2017. 114: 1910-1915. DOI: 10.1073/pnas.1615625114

79. Klein, A.P., Sattely, E.S., *Two cytochromes P450 catalyze S-heterocyclizations in cabbage phytoalexin biosynthesis.* Nature Chemical Biology, 2015. 11: 837-839. DOI: 10.1038/nchembio.1914

80. Klepikova, A.V., Kasianov, A.S., Gerasimov, E.S., Logacheva, M.D., Penin, A.A., *A high resolution map of the Arabidopsis thaliana developmental transcriptome based on RNA-seq profiling.* The Plant Journal, 2016. 88: 1058-1070. DOI: 10.1111/tpj.13312

81. Kliebenstein, D.J., D'Auria, J.C., Behere, A.S., Kim, J.H., Gunderson, K.L., Breen, J.N., Lee, G., Gershenzon, J., Last, R.L., Jander, G., *Characterization of seed-specific benzoyloxyglucosinolate mutations in Arabidopsis thaliana.* The Plant Journal, 2007. 51: 1062-1076. DOI: 10.1111/j.1365-313X.2007.03205.x

82. Knill, T., Schuster, J., Reichelt, M., Gershenzon, J., Binder, S., *Arabidopsis Branched-Chain Aminotransferase 3 Functions in Both Amino Acid and Glucosinolate Biosynthesis.* Plant Physiology, 2008. 146: 1028-1039. DOI: 10.1104/pp.107.111609

83. Koornneef, M., Meinke, D., *The development of Arabidopsis as a model plant.* The Plant Journal, 2010. 61: 909-921. DOI: 10.1111/j.1365-313X.2009.04086.x

84. Koornneef, M., Van Eden, J., Hanhart, C.J., Stam, P., Braaksma, F.J., Feenstra, W.J., *Linkage map of Arabidopsis thaliana.* Journal of Heredity, 1983. 74: 265-272. DOI: 10.1093/oxfordjournals.jhered.a109781

85. Koprivova, A., Schwier, M., Volz, V., Kopriva, S., *Shoot-root interaction in control of camalexin exudation in Arabidopsis.* Journal of Experimental Botany, 2023. 74: 2667-2679. DOI: 10.1093/jxb/erad031

86. Korkina, L.G., *Phenylpropanoids as naturally occurring antioxidants: from plant defense to human health.* Cellular and Molecular Biology, 2007. 53: 15-25.

87. Kruszka, D., Sawikowska, A., Kamalabai Selvakesavan, R., Krajewski, P., Kachlicki, P., Franklin, G., *Silver nanoparticles affect phenolic and phytoalexin*

composition of Arabidopsis thaliana. Science of the Total Environment, 2020. 716: 135361. DOI: 10.1016/j.scitotenv.2019.135361

88. Lambrix, V., Reichelt, M., Mitchell-Olds, T., Kliebenstein, D.J., Gershenzon, J., *The Arabidopsis Epithiospecifier Protein Promotes the Hydrolysis of Glucosinolates to Nitriles and Influences Trichoplusia ni Herbivory.* The Plant Cell, 2001. 13: 2793-2807. DOI: 10.1105/tpc.010261

89. Liebrand, T.W.H., van den Berg, G.C.M., Zhang, Z., Smit, P., Cordewener, J.H.G., America, A.H.P., Sklenar, J., Jones, A.M.E., Tameling, W.I.L., Robatzek, S., Thomma, B.P.H.J., Joosten, M.H.A.J., *Receptor-like kinase SOBIR1/EVR interacts with receptor-like proteins in plant immunity against fungal infection.* Proceedings of the National Academy of Sciences, 2013. 110: 10010-10015. DOI: 10.1073/pnas.1220015110

90. Lin, J., Monsalvo, I., Ly, M., Jahan, M.A., Wi, D., Martirosyan, I., Kovinich, N., *RNA-Seq Dissects Incomplete Activation of Phytoalexin Biosynthesis by the Soybean Transcription Factors GmMYB29A2 and GmNAC42-1.* Plants, 2023. 12: 545. DOI: 10.3390/plants12030545

91. Lipka, V., Dittgen, J., Bednarek, P., Bhat, R., Wiermer, M., Stein, M., Landtag, J., Brandt, W., Rosahl, S., Scheel, D., Llorente, F., Molina, A., Parker, J., Somerville, S., Schulze-Lefert, P., *Pre- and Postinvasion Defenses Both Contribute to Nonhost Resistance in Arabidopsis.* Science, 2005. 310: 1180-1183. DOI: 10.1126/science.1119409

92. Liu, T., Zhang, X., Yang, H., Agerbirk, N., Qiu, Y., Wang, H., Shen, D., Song, J., Li, X., *Aromatic Glucosinolate Biosynthesis Pathway in Barbarea vulgaris and its Response to Plutella xylostella Infestation.* Frontiers in Plant Science, 2016. 7. DOI: 10.3389/fpls.2016.00083

93. Louveau, T., Osbourn, A., *The Sweet Side of Plant-Specialized Metabolism.* Cold Spring Harbor Perspectives in Biology, 2019. 11: a034744. DOI: 10.1101/cshperspect.a034744

94. Love, A.J., Yun, B.W., Laval, V., Loake, G.J., Milner, J.J., *Cauliflower mosaic virus, a Compatible Pathogen of Arabidopsis, Engages Three Distinct Defense-Signaling Pathways and Activates Rapid Systemic Generation of Reactive Oxygen Species.* Plant Physiology, 2005. 139: 935-948. DOI: 10.1104/pp.105.066803

95. Lu, X., Dittgen, J., Piślewska-Bednarek, M., Molina, A., Schneider, B., Svatoš, A., Doubský, J., Schneeberger, K., Weigel, D., Bednarek, P., Schulze-Lefert, P., *Mutant Allele-Specific Uncoupling of PENETRATION3 Functions Reveals Engagement of the ATP-Binding Cassette Transporter in Distinct Tryptophan Metabolic Pathways.* Plant Physiology, 2015. 168: 814-827. DOI: 10.1104/pp.15.00182

96. Lv, Q., Li, X., Fan, B., Zhu, C., Chen, Z., *The Cellular and Subcellular Organization of the Glucosinolate-Myrosinase System against Herbivores and Pathogens.* International Journal of Molecular Sciences, 2022. 23: 1577. DOI: 10.3390/ijms23031577

97. Lygin, A.V., Zernova, O.V., Hill, C.B., Kholina, N.A., Widholm, J.M., Hartman, G.L., Lozovaya, V.V., *Glyceollin is an Important Component of Soybean Plant Defense Against Phytophthora sojae and Macrophomina phaseolina.* Phytopathology, 2013. 103: 984-994. DOI: 10.1094/PHYTO-12-12-0328-R

98. Martin, R., Qi, T., Zhang, H., Liu, F., King, M., Toth, C., Nogales, E., Staskawicz, B.J., *Structure of the activated ROQ1 resistosome directly recognizing the pathogen effector XopQ.* Science, 2020. 370: eabd9993. DOI: 10.1126/science.abd9993

99. Martínez-Ballesta, M.D.C., Muries, B., Moreno, D.Á., Dominguez-Perles, R., García-Viguera, C., Carvajal, M., *Involvement of a glucosinolate (sinigrin) in the regulation of water transport in Brassica oleracea grown under salt stress.* Physiologia Plantarum, 2014. 150: 145-160. DOI: 10.1111/ppl.12082

100. Masyita, A., Mustika Sari, R., Dwi Astuti, A., Yasir, B., Rahma Rumata, N., Emran, T.B., Nainu, F., Simal-Gandara, J., *Terpenes and terpenoids as main bioactive compounds of essential oils, their roles in human health and potential application as natural food preservatives.* Food Chemistry: X, 2022. 13: 100217. DOI: 10.1016/j.fochx.2022.100217

101. Matern, A., Böttcher, C., Eschen-Lippold, L., Westermann, B., Smolka, U., Döll, S., Trempel, F., Aryal, B., Scheel, D., Geisler, M., Rosahl, S., *A substrate of the ABC transporter PEN3 stimulates bacterial flagellin (flg22)-induced callose deposition in Arabidopsis thaliana.* Journal of Biological Chemistry, 2019. 294: 6857-6870. DOI: 10.1074/jbc.RA119.007676

102. Mauch-Mani, B., Slusarenko, A.J., *Arabidopsis as a model host for studying plant-pathogen interactions.* Trends in Microbiology, 1993. 1: 265-270. DOI: 10.1016/0966-842X(93)90049-W

103. Meinke, D.W., Cherry, J.M., Dean, C., Rounsley, S.D., Koornneef, M., *Arabidopsis thaliana : A Model Plant for Genome Analysis.* Science, 1998. 282: 662-682. DOI: 10.1126/science.282.5389.662

104. Miya, A., Albert, P., Shinya, T., Desaki, Y., Ichimura, K., Shirasu, K., Narusaka, Y., Kawakami, N., Kaku, H., Shibuya, N., *CERK1, a LysM receptor kinase, is essential for chitin elicitor signaling in Arabidopsis.* Proceedings of the National Academy of Sciences, 2007. 104: 19613-19618. DOI: 10.1073/pnas.0705147104

105. Miyaji, S., Ito, T., Kitaiwa, T., Nishizono, K., Agake, S., Harata, H., Aoyama, H., Umahashi, M., Sato, M., Inaba, J., Fushinobu, S., Yokoyama, T., Maruyama-Nakashita, A., Hirai, M.Y., Ohkama-Ohtsu, N., *N²-Acetylornithine deacetylase functions as a Cys-Gly dipeptidase in the cytosolic glutathione degradation pathway in Arabidopsis thaliana.* The Plant Journal, 2024. 118: 1603-1618. DOI: 10.1111/tpj.16700

106. Moctezuma, C., Hammerbacher, A., Heil, M., Gershenzon, J., Méndez-Alonzo, R., Oyama, K., *Specific Polyphenols and Tannins are Associated with Defense Against Insect Herbivores in the Tropical Oak Quercus oleoides.* Journal of Chemical Ecology, 2014. 40: 458-467. DOI: 10.1007/s10886-014-0431-3

107. Møldrup, M.E., Salomonsen, B., Geu-Flores, F., Olsen, C.E., Halkier, B.A., *De novo genetic engineering of the camalexin biosynthetic pathway.* Journal of Biotechnology, 2013. 167: 296-301. DOI: 10.1016/j.jbiotec.2013.06.013

108. Monde, K., Takasugi, M., Lewis, J.A., Fenwick, G.R., *Time-Course Studies of Phytoalexins and Glucosinolates in UV-Irradiated Turnip Tissue.* Zeitschrift für Naturforschung C, 1991. 46: 189-193. DOI: 10.1515/znc-1991-3-405

109. Mucha, S., Heinzlmeir, S., Kriechbaumer, V., Strickland, B., Kirchhelle, C., Choudhary, M., Kowalski, N., Eichmann, R., Hückelhoven, R., Grill, E., Kuster, B., Glawischnig, E., *The formation of a camalexin-biosynthetic metabolon.* The Plant Cell, 2019. 31(11): 2697-2710. DOI: 10.1105/tpc.19.00403

110. Mucha, S., Walther, D., Müller, T.M., Hincha, D.K., Glawischnig, E., *Substantial reprogramming of the Eutrema salsugineum (Thellungiella salsuginea) transcriptome in response to UV and silver nitrate challenge.* BMC Plant Biology, 2015. 15: 137. DOI: 10.1186/s12870-015-0506-5

111. Müller, T.M., Böttcher, C., Morbitzer, R., Götz, C.C., Lehmann, J., Lahaye, T., Glawischnig, E., *TRANSCRIPTION ACTIVATOR-LIKE EFFECTOR NUCLEASE-Mediated Generation and Metabolic Analysis of Camalexin-Deficient cyp71a12 cyp71a13 Double Knockout Lines.* Plant Physiology, 2015. 168: 849-858. DOI: 10.1104/pp.15.00481

112. Mylona, P., Owatworakit, A., Papadopoulou, K., Jenner, H., Qin, B., Findlay, K., Hill, L., Qi, X., Bakht, S., Melton, R., Osbourn, A., *Sad3 and Sad4 Are Required for Saponin Biosynthesis and Root Development in Oat.* The Plant Cell, 2008. 20: 201-212. DOI: 10.1105/tpc.107.056531

113. Nafisi, M., Goregaoker, S., Botanga, C.J., Glawischnig, E., Olsen, C.E., Halkier, B.A., Glazebrook, J., *Arabidopsis cytochrome P450 monooxygenase 71A13 catalyzes the conversion of indole-3-acetaldoxime in camalexin synthesis.* The Plant Cell, 2007. 19: 2039-2052. DOI: 10.1105/tpc.107.051383

114. Nakano, R.T., Piślewska-Bednarek, M., Yamada, K., Edger, P.P., Miyahara, M., Kondo, M., Böttcher, C., Mori, M., Nishimura, M., Schulze-Lefert, P., Hara-Nishimura, I., Bednarek, P., *PYK10 myrosinase reveals a functional coordination between endoplasmic reticulum bodies and glucosinolates in Arabidopsis thaliana.* The Plant Journal, 2017. 89: 204-220. DOI: 10.1111/tpj.13377

115. NASC Bioinformatics.

116. Nemri, A., Atwell, S., Tarone, A.M., Huang, Y.S., Zhao, K., Studholme, D.J., Nordborg, M., Jones, J.D.G., *Genome-wide survey of Arabidopsis natural variation in downy mildew resistance using combined association and linkage mapping.* Proceedings of the National Academy of Sciences, 2010. 107: 10302-10307. DOI: 10.1073/pnas.0913160107

117. Ng, T.B., Ye, X.J., Wong, J.H., Fang, E.F., Chan, Y.S., Pan, W., Ye, X.Y., Sze, S.C.W., Zhang, K.Y., Liu, F., Wang, H.X., *Glyceollin, a soybean phytoalexin with medicinal properties.* Applied Microbiology and Biotechnology, 2011. 90: 59-68. DOI: 10.1007/s00253-011-3169-7

118. Ngou, B.P.M., Ahn, H.-K., Ding, P., Jones, J.D.G., *Mutual potentiation of plant immunity by cell-surface and intracellular receptors.* Nature, 2021. 592: 110-115. DOI: 10.1038/s41586-021-03315-7

119. N'Guyen, G.Q., Raulo, R., Porquier, A., Iacomi, B., Pelletier, S., Renou, J.-P., Bataillé-Simoneau, N., Campion, C., Hamon, B., Kwasiborski, A., Colou, J., Benamar, A., Hudhomme, P., Macherel, D., Simoneau, P., Guillemette, T., *Responses of the Necrotrophic Fungus Alternaria brassicicola to the Indolic Phytoalexin Brassinin.* Frontiers in Plant Science, 2021. 11: 611643. DOI: 10.3389/fpls.2020.611643

120. Nintemann, S.J., Hunziker, P., Andersen, T.G., Schulz, A., Burow, M., Halkier, B.A., *Localization of the glucosinolate biosynthetic enzymes reveals distinct spatial patterns for the biosynthesis of indole and aliphatic glucosinolates.* Physiologia Plantarum, 2018. 163: 138-154. DOI: 10.1111/ppl.12672

121. Nishimura, M.T., Dangl, J.L., *Arabidopsis and the plant immune system.* The Plant Journal, 2010. 61: 1053-1066. DOI: 10.1111/j.1365-313X.2010.04131.x

122. Nützmann, H.-W., Doerr, D., Ramírez-Colmenero, A., Sotelo-Fonseca, J.E., Wegel, E., Di Stefano, M., Wingett, S.W., Fraser, P., Hurst, L., Fernandez-Valverde, S.L., Osbourn, A., *Active and repressed biosynthetic gene clusters have spatially distinct chromosome states.* Proceedings of the National Academy of Sciences, 2020. 117: 13800-13809. DOI: 10.1073/pnas.1920474117

123. Pastorczyk, M., Bednarek, P., *The Function of Glucosinolates and Related Metabolites in Plant Innate Immunity.* In: Advances in Botanical Research. Elsevier, 2016. pp. 171-198. DOI: 10.1016/bs.abr.2016.06.007

124. Pastorczyk, M., Kosaka, A., Piślewska-Bednarek, M., López, G., Frerigmann, H., Kułak, K., Glawischnig, E., Molina, A., Takano, Y., Bednarek, P., *The role of CYP 71A12 monooxygenase in pathogen-triggered tryptophan metabolism and Arabidopsis immunity.* New Phytologist, 2020. 225: 400-412. DOI: 10.1111/nph.16118

125. Paxton, J.D., *Phytoalexins: A Working Redefinition.* Journal of Phytopathology, 1981. 101: 106-109. DOI: 10.1111/j.1439-0434.1981.tb03327.x

126. Pedras, M.S.C., Abdoli, A., *Pathogen inactivation of cruciferous phytoalexins: detoxification reactions, enzymes and inhibitors.* RSC Advances, 2017. 7: 23633-23646. DOI: 10.1039/C7RA01574G

127. Pedras, M.S.C., Adio, A.M., *Phytoalexins and phytoanticipins from the wild crucifers Thellungiella halophila and Arabidopsis thaliana: Rapalexin A, wasalexins and camalexin.* Phytochemistry, 2008. 69: 889-893. DOI: 10.1016/j.phytochem.2007.10.032

128. Pedras, M.S.C., Adio, A.M., Suchy, M., Okinyo, D.P.O., Zheng, Q.-A., Jha, M., Sarwar, M.G., *Detection, characterization and identification of crucifer phytoalexins using high-performance liquid chromatography with diode array detection and electrospray ionization mass spectrometry.* Journal of Chromatography A, 2006. 1133: 172-183. DOI: 10.1016/j.chroma.2006.08.015

129. Pedras, M.S.C., Alavi, M., *Expanding the Phytoalexin Chemical Space: Tropalexins a and B from Tropaeolum Majus Suggest Evolutionary Conservation of Biosynthetic Enzymes.* Preprint, 2020. DOI: 10.26434/chemrxiv.13350335.v1

130. Pedras, M.S.C., Alavi, M., To, Q.H., *Expanding the nasturlexin family: Nasturlexins C and D and their sulfoxides are phytoalexins of the crucifers Barbarea vulgaris and B. verna.* Phytochemistry, 2015. 118: 131-138. DOI: 10.1016/j.phytochem.2015.08.009

131. Pedras, M.S.C., Minic, Z., Abdoli, A., *The phytoalexin camalexin induces fundamental changes in the proteome of Alternaria brassicicola different from those caused by brassinin.* Fungal Biology, 2014. 118: 83-93. DOI: 10.1016/j.funbio.2013.11.005

132. Pedras, M.S.C., Montaut, S., Suchy, M., *Phytoalexins from the Crucifer Rutabaga: Structures, Syntheses, Biosyntheses, and Antifungal Activity.* The Journal of Organic Chemistry, 2004. 69: 4471-4476. DOI: 10.1021/jo049648a

133. Pedras, M.S.C., Thapa, C., *Unveiling fungal detoxification pathways of the cruciferous phytoalexin rapalexin A: Sequential L-cysteine conjugation, acetylation and oxidative cyclization mediated by Colletotrichum spp.* Phytochemistry, 2020. 169: 112188. DOI: 10.1016/j.phytochem.2019.112188

134. Pedras, M.S.C., Yaya, E.E., *Phytoalexins from Brassicaceae: News from the front.* Phytochemistry, 2010. 71: 1191-1197. DOI: 10.1016/j.phytochem.2010.03.020

135. Pedras, M.S.C., Yaya, E.E., Glawischnig, E., *The phytoalexins from cultivated and wild crucifers: Chemistry and biology.* Natural Product Reports, 2011. 28: 1381. DOI: 10.1039/c1np00020a

136. Pedras, M.S.C., Yaya, E.E., Hossain, S., *Unveiling the phytoalexin biosynthetic puzzle in salt cress: unprecedented incorporation of glucobrassicin into wasalexins A and B.* Organic & Biomolecular Chemistry, 2010. 8: 5150. DOI: 10.1039/c0ob00265h

137. Pedras, M.S.C., Zheng, Q.-A., Gadagi, R.S., *The first naturally occurring aromatic isothiocyanates, rapalexins A and B, are cruciferous phytoalexins.* Chemical Communications, 2007. 4: 368-370. DOI: 10.1039/B615424G

138. Peng, Z., Cao, M., Zhu, S., Yang, J., Yan, B., Wan, X., Kang, C., Wang, S., Lv, C., Zhang, Yufei, Yuan, F., Zhao, Z., Xiang, Z., Xue, W., Zhang, Yan, He, Y., Guo, L., *Interspecific rhizosphere interactions enhance secondary metabolite synthesis and volatile oil content in Atractylodes lancea through root exudates.* Industrial Crops and Products, 2025. 236: 122084. DOI: 10.1016/j.indcrop.2025.122084

139. Pfalz, M., Mikkelsen, M.D., Bednarek, P., Olsen, C.E., Halkier, B.A., Kroymann, J., *Metabolic Engineering in Nicotiana benthamiana Reveals Key Enzyme Functions in Arabidopsis Indole Glucosinolate Modification.* The Plant Cell, 2011. 23: 716-729. DOI: 10.1105/tpc.110.081711

140. Pfalz, M., Mukhaimar, M., Perreau, F., Kirk, J., Hansen, C.I.C., Olsen, C.E., Agerbirk, N., Kroymann, J., *Methyl Transfer in Glucosinolate Biosynthesis Mediated by Indole Glucosinolate O-Methyltransferase 5.* Plant Physiology, 2016. 172: 2190-2203. DOI: 10.1104/pp.16.01402

141. Pfalz, M., Vogel, H., Kroymann, J., *The Gene Controlling the Indole Glucosinolate Modifier1 Quantitative Trait Locus Alters Indole Glucosinolate Structures and Aphid Resistance in Arabidopsis.* The Plant Cell, 2009. 21: 985-999. DOI: 10.1105/tpc.108.063115

142. Pickens, L.B., Tang, Y., Chooi, Y.-H., *Metabolic Engineering for the Production of Natural Products.* Annual Review of Chemical and Biomolecular Engineering, 2011. 2: 211-236. DOI: 10.1146/annurev-chembioeng-061010-114209

143. Piślewska-Bednarek, M., Nakano, R.T., Hiruma, K., Pastorczyk, M., Sanchez-Vallet, A., Singkaravanit-Ogawa, S., Ciesiołka, D., Takano, Y., Molina, A., Schulze-Lefert, P., Bednarek, P., *Glutathione Transferase U13 Functions in Pathogen-Triggered Glucosinolate Metabolism.* Plant Physiology, 2018. 176: 538-551. DOI: 10.1104/pp.17.01455

144. Plaszkó, T., Szűcs, Z., Vasas, G., Gonda, S., *Effects of Glucosinolate-Derived Isothiocyanates on Fungi: A Comprehensive Review on Direct Effects, Mechanisms, Structure-Activity Relationship Data and Possible Agricultural Applications.* Journal of Fungi, 2021. 7: 539. DOI: 10.3390/jof7070539

145. Pucker, B., Kleinbölting, N., Weisshaar, B., *Large scale genomic rearrangements in selected Arabidopsis thaliana T-DNA lines are caused by T-DNA insertion mutagenesis.* BMC Genomics, 2021. 22: 599. DOI: 10.1186/s12864-021-07877-8

146. Rajniak, J., Giehl, R.F.H., Chang, E., Murgia, I., Von Wirén, N., Sattely, E.S., *Biosynthesis of redox-active metabolites in response to iron deficiency in plants.* Nature Chemical Biology, 2018. 14: 442-450. DOI: 10.1038/s41589-018-0019-2

147. Ramírez-Zavaleta, C.Y., García-Barrera, L.J., Rodríguez-Verástegui, L.L., Arrieta-Flores, D., Gregorio-Jorge, J., *An Overview of PRR- and NLR-Mediated Immunities: Conserved Signaling Components across the Plant Kingdom That Communicate Both Pathways.* International Journal of Molecular Sciences, 2022. 23: 12974. DOI: 10.3390/ijms232112974

148. Redei, G.P., *Arabidopsis as a genetic tool.* Annual Review of Genetics, 1975. 9: 111-127. DOI: 10.1146/annurev.ge.09.120175.000551

149. Roell, M.-S., Zurbriggen, M.D., *The impact of synthetic biology for future agriculture and nutrition.* Current Opinion in Biotechnology, Plant Biotechnology - Food Biotechnology, 2020. 61: 102-109. DOI: 10.1016/j.copbio.2019.10.004

150. Rogers, E.E., *Mode of Action of the Arabidopsis thaliana Phytoalexin Camalexin and Its Role in Arabidopsis-Pathogen Interactions.* Molecular Plant-Microbe Interactions, 1996. 9: 748. DOI: 10.1094/MPMI-9-0748

151. Rouxel, T., Kollmann, A., Boulidard, L., Mithen, R., *Abiotic elicitation of indole phytoalexins and resistance to Leptosphaeria maculans within Brassiceae.* Planta, 1991. 184: 271-278. DOI: 10.1007/BF00197957

152. Sanchez-Vallet, A., Ramos, B., Bednarek, P., López, G., Piślewska-Bednarek, M., Schulze-Lefert, P., Molina, A., *Tryptophan-derived secondary metabolites in Arabidopsis thaliana confer non-host resistance to necrotrophic Plectosphaerella cucumerina fungi.* The Plant Journal, 2010. 63(1): 115-127. DOI: 10.1111/j.1365-313X.2010.04224.x

153. Schlaeppi, K., Abou-Mansour, E., Buchala, A., Mauch, F., *Disease resistance of Arabidopsis to Phytophthora brassicae is established by the sequential action of indole glucosinolates and camalexin: Glucosinolates and camalexin in disease resistance.* The Plant Journal, 2010. 62: 840-851. DOI: 10.1111/j.1365-313X.2010.04197.x

154. Schouten, A., Wagemakers, L., Stefanato, F.L., Kaaij, R.M. van der, Kan, J.A.L. van, *Resveratrol acts as a natural profungicide and induces self-intoxication by a specific laccase.* Molecular Microbiology, 2002. 43: 883-894. DOI: 10.1046/j.1365-2958.2002.02801.x

155. Schroeder, N.E., Macguidwin, A.E., *Mortality and behavior in Heterodera glycines juveniles following exposure to isothiocyanate compounds.* Journal of Nematology, 2010. 42: 194-200.

156. Schuhegger, R., Nafisi, M., Mansourova, M., Petersen, B.L., Olsen, C.E., Svatoš, A., Halkier, B.A., Glawischnig, E., *CYP71B15 (PAD3) Catalyzes the Final Step in Camalexin Biosynthesis.* Plant Physiology, 2006. 141: 1248-1254. DOI: 10.1104/pp.106.082024

157. Sellam, A., Dongo, A., Guillemette, T., Hudhomme, P., Simoneau, P., *Transcriptional responses to exposure to the brassicaceous defence metabolites camalexin and allyl-isothiocyanate in the necrotrophic fungus Alternaria brassicicola.* Molecular Plant Pathology, 2007. 8: 195-208. DOI: 10.1111/j.1364-3703.2007.00387.x

158. Sharma, A., Sinharoy, S., Bisht, N.C., *The mysterious non-arbuscular mycorrhizal status of Brassicaceae species.* Environmental Microbiology, 2023. 25: 917-930. DOI: 10.1111/1462-2920.16339

159. Shimura, K., Okada, A., Okada, K., Jikumaru, Y., Ko, K.-W., Toyomasu, T., Sassa, T., Hasegawa, M., Kodama, O., Shibuya, N., Koga, J., Nojiri, H., Yamane, H., *Identification of a biosynthetic gene cluster in rice for momilactones.* Journal of Biological Chemistry, 2007. 282: 34013-34018. DOI: 10.1074/jbc.m703344200

160. Somssich, M., Kliebenstein, D.J., Andersen, T.G., *Guns in rosettes: The Arabidopsis chemical weapons arsenal.* Plant Physiology, 2025. 199: kiaf411. DOI: 10.1093/plphys/kiaf411

161. Sønderby, I.E., Geu-Flores, F., Halkier, B.A., *Biosynthesis of glucosinolates - gene discovery and beyond.* Trends in Plant Science, 2010. 15: 283-290. DOI: 10.1016/j.tplants.2010.02.005

162. Stein, M., Dittgen, J., Sánchez-Rodríguez, C., Hou, B.-H., Molina, A., Schulze-Lefert, P., Lipka, V., Somerville, S., *Arabidopsis PEN3/PDR8, an ATP Binding Cassette Transporter, Contributes to Nonhost Resistance to Inappropriate Pathogens That Enter by Direct Penetration.* The Plant Cell, 2006. 18: 731-746. DOI: 10.1105/tpc.105.038372

163. Stringlis, I.A., De Jonge, R., Pieterse, C.M.J., *The Age of Coumarins in Plant-Microbe Interactions.* Plant and Cell Physiology, 2019. 60: 1405-1419. DOI: 10.1093/pcp/pcz076

164. Su, T., Xu, J., Li, Y., Lei, L., Zhao, L., Yang, H., Feng, J., Liu, G., Ren, D., *Glutathione-Indole-3-Acetonitrile Is Required for Camalexin Biosynthesis in Arabidopsis thaliana.* The Plant Cell, 2011. 23: 364-380. DOI: 10.1105/tpc.110.079145

165. Sugawara, S., Hishiyama, S., Jikumaru, Y., Hanada, A., Nishimura, T., Koshiba, T., Zhao, Y., Kamiya, Y., Kasahara, H., *Biochemical analyses of indole-3-acetaldoxime-dependent auxin biosynthesis in Arabidopsis.* Proceedings of the National Academy of Sciences, 2009. 106: 5430-5435. DOI: 10.1073/pnas.0811226106

166. Taguchi, G., Ubukata, T., Nozue, H., Kobayashi, Y., Takahi, M., Yamamoto, H., Hayashida, N., *Malonylation is a key reaction in the metabolism of xenobiotic phenolic glucosides in Arabidopsis and tobacco: Phenolic-xenobiotics metabolism in Arabidopsis.* The Plant Journal, 2010. 63: 1031-1041. DOI: 10.1111/j.1365-313X.2010.04298.x

167. Tal, B., Robeson, D.J., *The Metabolism of Sunflower Phytoalexins Ayapin and Scopoletin: Plant-Fungus Interactions.* Plant Physiology, 1986. 82: 167-172. DOI: 10.1104/pp.82.1.167

168. Tariq, H., Asif, S., Andleeb, A., Hano, C., Abbasi, B.H., *Flavonoid Production: Current Trends in Plant Metabolic Engineering and De Novo Microbial Production.* Metabolites, 2023. 13: 124. DOI: 10.3390/metabo13010124

169. The Arabidopsis Genome Initiative, *Analysis of the genome sequence of the flowering plant Arabidopsis thaliana.* Nature, 2000. 408: 796-815. DOI: 10.1038/35048692

170. The European Arabidopsis Stock Centre - The University of Nottingham.

171. Thomma, B.P.H.J., Nelissen, I., Eggermont, K., Broekaert, W.F., *Deficiency in phytoalexin production causes enhanced susceptibility of Arabidopsis thaliana to the fungus Alternaria brassicicola.* The Plant Journal, 1999. 19: 163-171. DOI: 10.1046/j.1365-313X.1999.00513.x

172. Thompson, J.N., *Interaction and Coevolution.* University of Chicago Press, Chicago, Illinois, 1982.

173. Tiedge, K.J., Roda, F., Smith, S.D., Moghe, G.D., *Advances in analyzing and engineering plant metabolic diversity.* Applications in Plant Sciences, 2025. 13: e70017. DOI: 10.1002/aps3.70017

174. Ting, H.-M., Cheah, B.H., Chen, Y.-C., Yeh, P.-M., Cheng, C.-P., Yeo, F.K.S., Vie, A.K., Rohloff, J., Winge, P., Bones, A.M., Kissen, R., *The Role of a Glucosinolate-Derived Nitrile in Plant Immune Responses.* Frontiers in Plant Science, 2020. 11: 257. DOI: 10.3389/fpls.2020.00257

175. Treutter, D., *Significance of flavonoids in plant resistance: a review.* Environmental Chemistry Letters, 2006. 4: 147-157. DOI: 10.1007/s10311-006-0068-8

176. Tripathi, M.K., Mishra, A.S., *Glucosinolates in animal nutrition: A review.* Animal Feed Science and Technology, 2007. 132: 1-27. DOI: 10.1016/j.anifeedsci.2006.03.003

177. Tsai, H.-H., Rodríguez-Celma, J., Lan, P., Wu, Y.-C., Vélez-Bermúdez, I.C., Schmidt, W., *Scopoletin 8-Hydroxylase-Mediated Fraxetin Production Is Crucial for Iron Mobilization.* Plant Physiology, 2018. 177: 194-207. DOI: 10.1104/pp.18.00178

178. Tully, J.P., Hill, A.E., Ahmed, H.M., Whitley, R., Skjellum, A., Mukhtar, M.S., *Expression-based network biology identifies immune-related functional modules involved in plant defense.* BMC Genomics, 2014. 15: 421. DOI: 10.1186/1471-2164-15-421

179. Van de Weyer, A.-L., Monteiro, F., Furzer, O.J., Nishimura, M.T., Cevik, V., Witek, K., Jones, J.D.G., Dangl, J.L., Weigel, D., Bemm, F., *A Species-Wide Inventory of NLR Genes and Alleles in Arabidopsis thaliana.* Cell, 2019. 178: 1260-1272.e14. DOI: 10.1016/j.cell.2019.07.038

180. Van Hulten, M., Chatterjee, S., Van Den Burg, H.A., *Infection Assay for Xanthomonas campestris pv. campestris in Arabidopsis thaliana Mimicking Natural Entry via Hydathodes.* In: Gassmann, W. (Ed.), Plant Innate Immunity, Methods in Molecular Biology. Springer New York, New York, NY, 2019. pp. 159-185. DOI: 10.1007/978-1-4939-9458-8_16

181. VanEtten, H.D., Mansfield, J.W., Bailey, J.A., Farmer, E.E., *Two Classes of Plant Antibiotics: Phytoalexins versus "Phytoanticipins".* The Plant Cell, 1994. 6: 1191-1192. DOI: 10.1105/tpc.6.9.1191

182. Wang, S., Alseekh, S., Fernie, A.R., Luo, J., *The Structure and Function of Major Plant Metabolite Modifications.* Molecular Plant, 2019. 12: 899-919. DOI: 10.1016/j.molp.2019.06.001

183. Winkel-Shirley, B., *Biosynthesis of flavonoids and effects of stress.* Current Opinion in Plant Biology, 2002. 5: 218-223. DOI: 10.1016/S1369-5266(02)00256-X

184. Wittstock, U., Burow, M., *Glucosinolate Breakdown in Arabidopsis: Mechanism, Regulation and Biological Significance.* The Arabidopsis Book, 2010. 8: e0134. DOI: 10.1199/tab.0134

185. Wittstock, U., Kurzbach, E., Herfurth, A.-M., Stauber, E.J., *Glucosinolate Breakdown.* In: Advances in Botanical Research. Academic Press, 2016. pp. 125-169. DOI: 10.1016/bs.abr.2016.06.006

186. Wu, Y., Hillwig, M.L., Wang, Q., Peters, R.J., *Parsing a multifunctional biosynthetic gene cluster from rice: Biochemical characterization of CYP71Z6 & 7.* FEBS Letters, 2011. 585: 3446-3451. DOI: 10.1016/j.febslet.2011.09.038

187. Xiang, M.-L., Hu, B.-Y., Qi, Z.-H., Wang, X.-N., Xie, T.-Z., Wang, Z.-J., Ma, D.-Y., Zeng, Q., Luo, X.-D., *Chemistry and bioactivities of natural steroidal alkaloids.* Natural Products and Bioprospecting, 2022. 12: 23. DOI: 10.1007/s13659-022-00345-0

188. Yadav, V., Wang, Z., Wei, C., Amo, A., Ahmed, B., Yang, X., Zhang, X., *Phenylpropanoid Pathway Engineering: An Emerging Approach towards Plant Defense.* Pathogens, 2020. 9: 312. DOI: 10.3390/pathogens9040312

189. Yamada, K., Hara-Nishimura, I., Nishimura, M., *Unique Defense Strategy by the Endoplasmic Reticulum Body in Plants.* Plant and Cell Physiology, 2011. 52: 2039-2049. DOI: 10.1093/pcp/pcr156

190. Yuan, M., Jiang, Z., Bi, G., Nomura, K., Liu, M., Wang, Y., Cai, B., Zhou, J.-M., He, S.Y., Xin, X.-F., *Pattern-recognition receptors are required for NLR-mediated plant immunity.* Nature, 2021. 592: 105-109. DOI: 10.1038/s41586-021-03316-6

191. Zasada, I.A., Ferris, H., *Sensitivity of Meloidogyne javanica and Tylenchulus semipenetrans to Isothiocyanates in Laboratory Assays.* Phytopathology, 2003. 93: 747-750. DOI: 10.1094/PHYTO.2003.93.6.747

192. Zhao, N., Wang, G., Norris, A., Chen, X., Chen, F., *Studying Plant Secondary Metabolism in the Age of Genomics.* Critical Reviews in Plant Sciences, 2013. 32(6): 369-382. DOI: 10.1080/07352689.2013.789648

193. Zipfel, C., *Plant pattern-recognition receptors.* Trends in Immunology, 2014. 35: 345-351. DOI: 10.1016/j.it.2014.05.004